The University Of Sheffield.

Data-driven methodologies to estimate process parameters, design parameters and mechanical properties of fused deposition modelling polylactide components

Ruixuan Tu

A thesis submitted in fulfilment of the requirements for the degree of Doctor of Philosophy

University of Sheffield
Faculty of Engineering
Department of Mechanical Engineering

February 2023

Declaration of Authorship

I hereby confirm that this thesis titled, “Data-driven methodologies to estimate process parameters, design parameters and mechanical properties of fused deposition modelling PLA components,” and the work presented in it is entirely my own. Where I have consulted the work of others is always clearly stated. All statements taken literally from other writings or referred to by analogy are marked, and the source is always given. Where any part of this thesis has previously been submitted for publication, this has been clearly stated.

Name: Ruixuan Tu

Date: February 2023

Abstract

Due to the high complexity of relationships between the various process parameters and the mechanical properties of the polylactide (PLA) components produced by the fused deposition modelling (FDM), predictions of their mechanical behaviour could be a complicated task to complete using the conventional approaches. Hence, alternative data-driven methodologies are adopted in the present investigation to serve this goal.

The present research has included the development of two alternative frameworks: dependent on the user needs, “direct” and “inverse” schemes. The former could be used to estimate mechanical properties with given process parameters, whereas the latter could identify the optimal combination of the process parameter ensuring the required mechanical behaviour. The process parameters estimated from the inverse framework can be adjusted with respect to the specifications of the printer and the software.

Three various data-driven methodologies were adopted in the present investigations, including the fuzzy inference system (FIS), artificial neural network (NN) and adaptive neural fuzzy inference system (ANFIS). The research has confirmed that with the priority being accuracy, the ANFIS is seen to be the most accurate approach, which requires particular computing power. However, FIS is reported to be the most efficient approach, which has a similar level of accuracy to the ANFIS approach.

The intrinsic versatility of the analysed data-driven methodologies has proven that these approaches could be adopted not only for process and geometrical design parameters, but also they are successful in analysing cost-relevant parameters such as printing time and material consumption. It has been shown that data-driven methodologies could be an effective and robust decision-making tool in design and cost management problems.

Acknowledgement

It has been an amazing experience for me to work on this project because not only have I learnt so much, but also I have known so many people as my colleagues and friends. The present work would not have been possible without their support and guidance.

Firstly, I would like to thank my supervisor Professor Inna Gitman, who is patient, kind and not only just a supervisor but also a mentor to me. With her unceasing support and encouragement, I have learnt a lot about how to become an independent researcher. I am so fortunate to have Inna as my supervisor, without whom the project could not have been successful. I will never forget the fascinating analogy of the “fairy tale” style of academic writing.

I would also like to thank Professor Luca Susmel, who expanded my research areas in 3D printing and paved the way for the success of this project. The project would not have succeeded without his generosity in sharing the data. The collaborative work with Luca significantly increases my confidence and has successfully become a part of this project.

Many other people have helped and supported me during my PhD study. I appreciate my colleagues Sinan Eraslan, Iwo Slodczyk and Zakaria Alshkmak whom I have had highly informative and essential discussions. I would like to thank Martyn Aspinall and Jeremy Stakes from the Engineering Application lab in Multidisciplinary Engineering Education for teaching me the basic knowledge of engineering applications and how to become a good lab demonstrator. I thank Dr David Polson, Dr Kamran Mumtaz and Dr Candice Majewski for their courses delivered.

Finally, during the Covid-19 pandemic, family support has given me great motivation and energy to carry on with my work. My deepest appreciation to my parents, without whom I would never achieve such success. I would also like to thank my partner Yuhan Bian, who took meticulous care of me during the pandemic and gave me powerful confidence during the thesis writing-up period. Moreover, special thanks go to my friends – Harry, Kai, Fang, Hao Guan, Yuetong Xu, Cynthia, and Gabi, who were always by my side during the last four years.

Contents

List of Figures

List of Tables

List of Abbreviations

ABS	Acrylonitrile Butadiene Styrene
AI	Artificial Intelligence
AM	Additive Manufacturing
ANFIS	Adaptive Neural Fuzzy Inference System
ANOVA	Analysis of Variance
CAD	Computer-Aided-Design
COG	Centre of Gravity
DOE	Design of Experiments
FDM	Fused Deposition Modelling
FEA	Finite Element Analysis
FIS	Fuzzy Inference System
GD	Gradient Descent
GDM	Gradient Descent with Momentum
LSE	Least Squared Estimate
MF	Membership Function
ML	Machine Learning
MSE	Mean Squared Error
NN	Neural Network
OFAT	One Factor at a Time
PLA	Polylactide
TS	Tensile strength
3D	Three-Dimensional

Nomenclature

d_v	Effective size of manufacturing voids	mm
e	Exponential constant	
E	General estimation error	
f	Output membership functions of ANFIS	
F_1	Inverse estimation	
F_2	Direct estimation	
I	Identity matrix	
L	Learning rate	
n	Number of experiments	
P_{est}	Estimated output	
P_{exp}	Experimental output	
W_a	The value of the weighted average	
y_p	Main printing direction	
Y	The output of the neuron in NN	
Z	Calculated value of the neuron in NN	
β	Momentum constant	
θ_p	Manufacturing angle	Degree
μ	Membership value	
σ_f	Failure tensile strength	MPa
σ_e	Estimated failure tensile strength	MPa
ω	Weight values of neural network	

This thesis is dedicated to my parents and my beloved partner, without whose unwavering support and meticulous care during the COVID-19 crisis, this thesis would not be possible to come to fruition.

Chapter 1

Introduction

1.1 Additive manufacturing technology

As modern society is entering the era of digital manufacturing, numerous innovative technologies have appeared and shown daily increasing competitiveness compared with conventional manufacturing solutions. Additive manufacturing (AM), which is one of these novel techniques, has raised a revolution in modern industries due to its unique characteristics. Different from the conventional manufacturing process such as machining, milling, shaping, etc., AM, also known as 3D-printing technologies, replaces "subtraction" with "addition", which allows materials to be processed more efficiently without extra waste. Although it is not the main focus of the thesis, the AM technology will still be explained in detail in this chapter[1] to fulfil the background knowledge of the 3D-printing techniques for readers.

1.1.1 Working principle

Based on the "additional" manufacturing strategy, various materials could be used for 3D printing, such as metals,[1] ceramics,[2] thermoplastics,[3] etc., depending on the specific choice of the technique. In the present study, the experimental specimens are manufactured with the fused

[1] This chapter is partly adopted from:

Tu R, Gitman I, Susmel L. Fuzzy inference system for failure strength estimation of plain and notched 3D-printed polylactide components. *Fatigue Fract Eng Mater Struct*. 2022;45: 1663–1677.

Tu R, Gitman I, Susmel L. Fuzzy sets based methodology for manufacturing parameter determination of 3D-printed PLA components: optimisation of strength, design and cost requirements. (under review)

deposition modelling (FDM) technique, which is an extrusion-based 3D-printing solution. Hence, the adopted material here is polylactide (PLA) which is a commonly used FDM material.

PLA is an economical and biodegradable material as it can be manufactured at a low cost, particularly from renewable resources such as corn starch and sugarcane.[4] Hence, it has been considered one of the environmentally sustainable materials. Another reason for PLA to become one of the common materials of FDM is that it is a thermoplastic which has a relatively low melting temperature of around 180°C[5] and is suitable for the FDM processing of the material.

Specifically, during the process of FDM, melted material filaments are extruded from a heated nozzle and then deposited selectively on a printing platform.[6] Upon touching, melted materials start to cool down and solidify, eventually forming a layer of predetermined geometry. This could be achieved as the path of the nozzle is generated based on the layer geometry, which is the outcome of the part being sliced into super-thin layers with the help of computer-aided design (CAD) software packages.[7]

After the layer geometry has been finished, the platform will be lowered so that the following materials can be bedded on top of the previously deposited ones. After this stage, layers of thermoplastic materials bond together and a three-dimensional part is eventually achieved as designed.

1.1.2 Processing parameters

During the manufacturing process, there are various processing parameters influencing the ultimate mechanical property of the printed object, such as infill density, manufacturing orientation and angle,[8] temperatures,[9] layer height,[10] etc. Among all these parameters, infill density, which represents the inner volume occupied by filled materials, is reported to have a significant impact on the mechanical properties of printed parts.[11–13]

The idea of the infill density is a compromise between a solid and a hollow object where the former is both material and time-consuming for FDM printing, and the latter is characterised by a strength which is too low.[14] As such, the infill density is directly connected with the strength and the weight of an object as well as the printing duration, and all these parameters vary between a solid and a hollow object.

It has been validated that the impact,[15] flexural and ultimate tensile strength[16] could peak at 100% (maximum) infill density, whereas the optimum infill density still depends on the actual application. This is not only for material saving but also for other important criteria. For example, Porter et al.[17] have found that 10% to 20% is the optimum range for infill percentage in order to

maximise the stiffness-to-mass for the 3D-printed object. However, a bit higher infill density is also suggested to avoid the reduction of flexural rigidity in their study. Similarly, Schmitt et al.[18] have also proven that various infill selections are necessary for regions with different stress situations, considering the prevailing trend of the light-weighting of components in the automotive industry. Therefore, the determination of the optimum infill density is definitely worth particular attention.

Apart from the infill density, printing direction has proven to significantly impact the mechanical behaviour of the printed parts.[19] In the present work, as far as the mechanical behaviour of 3D-printed polymers is concerned, much experimental evidence suggests that the anisotropy associated with the building direction plays a role of primary significance.[20–23]

For instance, it is seen from the experiments that the ultimate tensile strength and the yield stress of 3D-printed PLA parts manufactured perpendicularly to the build plate are lower than the corresponding mechanical properties that are obtained when objects are manufactured either on-edge or flat.[20,21] Similarly, when components are fused-filament fabricated flat on the built plate, their mechanical response is influenced by the intrinsic anisotropy resulting from the value being set for the manufacturing raster angle.[22,23] In more detail, the mechanical performance of 3D-printed polymers is seen to be higher when the loading is applied along directions that are parallel to the 3D-printed filaments. It has also been investigated that the building orientation with a higher proportion of extruded filaments along the loading direction shows a better strength performance of the part than those with more offset.[24] More specifically, Weake et al.[25] found that the tensile strength of an Acrylonitrile Butadiene Styrene (ABS) part could be up to 150% higher when the applied force is parallel to the material filaments (manufacturing angle equals 0°) than perpendicular (manufacturing angle equals 90°).

The anisotropy of 3D printing is usually related to manufacturing factors. The evident level of anisotropy has been reported to affect the overall mechanical response of the printed parts,[26] with this holding true under both static[27] and fatigue loading.[28–30] This is because, under the above circumstances, the overall mechanical response of additively manufactured polymers mainly depends on the axial mechanical strength of the extruded filaments.[20–23] In contrast, when the loading is applied along directions perpendicular to the 3D-printed filaments, the overall strength of the polymer under investigation markedly depends on the forces bonding together adjacent filaments/layers.[31] Since, by their nature, these bonding forces result in a lower mechanical performance than the corresponding mechanical performance characterising the extruded filaments themselves, overall 3D-printed materials are seen to be weaker when the loading is

applied along a direction perpendicular to the direction of the filaments.[21] Hence, it is seen from the above studies that the identification of the optimal manufacturing orientation for the 3D-printing process is worth necessary investigations.

1.2 Data-driven methodology

It has been seen in numerous experimental studies that both infill density and manufacturing angle can simultaneously influence the mechanical behaviour of 3D-printed objects. Although the individual effect of these parameters was analysed,[25,32] due to the complexity of the cross-correlations between them, the estimation of the mechanical strength can be highly inaccurate where both infill density and manufacturing angle vary. Considering the large variety of the possible combinations of aforementioned parameters, the evident level of non-linearity between these parameters and the mechanical behaviour[31] has become the main problem to be solved.

Conventionally, the determination of the mechanical behaviour of a 3D-printed part relies on either numerous tests or empirical relations, which are, in any case, the outcome of comprehensive experimental investigations.[33] Such investigations are normally costly and time-consuming for the required level of precision.[34] Hence, it has become a priority to provide an alternative methodology requiring fewer experimental tests for formulating the relationship between the mechanical behaviour of a 3D-printed object and multiple manufacturing parameters.

In recent years, the international scientific community has made a considerable effort to formulate alternative approaches, such as data-driven methods. Data-driven techniques have shown their capability of overcoming the above difficulties by gaining knowledge, recognising and creating patterns among the data directly. So far, data-driven methodologies have shown great potential to obtain knowledge as they learn the correlation between input and output parameters based on the provided data. Instead of developing various physical equations, data-driven methodologies aim to create patterns that could be used to map the non-linearity among parameters based on existing data. Thus, data-driven methods learn from a group of existing raw data and can estimate the behaviour of required variables based on this previous learning process.

Typical data-driven methods, including artificial neural network (NN), fuzzy inference system (FIS), adaptive neural fuzzy inference system (ANFIS), design of experiments (DOE) and other techniques, are widely applied to study the mechanical behaviour of a 3D-printed object.[25,35] The complexity caused by the joint effect of multiple parameters is seen to be effectively solved by the application of non-linear regression solutions included in the aforementioned techniques.[36] In

the following sections, the common data-driven techniques to be adopted in the present work will be briefly introduced in order to compare both the estimation accuracy and efficiency of all adopted methods.

1.2.1 Fuzzy inference system

One of the data-driven approaches is known as fuzzy inference system (FIS), which is based on the theory of fuzzy sets. Fuzzy inference system is a methodology that formulates the non-linear mapping from a given input to an output based on the theory of fuzzy logic.[37] The inference of the method is similar to the human reasoning process, which helps make decisions based on the known fuzzy rules from the historical data.[38] Details of the FIS methodology will be introduced in Chapter 2, whereas the background of the FIS application is mainly introduced here.

FIS methodology has been reported to be used for the prediction of the wear rate in selective inhibition sintered high-density polyethene (HDPE) parts based on processing parameters, including layer thickness, heat energy, heater feed rate and printer feed rate.[39] Note here that selective inhibition sintering (SIS) is another type of additive manufacturing technique. A 3-level & 3-parameter FIS has also been developed by Esakki et al.[35] for the prediction of mechanical strength. Hence, it is seen that the FIS methodology could be a useful tool for the property prediction of 3D-printed parts.

For the strength estimation with a fuzzy-based system, innovative studies have been carried out using a fuzzy-based methodology for the estimation of the strength properties of functional materials.[40] The fuzzy rule setup strategy with the deterministic values in the present work is inspired by the previous study of Gitman et al.[41] where the fuzzy relation is set up according to the adjacent values of the data. Successful predictions of strength and hardness have been observed by the FIS model in Gitman et al.[41], indicating that the fuzzy system could be a useful modelling tool in strength estimation problems.

In what follows, the FIS framework will be used to perform the failure strength assessment of 3D-printed plain and notched components of PLA. *It is the first time that the prediction will not only include the process parameters in the current study but also involve the geometrical design parameters as an additional criterion*. After the strength prediction, an attempt will be made to use the FIS framework to identify the *optimal manufacturing parameters*, which is the inverse estimation of the aforementioned framework.

1.2.2 Artificial neural network

Other data-driven methodologies, which are usually compared with FIS, include artificial neural network (NN) and adaptive neural fuzzy inference system (ANFIS). The NN model simulates the signal-transmitting pattern between biological neurons in human brains.[42] The network is recursively updated in order to achieve the desired estimation accuracy. Due to the current enormous databases and computational resources, artificial neural network is under continuous development.[43] Details of NN will be illustrated in the latter chapters, with the current research progress of NN introduced in this section.

NN has been widely applied to various fields such as vocal recognition,[44] self-governing driving,[45] machine vision,[46] etc. It has been used to estimate the stiffness and toughness of composites where NN was found to be 250 times faster than the finite element analysis (FEA).[47] Liang et al.[48] have also demonstrated that NN could be a fast and accurate surrogate of FEA for stress analysis. For the particular application in the 3D-printing field, NN has also played a significant role in process monitoring and designing.

Everton et al.[49] have successfully applied NN in process monitoring during the printing process, aiming for quality supervision and control. Shevchik et al.[50] have also investigated quality monitoring during the printing process by combining the acoustic emission sensor with the NN. Williams et al.[51] reported that the convolutional neural network (CNN) was more accurate than the linear regression model when being used to estimate quantitative manufacturing metrics directly from voxel-based component geometries. Khadilkar et al.[52] introduced an NN-based framework which was applied to predict the stress distribution on the curved layer of the stereolithography (SLA)-based printed part in real-time.

Apart from the process monitoring and designing, it is necessary to point out that the NN has also been useful for the correlation between process parameters and printed parts' characteristics. It is reported that NN has been used to predict compressive strength and sliding wear of FDM printed parts with layer thickness, positioning, raster angle and width, and air gap.[53,54] Vahabli et al.[55] have managed to estimate the surface roughness distribution of FDM printed parts with the NN approach with particularly optimised process parameters such as time, cost and quality. Mohamed et al.[56] successfully predict the dynamic modulus of elasticity of 3D-printed parts with multiple common process parameters with better accuracy than the fractional factorial model.

In what follows, NN will be used to formulate the prediction of the failure strength of the 3D-printed parts based on *not only the process parameters but also notch-relevant parameters*, i.e., geometrical design characteristics. Furthermore, NN will also be applied to identify the *optimal*

combination of the process parameters with the particular requirement of geometrical design and strength.

1.2.3 Adaptive neural fuzzy inference system

With the above two methodologies proposed, an integrated methodology has been developed to combine FIS and NN methods, known in the field as the adaptive neural fuzzy inference system (ANFIS). The adaptive system inherits the idea of human reasoning and fuzzy rules from FIS but optimises the fuzzy rules with NN methods. Hence, with a particular emphasis on the accuracy of the fuzzy model in the adaptive system, ANFIS has been widely applied as a data-driven solution to various real-world problems, such as medical diagnosis,[57] mobile learning,[58] flammability parameter prediction,[59] etc.

The ANFIS methodology has also been used in 3D-printing areas. Raju et al.[60] have successfully used the ANFIS model to predict the printing time, part thickness and surface roughness based on the infill density and printing speed. It is also reported that the surface roughness of the FDM PLA parts could be estimated using ANFIS based on the given building orientation, layer thickness and impact angle.[61] Sedigh et al.[62] applied ANFIS to estimate the scaffold line width for 3-dimensional bioprinting with provided inputs (gelatin concentration, bioink temperature, pressure and printing speed).

Particularly for the strength prediction of 3D-printed parts, Yadav et al.[63] have investigated the prediction of tensile strength of materials like PETG, ABS and multi-material (60% ABS + 40% PETG) based on the given layer height and extrusion temperature. It is also reported that the flexural stress of the 3D-printed carbon fibre-based composites can be estimated with a high accuracy using ANFIS methodology as compensation for experimental work assessments.[64]

There has yet to be a study using both process and design parameters to estimate the mechanical strength of FDM parts with ANFIS. Hence, in what follows, *ANFIS will be applied to estimate the failure tensile strength of FDM parts based on the infill density, manufacturing angle and notch root radius*. This strength-orientated estimation framework is referred to as direct estimation. An extensive study will also include using ANFIS methodology to identify the *optimal combination of manufacturing parameters based on required strength performance*, referred to as the inverse estimation.

1.2.4 Design of experiments

Conventionally, experiments are conducted by holding certain factors constant and varying the value of another variable. Such the "one factor at a time" (OFAT) approach could be inefficient when each of the multiple factors has various levels, compared with varying factor levels simultaneously in DOE.

Design of experiments is a statistical approach widely used in experiments planning, parameters analysis, etc. It has been used for analysing and interpreting data obtained from experiments.[65] DOE is an effective systematic procedure carried out under controlled conditions to study the complex relationship between the multiple input and output parameters, with the particular capability of identifying the significance of each input parameter. Being itself an effective tool in decision-making process, DOE has played a significant role in not only engineering areas, but also in pharmaceutical,[66] food industry,[67] architecture and energy.[68,69]

Although DOE has been applied in various areas, there are very few comparative studies regarding the estimation performance of DOE and other data-driven methods. In the research of Aengchuan and Phruksaphanrat,[70] DOE was shown to be less accurate than FIS, but with the capability to identify the main factors and their interactions. Although reportedly less accurate, DOE method benefits from the high accessibility, as it is currently built into MS excel toolbox. Utilising the ease of use and ease of accessibility, the DOE is adopted here as a contrast method in later sections for comparing all the adopted data-driven methods.

To help the readers' understanding, a simple example is included here for illustration. Suppose there are three input parameters (x_1, x_2 & x_3) relevant to the output parameter (y) of the problem, and each of the input parameters has three levels of value (Level 1, 2 & 3). According to the OFAT approach, there are supposed to be $3^3 = 27$ tests to include all possible combinations. However, according to the Taguchi arrays for the DOE,[71] only nine tests are needed for the problem, and the test setup is as shown in Table 1.1.

Following the Taguchi design, a statistical model is proposed here to represent the relationship between the input and output parameters in Equation (1):

$$y = b + m_1x_1 + m_2x_2 + m_3x_3 + m_4x_1x_2 + m_5x_1x_3 + m_6x_2x_3 + m_7x_1x_2x_3\,, \qquad (1)$$

where b (to be determined) is the average y-value when all x equal to zero;[72] m_1 to m_7 are coefficients to be determined by the regression. In the present investigation, the built-in data analysis tool of MS Excel is adopted for the regression calculations of the coefficients. Note that

with a user-defined confidence level of 95%, the generated analysis of variance (ANOVA) table directly shows the value of each coefficient. Finally, following the determination of the coefficients, extra data is required to validate the accuracy of the calculated regression model.

Note here that the above test setup in Table 1.1 is only for model setup, similar to the data for setting up the fuzzy rules in FIS and the training data group in NN and ANFIS (to be introduced in following sections). Hence, in the following sections, the historical data for coefficient calculations with DOE method will be referred to as "training data" for clarification.

Table 1.1 The Taguchi array for a 3-parameter and 3-level problem.[71]

Tests No.	x_1	x_2	x_3	y
1	1	1	1	y_1
2	1	2	2	y_2
3	1	3	3	y_3
4	2	1	2	y_4
5	2	2	3	y_5
6	2	3	1	y_6
7	3	1	3	y_7
8	3	2	1	y_8
9	3	3	2	y_9

1.3 Summary of existing work

After introducing the main methods adopted in this research, it is author's pleasure to introduce the existing work done by Luca Susmel and Adnan A. Ahmed,[73] which the current investigation is based on. Experimental specimens and relevant data are adopted from their past work. Specimens used in the present investigation, were manufactured with the FDM 3D-printing technique. Being in itself not the main part of the present investigation, some important terminology and necessary variables during the manufacturing process used in what follows will be introduced here.

1.3.1 Specimen geometry design

In the present investigation, two different geometries will be analysed in the investigation: plain and notched (U-shape) components (see Figure 1.1A and Figure 1.1B for illustration). The particular choice of 3D-printed specimens' geometries was dictated by:

- extensive testing of the various data-driven methodologies on relatively simple geometry where the parameters of interest are *only* manufacturing process parameters (plain specimens in Figure 1.1A);
- the desire to expand and test data-driven methodologies on mixed types of input parameters, i.e., manufacturing *and* geometrical/design parameters (U-notched specimens in Figure 1.1B). The latter, potentially, will pave the way to a class of design-related problems, which is particularly important in industrial applications.

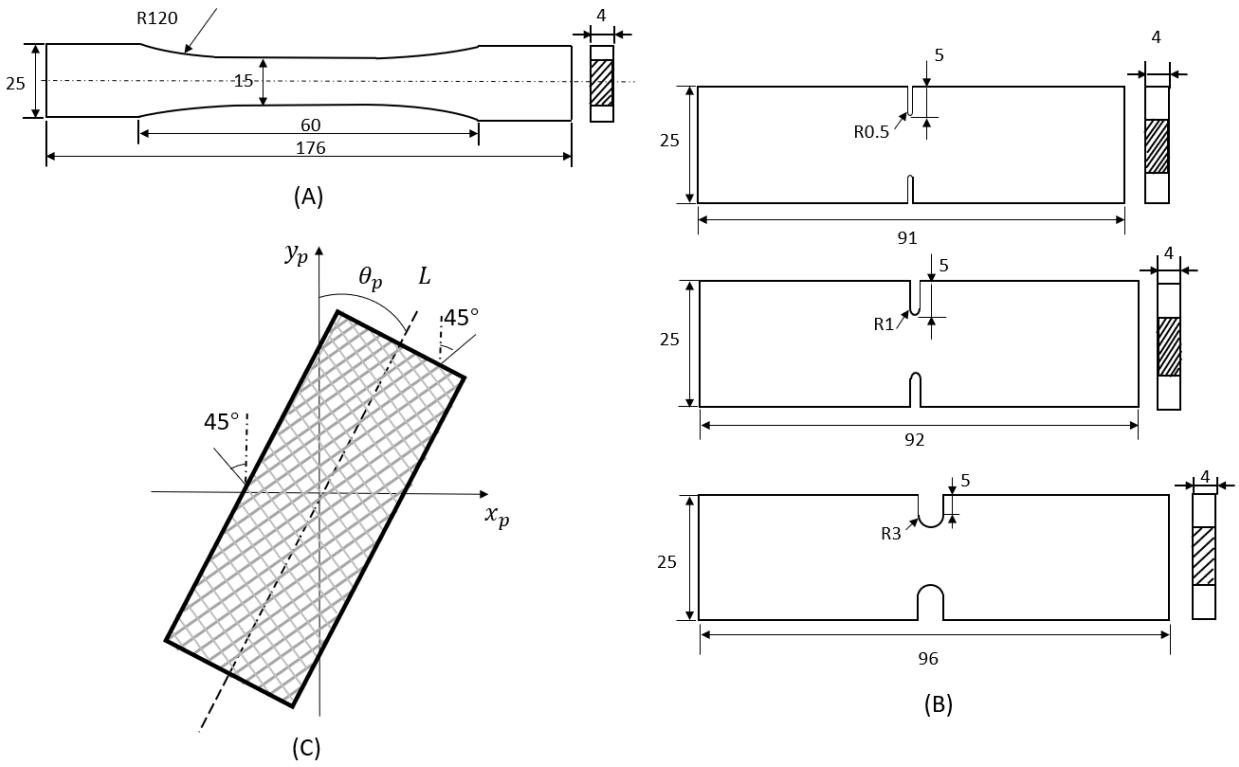

Figure 1.1 A) Geometrical design of the plain specimen; B) Geometrical design of the U-shape notched specimens with various notch root radius; C) Manufacturing angle θ_p is between the longitudinal axis L and the main printing direction y_p.

1.3.2 Parameters of interest

Following the introduction of process parameters, infill density and manufacturing angle were the main processing parameters chosen to support the estimation of the mechanical property. The infill density quantifies the percentage of volume infilled with filaments, and it is normally larger than 0% and could be up to 100%. The unfilled space forms manufacturing voids, which could allow a considerable reduction of material consumption and object weight with tolerable sacrifice in general structural strength. In order to study the impact of infill density on failure tensile strength, nine levels of infill density were fabricated and used in this study[73] (10% to 90% with a 10% interval) for the plain specimens, whereas three levels of infill density (30%, 50% & 70%) were fabricated[73] for the U-notched specimens.

The manufacturing angle, denoted here as θ_p, is defined as the angle between the printing direction y_p (see Figure 1.1C) and the longitudinal axis L of the specimen. Note that it is different from the raster angle, which is the angle between the path of the nozzle and the x-axis of the printing platform.[74] In this study, the 3D printer used for manufacturing specimens always has a $\pm 45^{\circ}$ angle between the nozzle path and the x-axis. Therefore changes in θ_p can effectively vary the raster angle with respect to the axial loading direction.[73] The specimens shown in Figure 1.1 were all manufactured flat on the build-plate where the manufacturing angle θ_p was set to be 0°, 30° and 45°, respectively.

For the U-notched specimens, each part had a U-shape notch on each longitudinal side. The notch root radius was taken as a geometrical design factor, which was equal to 0.5mm, 1mm and 3mm for various specimens. In further analysis, it could also pave the way to the study of the fracture behaviour of FDM parts.

1.3.3 Manufacturing and testing process

Both plain and notched specimens were manufactured using 3D-printer Ultimaker 2+ Extended[75] with PLA filaments having a diameter equal to 2.85 mm. The manufacturing parameters of the FDM parts were set as shown in Table 1.2, and all specimens were tested with a Shimadzu universal axial machine where the displacement rate was equal to 2mm/min.[73] Both plain and U-notched specimens were tested up to complete breakage.

As introduced in the previous section, process parameters can significantly impact various mechanical properties of a 3D-printed part. Being one of the important mechanical parameters of interest, tensile strength (TS) describes the ability of the printed component to resist fracture due

to tension.

Hence, the failure tensile strength was evaluated in the present investigation. Apart from the importance of this parameter, the other reason for the tensile strength being evaluated was the adopted here experimental work of Luca Susmel and Adnan A. Ahmed.[73] The only mechanical-behaviour parameter available in the original work was the failure tensile strength. Last but not least, considering the intrinsic versatility of data-driven methodologies, other mechanical properties or even those material properties (surface finish, toughness, etc.) should work as successful as the TS if the application of methodologies and the proposed framework are proven to be applicable.

Table 1.2 Predetermined manufacturing parameters for 3D-printing process.[73]

Manufacturing parameters	Values
Layer height	0.1mm
Shell thickness	0.4mm
Build-plate temperature	60℃
Printing speed	30mm/s
Nozzle size	0.4mm
Nozzle temperature	240℃

The experimental results for the plain and U-notched specimens are shown in Table 1.3 and

Table 1.4, respectively. Considering both plain and U-notched specimens, there are three manufacturing/design parameters related to the failure tensile strength. Hence, the total number of configurations should be $3^3 = 27$, which can cover all possible configurations. Note that in the original study, three samples were manufactured and tested for any geometry/manufacturing configuration being investigated. Hence, there were $27 \times 3 = 81$ specimens tested in total for the original experimental data, which are shown in Table 1.3 and

Table 1.4. Given the fact that data-driven methods need sole values for each parameter in the process of calculation, the three tested failure strengths for each configuration were averaged to a single value. Hence, the data to be used in later sections will only include 27 specimens/configurations. It is worth mentioning that the above averaging process (81 specimens to 27 specimens) could have negatively influenced the final estimation result due to the uncertainty caused by numerical errors. Therefore, the actual performance of the framework and

methodologies could potentially be better than presented in later chapters. Note in following tables, the d_v refers to effective size of manufacturing voids and Radius refers to the notch root radius, both of which will be introduced in detail in later chapters.

Table 1.3 Summary of 81 experimental results for plain specimens.[73]

Specimen	θ_p (°)	Infill density (%)	d_v (mm)	σ_f (MPa)
1-1	0	10	10.7	7.8
1-2				8.7
1-3				8.7
2-1	0	20	4.98	9.4
2-2				9.1
2-3				9
3-1	0	30	1.36	9.9
3-2				10.7
3-3				10.6
4-1	0	40	0.88	12
4-2				11.8
4-3				12
5-1	0	50	0.62	13.7
5-2				13.9
5-3				13.3
6-1	0	60	0.45	15.9
6-2				16.6
6-3				16.7
7-1	0	70	0.33	19.6
7-2				20.4
7-3				19.5
8-1	0	80	0.24	22.3
8-2				22.9
8-3				22.4
9-1	0	90	0.14	26
9-2				26.2
9-3				25.2
10-1	30	10	10.72	8.7
10-2				8.8
10-3				8.7
11-1	30	20	5.06	7.9
11-2				7.9
11-3				7.9
12-1	30	30	1.39	9.8
12-2				9.9
12-3				9.8
13-1	30	40	0.96	10.1
13-2				10.1
13-3				10.2

Table 1.3 (Continued)

Specimen	θ_p (°)	Infill density (%)	d_v (mm)	σ_f (MPa)
14-1	30	50	0.66	14.3
14-2				14
14-3				13.6
15-1	30	60	0.41	16.2
15-2				16
15-3				15.5
16-1	30	70	0.29	18.5
16-2				18.4
16-3				18.5
17-1	30	80	0.25	18.7
17-2				19.6
17-3				19.7
18-1	30	90	0.11	23.6
18-2				23.6
18-3				23
19-1	45	10	10.65	9.1
19-2				7.6
19-3				8.1
20-1	45	20	5.12	10.7
20-2				8.9
20-3				8.9
21-1	45	30	1.37	11.1
21-2				10.6
21-3				10.7
22-1	45	40	0.93	12.7
22-2				12.4
22-3				12
23-1	45	50	0.65	14.6
23-2				14.3
23-3				13.4
24-1	45	60	0.43	16.6
24-2				15.8
24-3				15.2
25-1	45	70	0.31	19.1
25-2				17.8
25-3				17.5
26-1	45	80	0.22	20.8
26-2				20.5
26-3				20.3
27-1	45	90	0.13	23.8
27-2				22.4
27-3				22.2

Table 1.4 Summary of 81 experimental results for U-notched specimens.

Specimen	θ_p (°)	Infill density(%)	Radius (mm)	σ_f (MPa)
1-1	0	30	0.5	11.58
1-2				8.48
1-3				9.06
2-1	0	30	1	8.17
2-2				8.81
2-3				11.63
3-1	0	30	3	11.63
3-2				11.48
3-3				9.51
4-1	0	50	0.5	12.64
4-2				12.7
4-3				13.86
5-1	0	50	1	13.25
5-2				13.66
5-3				14.35
6-1	0	50	3	14.17
6-2				13.83
6-3				15.37
7-1	0	70	0.5	19.17
7-2				16.33
7-3				16.61
8-1	0	70	1	16.81
8-2				15.06
8-3				18.89
9-1	0	70	3	19.55
9-2				16.85
9-3				19.39
10-1	30	30	0.5	9.15
10-2				7.83
10-3				7.58
11-1	30	30	1	8.23
11-2				8.79
11-3				8.33
12-1	30	30	3	10.03
12-2				10.22
12-3				9.85
13-1	30	50	0.5	12.74
13-2				11.22
13-3				10.43

Table 1.5 (Continued)

Specimen	θ_p (°)	Infill density(%)	Radius (mm)	σ_f (MPa)
14-1	30	50	1	12.02
14-2				11.62
14-3				12.31
15-1	30	50	3	12.9
15-2				12.47
15-3				12.27
16-1	30	70	0.5	14.52
16-2				11.77
16-3				10.26
17-1	30	70	1	12.23
17-2				11.7
17-3				11.81
18-1	30	70	3	13.78
18-2				14.2
18-3				13.78
19-1	45	30	0.5	7.3
19-2				7.26
19-3				9.52
20-1	45	30	1	8.76
20-2				8.33
20-3				7.22
21-1	45	30	3	10.09
21-2				9.78
21-3				9.65
22-1	45	50	0.5	13.15
22-2				10.05
22-3				9.81
23-1	45	50	1	10.39
23-2				11.5
23-3				13.81
24-1	45	50	3	13.96
24-2				13.57
24-3				12.84
25-1	45	70	0.5	14.65
25-2				13.75
25-3				16.72
26-1	45	70	1	15.66
26-2				16.08
26-3				13.79
27-1	45	70	3	16.12
27-2				17.11
27-3				15.87

1.4 Main aim and objectives of the thesis

The main aim of the present work is to evaluate the performance of data-driven methodologies used for estimating the mechanical behaviour of 3D-printed components based on given manufacturing parameters of the printing process and geometrical design characteristics of components, as well as the inverse: the identification of the optimal process parameters ensuring the desired mechanical characteristics of 3D-printed components. To achieve this aim, the objectives of this thesis are:

- To develop a framework that could be used for the direct estimation of mechanical property with provided manufacturing and geometrical parameters.
- To develop a framework that could be used for inverse estimation of optimal manufacturing parameters with given requirements of mechanical response and geometrical design.
- To compare all the adopted data-driven methodologies with respect to their estimation accuracy and efficiency.

The first objective will be applying the data-driven methodology to property prediction in the FDM 3D printing area. Then the second objective will be conducted with each methodology to achieve the optimal combination of manufacturing parameters. At this stage, in order to find out the full capability of the adopted method, various types of parameters will be included, such as manufacturing relevant, geometrical design relevant and cost-control relevant. Finally, following a comparative analysis, the best methodology regarding the estimation performance can be concluded . The present study is aimed to fill the lack of knowledge in evaluating the performance of FIS, NN and ANFIS methodologies being applied in FDM with geometrical and cost-relevant parameters included. Apart from the direct estimation framework, the development of inverse framework could potentially become an effective decision-making tool in modern industries.

1.5 Outline of the thesis

Chapter 2 will include the main aspects of the fuzzy inference system and the performance evaluation of the FIS methodology. Both direct and inverse estimation frameworks will be introduced here in detail. Chapter 3 will introduce the neural network, followed by the analysis of the NN methodology with respect to accuracy and efficiency. Chapter 4 will present the adaptive

neural fuzzy inference system with a particular analysis of its estimation performance. Then in Chapter 5, a comparative study will be illustrated with a contrast approach – design of experiments, for the analysis of all the adopted methodologies. Finally, Chapter 6 will list the goals achieved and the corresponding conclusions in the present investigation, and potential future work will also be illustrated.

Chapter 2

Fuzzy Inference System

Starting from this chapter[2], the topic will return to the aforementioned data-driven techniques. The main focus of the current chapter is the introduction and analysis of a data-driven approach, named fuzzy inference system, allowing the estimation of the strength performance of 3D-printed objects. In this section, the main aspects of fuzzy inference system methodology will be discussed in detail with a simplified illustrative example, with attention given to all necessary stages of building up FIS models.

A fuzzy inference system (FIS) is based on the theory of fuzzy sets, which was first proposed by Zadeh.[76] It can be used to model complicated systems with simple logic rules, similar to the human reasoning process. The term *fuzzy* refers to the indeterministic relationships between the input and the output of a FIS. In the first part of this study, the *input* relates to manufacturing and geometrical parameters, and the *output* refers to the object's strength performance. Such a pattern (from manufacturing parameters to mechanical property) is referred to as the direct estimation framework, previously mentioned in Chapter 1.

The main steps of FIS consist of (i) formulating aforementioned indeterministic relationships, in the form of fuzzy rules, between *known* input and output parameters (historical data) where the

[2] This chapter is partly adopted from:

Tu R, Gitman I, Susmel L. Fuzzy inference system for failure strength estimation of plain and notched 3D-printed polylactide components. *Fatigue Fract Eng Mater Struct*. 2022;45: 1663–1677.

Tu R, Gitman I, Susmel L. Fuzzy sets based methodology for manufacturing parameter determination of 3D-printed PLA components: optimisation of strength, design and cost requirements. (under review)

process can be considered as the *training* of a FIS; and (ii) using this trained FIS to provide an estimation of an *unknown* output (strength performance) for the case of new inputs (manufacturing and geometrical parameters).

Although there are alternative data-driven methodologies that can be used for estimation, such as artificial neural network (discussed later),[77] the FIS is still popular due to its structural simplicity. As shown in Figure 2.1, a FIS is composed of 4 sections which are *fuzzification, fuzzy rule base, fuzzy inference engine,* and *defuzzification*. With the assistance of fuzzy rules, mapping can be performed between input and output variables, which aligns with human thoughts. The detailed setup of all four FIS components is illustrated in section 2.1 using, as an example, parameters of 3D printing.

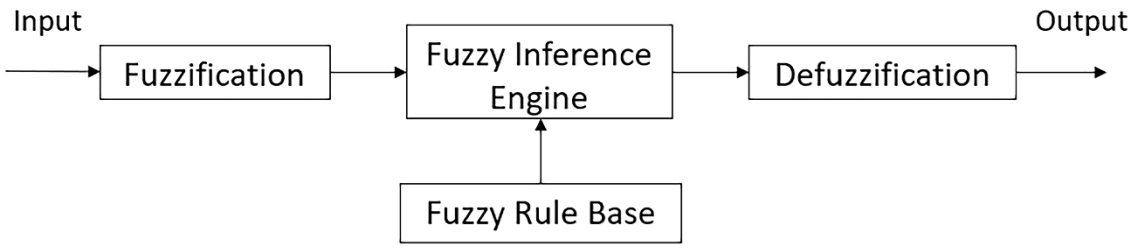

Figure 2.1 Illustration of a fuzzy inference system.[36]

2.1 Structure of a Mamdani fuzzy inference system

2.1.1 Fuzzification

First of all, the inputs of a FIS have to be fuzzified before being fed into the system. In fuzzification, each input data is mapped according to its degree of membership, ranging from zero to one, and all these membership values together are defined as fuzzy sets. The membership value represents how much the data belongs partially to each subset of a universal set.[78] Numerically, this mapping of each membership value is characterised by membership functions (MF), whose types and parameters are defined by users.

There are several existing MFs such as triangular MF, Gaussian MF, Trapezoidal MF, etc. Zhao and Bose[79] showed that the triangular MF, consisting of simple straight line segments, had the best performance in fuzzy control, compared with the Gaussian and trapezoidal MF. In the study of Harliana and Rahim,[80] triangular MF has proven to be as good as the trapezoidal and Gaussian MF, but easier for taking parameter values due to its simple structure. Adil and Ali also proved that the triangular MF showed a better performance compared with other MFs in Antenna Azimuth Position control system.[81] Hence, the triangular MF is adopted in the present

investigation.

Being particularly known for its simplicity, the triangular MF can be expressed mathematically as Equation (*2*).[82] Users can define the MF by changing parameters (a, b and c in Equation (*2*)), or graphically in Figure 2.2. In Figure 2.2, line segments aAc represent the MF of x ranging from a to c, where the lower limit (a) and the upper limit (c) both locate the "feet" of the triangle. The MF will reach the peak and be equal to 1 when x is equal to b ($a< b< c$).

$$\mu(x) = \begin{cases} 0, & x \leq a \\ \dfrac{x-a}{b-a}, & a < x \leq b \\ \dfrac{c-x}{c-b}, & b < x < c \\ 0, & x \geq c \end{cases} \tag{2}$$

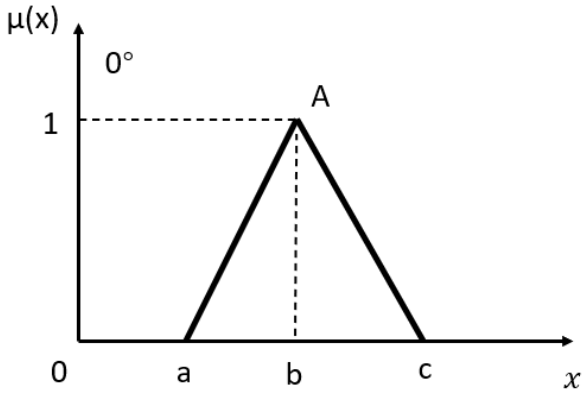

Figure 2.2 Illustration of triangular membership function where x is the input of MF and μ is membership value.[36]

To illustrate fuzzification, two 3D-printed parts with 10% and 90% infill densities separately are synthesised and considered. Here the infill density is treated as an input variable which will be fuzzified. Assuming the lowest and the highest possible infill densities (known from performed experiments) are 0% and 100%, both 10% and 90% are *high* infill densities to *some* extent. The term *high* here refers to the maximum known infill density of 100%. In this case, 90% infill density is significantly *higher* than 10%, i.e., it (90%) *belongs* to the category *high* significantly more than 10% infill density *belongs* to the same category.

Mathematically, the above phrase can be interpreted using membership values. Following the second row of Equation (*2*), membership values of 10% and 90% infill density can be calculated. The results of this simple calculation are presented in Figure 2.3A, showing μ (MF value) for 10% is 0.1 and μ for 90% is 0.9. Note that, for the simplicity of illustration, a is set to be zero and b is equal to 100% infill density in this example for the case of Figure 2.2. Note also that, in general, triangular MF has a triangular shape, but here only the left half of the triangle is considered (Figure 2.3A). This is due to the *high* membership value being defined as 1 when the infill density reaches 100% (i.e., the maximum infill density has the highest potential membership degree). Therefore, there is no need to show the other half of the function, which lies out of the range of interest (0-100% infill density).

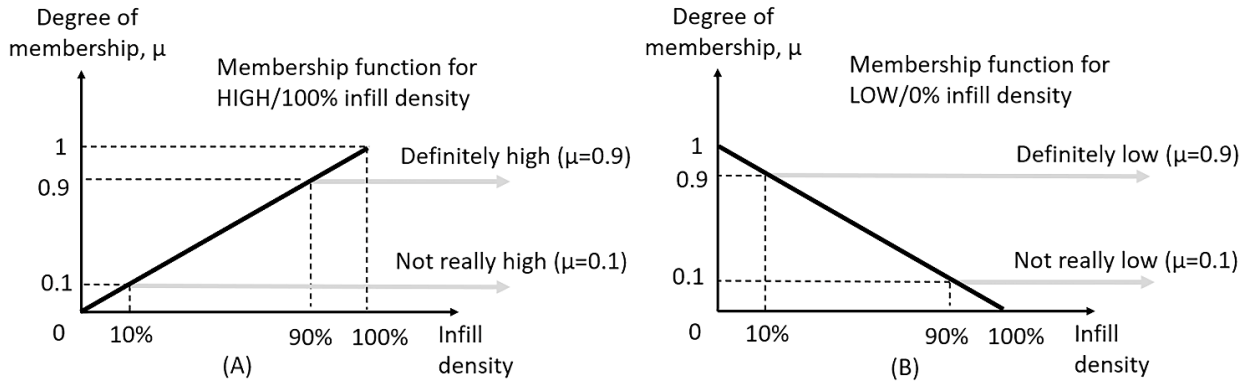

Figure 2.3 Degree of membership vs infill density with triangular membership function for (A) high infill density and (B) low infill density.[36]

Similarly, MFs can be formulated to describe how *low* the infill density is. The term *low* refers to the minimum known infill density, in our example, 0%. Considering again 10% and 90% infill densities in our 3D-printed parts, we can conclude that the former is considerably *lower* (and its new degree of membership, following the third row of Equation (*2*), is $\mu = 0.9$) than the latter (with the new degree of membership $\mu = 0.1$), see Figure 2.3B. Note that here only the right half of the triangle is considered because the highest potential membership value one can be achieved at the minimum (*lowest*) infill density 0%, and the membership value for 100% infill density is zero.

2.1.2 Fuzzy rule base

The fuzzy rule base contains all IF-THEN statements that build connections between inputs and outputs. With existing information or data, the mapping between input and output can be described as inference by these rules. A single rule consists of one or more antecedents and

consequents. For example, a fuzzy rule can be a sentence like "if the infill density is *high* (antecedent A) and the manufacturing angle is *large* (antecedent B), the failure strength is *large* (consequent)". If the corresponding experimental data, including both manufacturing parameters and failure strength, is already known as deterministic values, the fuzzy rule can also use values directly, for example: "if the infill density is 10% (antecedent A) and the manufacturing angle is 0° (antecedent B), the failure strength of a 3D-printed part is 1 MPa (consequent)". This is an updated fuzzy rule that contains two antecedents and one consequent. If another 3D-printed part is known to have an infill density of 90%, a manufacturing angle of 40° and a failure strength of 10 MPa, a second fuzzy rule can be written as "if the infill density is 90% and the manufacturing angle is 40°, the failure strength is 10 MPa". The detailed parameters and values depend on existing historical data, and there are normally two or more rules in a fuzzy rule base.

2.1.3 Fuzzy inference engine

The input of a fuzzy inference engine is multiple membership values acquired from fuzzification, and the output is one fuzzy set which contains membership values for each output variable. The main body of a fuzzy inference engine contains multiple operations such as *fuzzy operator*, *implication*, and *aggregation*.

To illustrate the working principle of fuzzy inference engine, a similar example (as discussed in section 2.1.2) will be used. Let us assume that for the two 3D-printed parts, infill densities, manufacturing angles and failure strengths are known and formulated as rules 1 and 2 (see Table 2.1, top two rows); then, for a new third part, with the new infill density and the manufacturing angle 50% and 30° respectively, the failure strength is to be estimated using FIS (see Table 2.1, third row).

Table 2.1 Synthetic fuzzy rules as illustrative examples.

Specimen No.	Infill density (%)	Manufacturing angle (°)	Failure strength (MPa)
1 (fuzzy rule 1)	90	40	10
2 (fuzzy rule 2)	10	0	1
3 (new)	50	30	To be estimated

Fuzzy operator[3]**.** Following the fuzzification of input values, the degree of membership for each antecedent can be obtained. Generally, a single rule can have multiple input parameters (see Table 2.1, where the infill density and the manufacturing angle are present for each rule). In this step, a *fuzzy operator* is applied to combine information from the aforementioned multiple input parameters to a single value corresponding to a resulting consequence. The standard logical operator *AND* is used at this stage, resulting in a consequence being *true* only when all antecedents are true (i.e., when all input requirements are met).

Mathematically, the logical operator *AND* refers here to the *minimum (min)* operator, so the output of this operation is the smaller membership value. With the input of the FIS in this example being 50% infill density and 30° manufacturing angle, corresponding membership values can be calculated using the second row of Equation (*2*) as follows:

$$\mu(50\%) = \frac{50-10}{90-10} = 0.5\,, \qquad \mu(30^{\circ}) = \frac{30-0}{40-0} = 0.75\,, \tag{3}$$

where the smaller (*min*) membership value is 0.5 (see Figure 2.4, step 1 and 2, top row). Note that the infill density in Figure 2.4 ranges from 10% to 90%, not 0% to 100%, and that is due to the minimum and the maximum values for a MF here being taken directly from the known experimental data (see fuzzy rules in Table 2.1). The same comment holds for the manufacturing angle.

Implication. The outcome of a *fuzzy operator* is a single membership value, and the next step is applying the *implication* method to each fuzzy rule and reshaping the output MF using the obtained single membership value. One of the commonly used implication methods is truncation, which is again based on *AND* (*min*) operator (see Figure 2.4, step 3 at first row).

As introduced at the beginning of Section 2.1.2, the failure strength ranges from 1 to 10MPa, and the MF of failure strength is chosen to be triangular, similar to MFs of the infill density and the manufacturing angle.[4] As a supplementary illustration for readers, note that here the MF for the output variable is still a triangular MF, which is a main characteristic of the Mamdani fuzzy system.[83]

[3] This step and the step below (*implication*) need to be performed for each fuzzy rule (rows in Table 2.1); however, for clarity of presentation, an example rule (rule 1) will be presented here.

[4] Note that although MFs in our example are all triangular for the simplicity of demonstration, both input and output parameters can have different types of membership functions in general cases and are determined by users.

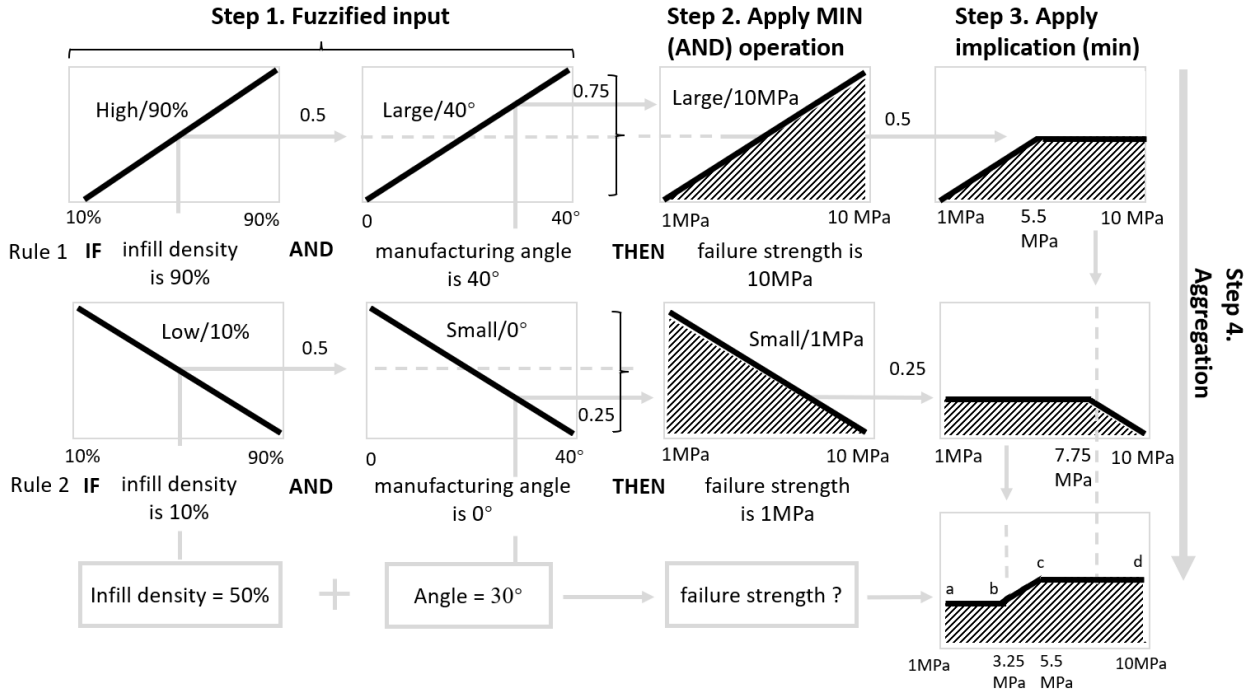

Figure 2.4 Decomposition of a fuzzy inference system.

Returning to the output variable in Figure 2.4, the term *large* for describing failure strength represents the maximum value which is 10MPa. Since 0.5 is the *min* membership value in fuzzy operator, the MF of failure strength is truncated by this single value (0.5), and with a simple step of bringing 0.5 back into Equation (2), the failure strength where the truncation starts can be calculated as $\frac{x-1}{10-1} = 0.5$, $x = 1 + 4.5 = 5.5$MPa. Note that the input of implication is the single membership value, and the output of implication is a fuzzy set (see Figure 2.4, shadow area from step 3 at first row) relevant to consequent. It can be represented mathematically as $\{\mu_1/x_1, \mu_2/x_2, \ldots, \mu_n/x_n\}$, here a set of pairs μ_i/x_i represents membership values μ_i of output parameters x_i (values of failure strength). For our example, the fuzzy set can be represented as $\{0/1, 0.5/5.5, 0.5/10\}$.

Aggregation. The final output of FIS is based on considering *all* rules together. In Figure 2.4, the first row represents fuzzy rule 1, and the second row represents fuzzy rule 2. The outcomes of each rule are *aggregated* so that the aggregation result is a single fuzzy set. One of the most common aggregation operations is *maximum* (*max*), which picks the maximum segments among all MFs and combines them (see Figure 2.4, step 4).

In our example, for rule 1, see Equation (*3*), $\mu(50\%) = 0.5$ and $\mu(30^{\circ}) = 0.75$, resulting in $\mu_1(50\% \,\&\, 30°) = \min_1(0.5,0.75) = 0.5$. For the second rule, where the MF describes the low infill density and small manufacturing angle, as explained at the end of section 2.1.1, the

membership values for both infill density and manufacturing angle are calculated using the third row of Equation (2) as follows:

$$\mu(50\%) = \frac{90-50}{90-10} = 0.5\,, \qquad \mu(30^{\circ}) = \frac{40-30}{40-0} = 0.25\,, \tag{4}$$

resulting in $\mu_2(50\% \,\&\, 30°) = min(0.5,0.25) = 0.25$.

Since the manufacturing angle has the smaller membership value in rule 2, the MF of failure strength for the second row is truncated at 0.25, where failure strength is calculated as $\frac{x-1}{10-1} = 1 - 0.25$, $x = 1 + 6.75 = 7.75$MPa. Then the *implication* result of the second row in Figure 2.4 can be represented as {0.25/1, 0.25/7.75, 0/10}.

The aggregation operation is essentially identifying the maximum membership value from both rules with various failure strength. Considering the implication result of both rules, the maximum membership value remains to be 0.25 from $x = 1$MPa to $x = 3.25$MPa ($\frac{x-1}{10-1} = 0.25$, $x = 1 + 2.25 = 3.25$). Then the membership value increases from 0.25 (3.25MPa) to 0.5 (5.5MPa) as previously calculated. Finally, from 5.5MPa to 10MPa, the membership value remains to be 0.5.

Thus, the inputs of the *aggregation* process are two fuzzy sets acquired from individual *implications* (top two graphs in the fourth column, Figure 2.4), and the output is a single *aggregated* fuzzy set (bottom graph in the fourth column, Figure 2.4). The output fuzzy set after aggregation operation can be represented mathematically as {0.25/1, 0.25/3.25, 0.5/5.5, 0.5/10}.

2.1.4 Defuzzification

Since the output of the fuzzy inference engine is still a fuzzy set (or a number of fuzzy sets if there is more than one output parameter) for a Mamdani fuzzy system, it is not a "meaningful" value yet. Considering that defuzzification is the inverse operation of fuzzification, similar to encoding and decoding, the fuzzy sets can be turned into a meaningful value after being defuzzified. There are different types of defuzzification techniques, such as the centre of gravity (COG), mean of maxima, bisector of area etc.[84] In this study, the centre-of-gravity technique is chosen since it is most commonly used in practical applications.[85] The defuzzified value x^* can then be expressed as Equation (*5*) if the fuzzy set is discrete or as Equation (*6*) if continuous:[41]

$$x^* = \frac{\sum_{i=1}^{n} \mu(x_i) x_i}{\sum_{i=1}^{n} \mu(x_i)}\,, \tag{5}$$

$$x^* = \frac{\int \mu(x) \cdot x\, dx}{\int \mu(x)\, dx}\,, \tag{6}$$

where $\mu(x_i)$ refers to the membership value of the element x_i (failure strengths), and n is the total number of elements in the sample. In order to calculate the failure strength x^* in our example (the most bottom right of Figure 2.4), three line equations from the image (ab, bc and cd) are calculated and listed in Table 2.2. Hence, the failure strength x^* can be calculated based on Equation (*6*) as shown in Equation (*7*). In conclusion, the result of the defuzzification step is 6.13MPa which is the estimated failure strength for the 3D-printed part with an infill density of 50% and a manufacturing angle of 30°.

Table 2.2 Summary of line equations

Line	Equation	Range
ab	$y = 0.25$	[1, 3.25]
bc	$y = \frac{x-1}{10-1}$	[3.25, 5.5]
cd	$y = 0.5$	[5.5, 10]

$$x^* = \frac{\int_1^{3.25} (0.25) x\, dx + \int_{3.25}^{5.5} \left(\frac{x-1}{10-1}\right) x\, dx + \int_{5.5}^{10} 0.5x\, dx}{\int_1^{3.25} (0.25)\, dx + \int_{3.25}^{5.5} \left(\frac{x-1}{10-1}\right)\, dx + \int_{5.5}^{10} 0.5\, dx} = 6.13 \tag{7}$$

2.2 Various types of fuzzy inference systems

After introducing the structure of fuzzy inference system, it is necessary to point out that there are two main types of fuzzy systems which are Mamdani and Sugeno systems. Mamdani fuzzy system was first proposed to imitate the performance of human operators in charge of controlling certain industrial processes.[86] The aim was to integrate the operators' experience into a set of IF-THEN rules so that the industrial process can be controlled automatically by a machine. The main

characteristic of a Mamdani fuzzy system is that the output of each rule is a fuzzy set, calculated from the output MFs. Each set is then aggregated into a single fuzzy set, which is then defuzzified into a crisp output value (as introduced in the previous section). This type of fuzzy system is well suited to industrial control system where human experts' experience are imperative.[87]

Different from that of Mamdani system, the output MF Sugeno fuzzy system[88] is either constant or a liner function of the input parameters. The defuzzification process of a Sugeno system is simply calculations of weighted average of previously calculated values, which is relatively more computationally efficient than calculating the centre of gravity for a 2D area in Mamdani system.[87] In this case, Sugeno FIS is more suitable for the current research than Mamdani FIS as the latter has a requirement of transforming crisp output values into membership functions before defuzzification, which could generate a further numerical error if the parameters of MFs are not set to optimal. Sugeno FIS is suitable for certain mathematical analysis as each rule is linearly dependent on the input variables. For example, the failure tensile strength of a 3D-printed part can vary depending on the infill density and the manufacturing angle.

The Mamdani system is presented in the first half of this chapter for the plain specimens to demonstrate how the basic fuzzy system works, including membership function calculations. It is demonstrated here also because it was the very first fuzzy system that the author adopted at the beginning of this study. Since the Sugeno FIS is more suitable for the present investigation, it will be applied later as a solution to evaluate the U-notched specimens which includes an additional geometrical parameter – notch root radius. The results from the Sugeno system (U-notched specimens) will be compared with the results from other methodologies regarding the accuracy and efficiency. The calculation of the Sugeno fuzzy system will be explained in detail with an illustrative example in later sections in order to keep the Mamdani section clear in order.

2.3 Experimental data and fuzzy inference system setup

After introducing the main steps of a fuzzy system, the topic in this section will return to the actual work conducted using FIS to estimate the failure tensile strength of the 3D-printed parts. Besides, the discussion will also include the analysis of the experimental data obtained from manufacturing and testing the 3D-printed specimens being considered in this study (see Chapter 1 for details). The construction and the performance of the FIS, following the methodology introduced in section 3.1, will then be evaluated using the data from the aforementioned experiments.

2.3.1 Manufacturing void size as an additional parameter

As mentioned in Chapter 1, infill density and manufacturing angle are parameters commonly chosen to assess the strength of 3D-printed components. Another parameter frequently associated with assessing strength is the size of manufacturing voids.[73] Note, however, that the manufacturing angle θ_p and infill density are independent variables that can be changed individually; contrary to that, the size of manufacturing voids (see Figure 2.5) depends on the infill density as void sizes will decrease if more internal space is infilled (higher infill density). Therefore, in order to demonstrate the performance of the FIS with multiple interconnected input parameters,[89] the effective size of manufacturing voids, d_v, is included in the research. In particular, parameter d_v was measured using an optical microscope[73] and the d_v reported in Table 2.3 is the calculated average value of measured void sizes with the same infill density. The analysis based on both infill density and d_v will show how an additional interconnected parameter can influence the performance of the FIS and which of the two parameters can lead to better accuracy.

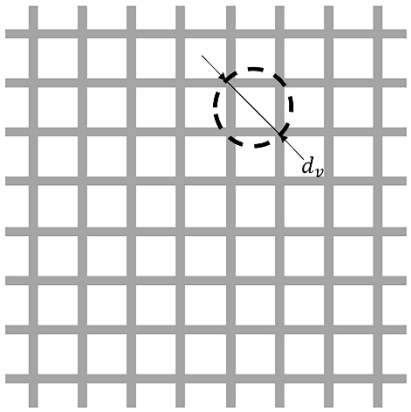

Figure 2.5 Manufacturing voids of a 3D-printed object: grey lines are printed filaments, and blank areas are the manufacturing voids.[36]

Table 2.3 Summary of experimental results for plain specimens.

	Input			Output
Specimen	θ_p (°)	Infill density (%)	d_v (mm)	σ_f (MPa)
1	0	10	10.7	8.6
2	0	20	4.98	9.2
3	0	30	1.36	10.4
4	0	40	0.88	11.9
5	0	50	0.62	13.6
6	0	60	0.45	16.4
7	0	70	0.33	19.8
8	0	80	0.24	22.5
9	0	90	0.14	25.8
10	30	10	10.72	8.7
11	30	20	5.06	7.9
12	30	30	1.39	9.8
13	30	40	0.96	10.1
14	30	50	0.66	14
15	30	60	0.41	15.9
16	30	70	0.29	18.5
17	30	80	0.25	19.4
18	30	90	0.11	23.4
19	45	10	10.65	8.3
20	45	20	5.12	9.6
21	45	30	1.37	10.8
22	45	40	0.93	12.4
23	45	50	0.65	14.1
24	45	60	0.43	15.8
25	45	70	0.31	18
26	45	80	0.22	20.5
27	45	90	0.13	22.8

2.3.2 Experimental results for the plain 3D-printed specimens

The experimental failure strength of plain specimens is calculated as the applied force upon breakage divided by the cross-sectional area of specimens. The calculation is based on the assumption that the mechanical strength of a 3D-printed part with infill density lower than 100% can be estimated via an equivalent material which is continuum, homogeneous, linear-elastic and isotropic.[73] The experimental data are summarised in Table 2.3 (adapted from Ahmed and Susmel[73]), where: θ_p (°)-manufacturing angle, infill density (%), d_v (mm)-the size of manufacturing voids and σ_f (MPa)-failure strength. According to the experimental investigation discussed in Ahmed and Susmel,[73] 27 combinations of input parameters were tested, with each

combination being based on three individual tests. For simplicity, in this chapter, an average value of the failure strength for these three tests is calculated and taken as the failure strength of the corresponding input parameter combination. Accordingly, 27 experimental results are presented in Table 2.3, each having a unique combination of manufacturing angle, infill density, manufacturing void size and failure strength. As introduced in section 1.3, 27 results are present as there are three input parameters, each of which has three levels. Hence, the total number of different configurations are $3^3 = 27$, which is sufficient for evaluating the performance of the methodology and framework.

2.3.3 Specimens for fuzzy rule base and validation

For examining the performance of the FIS in estimating failure strength properties, a number of results in Table 2.3 are used for building the necessary fuzzy rules, and the remaining samples are used later to validate the estimation accuracy of the FIS. Note that, to minimise the experimental errors, more than one sample was used for validation purposes.

In order to determine the specimens to be used for fuzzy rule base and validation, respectively, 27 specimens are divided into three sections (see dotted lines in Table 2.3): specimen 1-9, 10-18 & 19-27, respectively (9 specimens in each group). The groups are chosen so that, in each group, manufacturing angles are identical, and the infill density ranges from 10 to 90 in sequence. Every second, fourth, sixth and eighth specimens are chosen for validation in each group. For the representativeness of estimation results, the selected validation specimens are evenly distributed in each group. Note that this is not a unique way of choosing validation and FIS-building specimens, and it has been considered here for convenience reasons. All validation specimens are marked as grey rows in Table 2.3, and the rest of the specimens are used for building fuzzy rules of the FIS (see Figure 2.6). Thus, in our case, n – the total number of specimens is equal to 27; x – the number of specimens used for validation is 12; the number of specimens used for building fuzzy rules is $n - x = 15$.

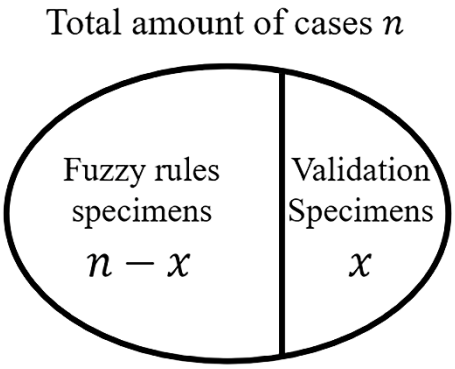

Figure 2.6 Classification of the validation and fuzzy rules specimens.[36]

2.3.4 Fuzzy inference system construction

As mentioned in section 2.1, one of the main stages in FIS construction is building a fuzzy rule base using historical data, and each rule can be presented in the form of "IF-THEN" statements. As discussed above, there are 27 data sets in total, where 15 of which are used for building the fuzzy rule base. The remaining 12 results are used to evaluate the estimation accuracy (as discussed in section 2.1.3).

To illustrate an example of MFs, Figure 2.7 presents the triangle MFs of one of the manufacturing parameters - manufacturing angle, θ_p. Rather than be in the adjective form of "Large, Medium & Small", MFs are named with their corresponding parameter values for simplicity of establishing rules.

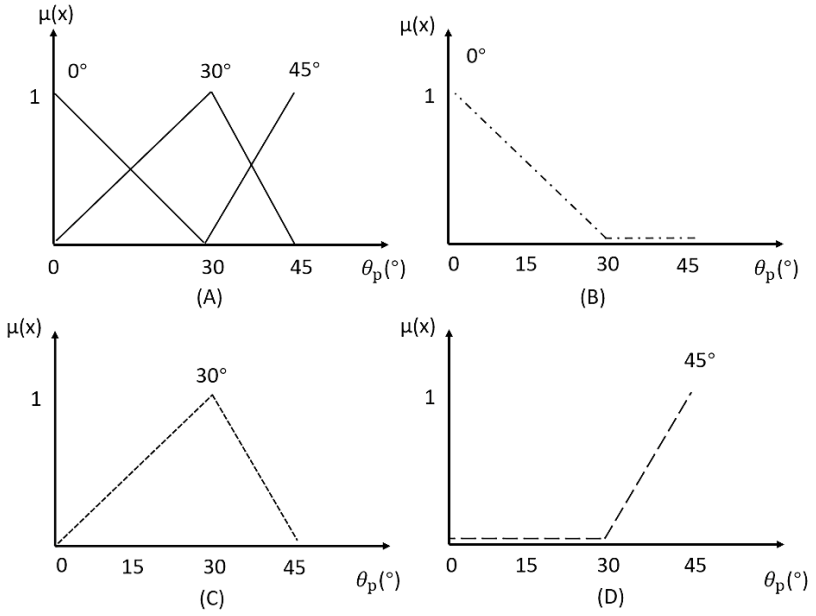

Figure 2.7 (A) Triangular membership functions for the manufacturing angle θ_p; (B), (C) & (D) Decomposition of membership functions for the manufacturing angle with respect to various membership terms.[36]

To clarify MFs presented in Figure 2.7A, Figure 2.7B-D show detailed MFs for all manufacturing angles separately: the MF of the manufacturing angle consists of three parts which are 0° (small), 30° (medium), 45° (large). For example, in Figure 2.7B, the manufacturing angle of 0° has the largest membership value of describing a "small manufacturing angle"; hence, $\mu(x) = 1$. However, with the increasing manufacturing angle, it can hardly be represented by the "small angle" category; hence, the membership value drops to 0 at 30°. Finally, three MFs (from Figure 2.7B-D) constitute the general MF of the parameter (Figure 2.7A). Note that similar logic is applied for the other parameters: infill density, d_v and σ_f.

It needs pointing out that the foot of the first triangular MF shares the same x value with the adjacent triangular MF. For example, the right foot of the triangle in Figure 2.7B locates at the bottom of the tip of the adjacent triangle in Figure 2.7C. The author adopted this strategy to develop a standard for selecting the parameter of each MF from the experimental data. Note also here although there is available fuzzy inference toolbox in MATLAB, the author did code the MF determination strategy and the whole estimation process by himself in MATLAB instead.

2.4 Estimation results of using fuzzy inference system

After the FIS is built, the input parameters of validation specimens are fed to the FIS, and the corresponding output is the *estimated* failure strength. The estimated results are then used to evaluate the accuracy of the FIS, represented by the error calculated as:

$$Error = \left| \frac{\sigma_e - \sigma_f}{\sigma_f} \right| \times 100\% , \tag{8}$$

where σ_f is the failure strength recorded in the experiment and σ_e is the estimated value obtained using the FIS. Errors for all validation specimens are then averaged, and this mean value is considered the estimation error of the FIS.

Table 2.4 Experimental and estimated results with the error between both results

	Input			Output	Estimation	
Spec	θ_p (°)	Infill density (%)	d_v (mm)	σ_f (MPa)	σ_e (MPa)	Error (%)
2	0	20	4.98	9.2	9.9	7.2
4	0	40	0.88	11.9	12.2	2.5
6	0	60	0.45	16.4	17.3	5.5
8	0	80	0.24	22.5	21.8	3.1
11	30	20	5.06	9.3	9.45	1.6
13	30	40	0.96	10.1	10.6	5
15	30	60	0.41	15.9	17.9	12.6
17	30	80	0.25	19.4	21.6	11.3
20	45	20	5.12	9.6	11.4	18.8
22	45	40	0.93	12.4	14	12.9
24	45	60	0.43	15.8	16.3	3.2
26	45	80	0.22	20.5	18.9	7.8
					Average error	**7.6**

The detailed experimental and estimation results, together with corresponding errors, are listed in Table 2.4, and the average error is calculated as 7.6%. As can be seen from Table 2.4, for the case of plain 3D-printed specimens, the FIS methodology can produce an accurate (with an average error of 7.6%) estimation result.

It is worth pointing out that despite the estimation accuracy of specimen 20 appears to be large enough as an "outlier", it is still acceptable in this case. Since the error calculation is based on the relative percentage, the estimation error of specimen 20 could be easily enlarged due to the significant fluctuation of experimental results (especially for the denominator). For example, on one hand, the absolute error between the estimation and experimental result for specimen 20 is $11.4 - 9.6 = 1.8$MPa. On the other hand, the absolute error for specimen 15 is $17.9 - 15.9 = 2$MPa, which is larger than that of specimen 20, and the estimation performance is seen to be better for specimen 20. However, contrary to this indication, the relative error of specimen 20 (18.8%) is much larger than that of specimen 15 (12.6%), which shows the estimation performance is seen to be better for specimen 15. Such contradiction is because the experimental σ_f is the denominator in the calculation of relative error, and specifically, the experimental σ_f of

specimen 20 is smaller than that of specimen 15. Thus, the estimation of specimen 20 is still accurate in general, and the absolute error will also be adopted for specific cases in following chapters in order to evaluate the methodology.

2.5 Analysis of estimation results

Following the estimation results of the 3D-printed plain specimens presented above, this section includes discussions of the effect of specimen numbers and the key manufacturing parameter on estimation accuracy.

2.5.1 The effect of the number of specimens on estimation accuracy

In order to analyse the effect of experiment quantity "n" on estimation accuracy, three groups of specimens are adapted from Table 2.3, where the composition of each group is also introduced. Group A has only $n = 9$ specimens, group B has $n = 18$, and group C has all $n = 27$ specimens. The FIS is then separately applied to Groups A, B & C to estimate failure strength. The contrast of the outcome for all three groups explains the effect of the number of specimens on estimation accuracy. The estimation error for group A, B and C are found to be:

A. 9 specimens (specimen 1-9): estimation error 10.3%;
B. 18 specimens (specimen 1-18): estimation error 8.6%;
C. 27 specimens (specimen 1-27): estimation error 7.6*%.

As such, it can be concluded that, first of all, with the given experimental data, the FIS can provide satisfying outcomes for estimating failure strength based on manufacturing angle and infill density with reasonable accuracy. Furthermore, the estimation accuracy improves with the growing number of specimens. However, it has to be said that, from an industrial design point of view, the increment in accuracy from using 9 calibration specimens to using 27 calibration specimens is very little. This suggests that estimates that are accurate from an engineering point of view can be obtained using a limited number of calibration values. In this context, further study can be focused on the minimum number of experiments required for user-defined estimation accuracy.

2.5.2 Key manufacturing parameter to the best estimation result

Next, an investigation of the *key* manufacturing parameters is performed. Following section 2.5.1, for the best estimation accuracy, group C (with all 27 specimens) has been analysed. The significance of each manufacturing parameter is addressed by evaluating the change of error, while excluding a respectful input variable one at a time.[90] It is important to recall here that the estimation error while considering all three parameters (manufacturing angle θ_p, infill density and manufacturing void size), is found to be 7.6%. Next, without changing θ_p, both infill density and d_v are excluded separately to study the importance of each parameter. The estimation error is found to be equal to 7.1% for considering θ_p & infill density and 8.2% for considering θ_p & d_v (see Table 2.5).

It shows the error is smaller than previously reported when excluding d_v, i.e. the estimation could be more accurate without considering the manufacturing void size as an input parameter of the FIS. On the contrary, the estimation error increases when excluding the infill density, i.e. a more accurate estimation result could be achieved when considering the infill density. As mentioned previously, d_v is a function of the infill density as it decreases while the infill density increases. So, it is recommended to consider only one of them as the input parameter of the FIS. Analysing the estimation errors, the infill density can be considered a slightly better choice.

Table 2.5 Estimation error (%) vs various input variable combinations

Parameters combination	θ_p, Infill density & dv	θ_p & Infill density	θ_p & d_v	θ_p	Infill density
Estimation error (%)	7.6	7.1	8.2	40.8	9.3

Next, the importance of the manufacturing angle and the infill density are compared. With only θ_p, the FIS gives an estimation error of 40.8%, and with only the infill density, the FIS has an error of 9.3%. As it can be seen, both errors increase considerably, indicating that having only one input parameter could lead to an unaccepted accuracy. Note also that excluding the infill density leads to a much larger estimation error (40.8%); thus, it can be concluded that it is very important to record the infill density for estimating failure strength.

Summarising the above outcomes, the manufacturing void size d_v leads to a slightly worse estimation accuracy when using the FIS, whereas both the manufacturing angle, θ_p, and the infill density lead to better estimation accuracy and, finally, the infill density has more significance on

the estimation result.

2.6 Fuzzy inference system for U-notched specimens

After analysing the effect of the number of specimens and the key parameters in the estimation process, this section we will take a further step in evaluating the performance of the FIS by considering two aspects:

(i) the ability of the FIS to estimate fracture strength as a function of manufacturing and *geometrical* parameters;

(ii) comparison of the FIS performance with the analytical method used in the literature.[73]

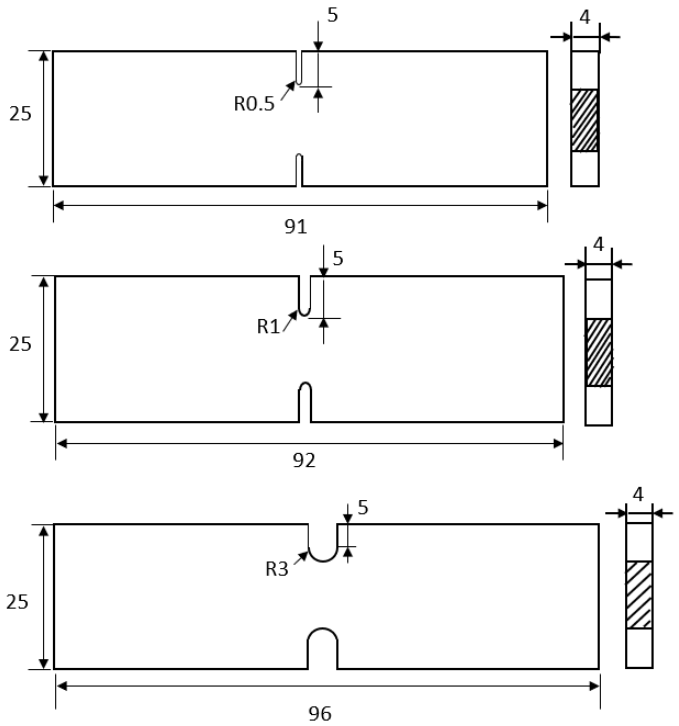

Figure 2.8 The U-notched specimens with symmetrical U-notch on both longitudinal sides where the notch root radius is equal to 0.5mm, 1mm and 3mm, respectively.

In order to address the first question, a new set of experimental data, namely data for U-notched specimens (Figure 2.8), are analysed. Experimental results used in this study (adapted from Ahmed and Susmel[73]) are presented in Table 2.6. A particular choice of the aforementioned data set is dictated by an introduction of a qualitatively new parameter: so far, the discussion has circled around the manufacturing input parameters (i.e., the manufacturing angle, the infill density, the size of manufacturing voids), but the analysis of U-notched specimens will allow introducing geometrical input characteristics of samples as well.

For the second aim, the FIS performance is compared to the analytical method, based on the equivalent homogenised material concept and the theory of critical distances as proposed by Ahmed and Susmel.[73]

Notched specimens have similar manufacturing and testing processes as discussed in chapter 2, but the previously mentioned difference is in sample geometry: notched specimens have symmetrical U-shape notches on each longitudinal side (Figure 2.8). There are three different geometries of notched specimens considered and all of them have 5mm notch depth, but the notch radius are 0.5mm, 1mm and 3mm, respectively.

Similar to the previously discussed plain specimens, notched specimens also have various combinations of manufacturing angles and infill densities. The varied radius of the notch is added as an extra (*geometrical*) input parameter. Therefore, for notched specimens, input parameters of the FIS are the manufacturing angle, the infill density and the radius of the notch, while the output remains failure strength (see Table 2.6). Note here that following section 2.6, manufacturing void size d_v is excluded from input parameters in the current chapter.

Experimental results of U-notched specimens (presented in Table 2.6), as mentioned before, are adapted from Ahmed and Susmel,[73] which contain failure strength of tested parts for different infill density levels, manufacturing angles and radius of notches. Note the difference in infill density: for U-notched analysis, it ranges between 30% and 70% (10% to 90% for the case of plain specimens). As for the output, similar to plain specimens, failure strength is calculated as the applied force upon breakage divided by the cross-section area of the breakage.

Table 2.6 Summary of experimental results for U-notched specimens.

	Input			Output
Specimen	θ_p (°)	Infill density(%)	Radius (mm)	σ_f (MPa)
1	0	30	0.5	9.7
2	0	30	1	9.5
3	0	30	3	10.9
4	0	50	0.5	13.1
5	0	50	1	13.8
6	0	50	3	14.4
7	0	70	0.5	17.4
8	0	70	1	16.9
9	0	70	3	18.6
10	30	30	0.5	8.2
11	30	30	1	8.5
12	30	30	3	10
13	30	50	0.5	11.5
14	30	50	1	12
15	30	50	3	12.5
16	30	70	0.5	12.2
17	30	70	1	11.9
18	30	70	3	13.9
19	45	30	0.5	8
20	45	30	1	8.1
21	45	30	3	9.8
22	45	50	0.5	11
23	45	50	1	11.9
24	45	50	3	13.5
25	45	70	0.5	15.1
26	45	70	1	15.2
27	45	70	3	16.4

The total number of 27 manufactured U-notched specimens is considered. The selection of fuzzy rules and validation specimens are chosen to be similar to the one discussed in section 2.3.3. Validation specimens are chosen to be specimens 2, 4, 6, 8, 11, 13, 15, 17, 20, 22, 24 and 26, i.e. 12 validation specimens (marked as grey rows in Table 2.6). The remaining 15 specimens (1, 3, 5, 7, 9, 10, 11, 12, 14, 16, 18, 19, 21, 23, 25 and 27) are taken to form fuzzy rules.

The comparison between the analytical method and the FIS methodology is based on the accuracy of using both techniques to estimate the failure strength of U-notched specimens. FIS-based estimation errors of failure strength for all 12 validation specimens are presented in Table 2.7 (middle column). For the accuracy of the adapted analytical method, error values are directly

acquired from Ahmed and Susmel,[73] these error values are also presented for readers' benefit in Table 2.7 (most right column). It is necessary to point out that the analytical method used the same 12 validation specimens mentioned above.

Table 2.7 Error contrast between the fuzzy inference system and the adapted analytical method

Specimen	FIS Error (%)	Analytical Method Error (%)
2	0.1	12.5
4	0.2	11.5
6	8.6	15.5
8	2.9	2.1
11	8.7	0.9
13	9	5.3
15	7.6	3.6
17	11.7	24.9
20	10.3	5.7
22	5.4	16.4
24	8.6	9
26	0.2	5.1
Average	**6.1**	**9.4**

As can be seen from Table 2.7, estimation errors lie within an interval of 11.7% for FIS and 24.9% for the analytical method, respectively. Note that the maximum estimation error is almost halved while using the FIS methodology. Interesting to point out that the average estimation error also decreases from 9.4% (for the analytical method) to 6.1% (for FIS). As such, it can be concluded that the fuzzy inference system is at least as functional as analytical methods in estimating failure strength and, in the above cases, shows improved accuracy.

As it has been mentioned above, a particular choice to analyse U-notched specimens has been made not only to validate the FIS using existing experimental data and to compare its performance to the existing methodologies but also to test its ability to perform on mixed types of data: manufacturing *and* geometrical input parameters. As can be seen, the FIS methodology reacts very well (with high accuracy) to the introduction of this new geometrical data. Notch root radius is an important geometrical characteristic, and the FIS approach has shown to be capable of estimating failure strength depending on the radius value (estimations show a similar trend in failure strength as a function of radius, as seen in experiments[73]). Considering the importance of

this geometrical characteristic as a possible *design* parameter, it can be concluded that the FIS has the potential to become a simple, robust and accurate methodology that can be expanded as a *decision-making* tool in design problems.

After the analysis of using FIS in the so-called *direct* estimation (from manufacturing and geometrical parameters to the mechanical property), the study in the next section will focus on extending the current usage of the FIS methodology to an *inverse* estimation framework. Such an inverse framework could potentially be a solution to the identification of the optimal combination of manufacturing parameters, ensuring user-defined mechanical characteristics of a component.

2.7 Inverse estimation of manufacturing parameters

Previous studies reported in sections 2.3-2.6 and published in [36] have proven that FIS has the capability to estimate tensile strength with given manufacturing and geometrical parameters. However, a common industrial problem is that with both strength and geometrical design requirements set for a 3D-printed object, the optimal combination of manufacturing parameters can be impossible to be determined a priori. Hence, starting from this section, attempts will be made to solve such a problem of ambiguous conformity by estimating manufacturing angle and infill density with the provided requirement of strength and geometry. Besides, adjustments will be conducted to the acquired manufacturing parameters in order to meet specific industrial needs, for example, with time-saving or material-saving as a top priority.

Due to the fact that the estimation here seeks manufacturing parameters which lead to required strength and geometry, it will be referred to as *inverse estimation* in the following sections and chapters, contrary to the *direct estimation*, which results in strength estimation based on the given manufacturing parameters reported in the previous section. [5]

[5] Note that the choice of "direct/inverse" terminology is arbitrary and dictated here by convenience and the order of analysis. Other researchers may use "reverse" terminology.

Table 2.8 Summary of experimental data for testing U-notched specimens

	Input		Output	
Specimen	Radius (mm)	σ_f (MPa)	θ_p (°)	Infill density(%)
1	0.5	9.7	0	30
2	1	9.5	0	30
3	3	10.9	0	30
4	0.5	13.1	0	50
5	1	13.8	0	50
6	3	14.4	0	50
7	0.5	17.4	0	70
8	1	16.9	0	70
9	3	18.6	0	70
10	0.5	8.2	30	30
11	1	8.5	30	30
12	3	10	30	30
13	0.5	11.5	30	50
14	1	12	30	50
15	3	12.5	30	50
16	0.5	12.2	30	70
17	1	11.9	30	70
18	3	13.9	30	70
19	0.5	8	45	30
20	1	8.1	45	30
21	3	9.8	45	30
22	0.5	11	45	50
23	1	11.9	45	50
24	3	13.5	45	50
25	0.5	15.1	45	70
26	1	15.2	45	70
27	3	16.4	45	70

2.7.1 Inverse problem setup

As mentioned previously, generally, the goal of an industrial process is to find the optimal solution of manufacturing parameters that ensures predetermined values of strength and geometry. Owing to the success of FIS in the previously investigated direct estimation (from manufacturing parameters to strength), the new input of the inverse FIS in the present investigation is set to be strength and geometrical parameters, i.e., tensile strength and notch root radius. Hence, the manufacturing angle and the infill density have become the output of this new inverse estimation.

2.7.2 Experimental data and classification for the inverse estimation

After the inverse problem has been formulated, the introduction of experimental data for training and validating the inverse FIS is also of great importance. The experimental data used in the inverse estimation is identical to that used in the direct estimation, which is originally adopted from Ahmed and Susmel[73] and reported in Table 2.8 but rearranged. There are 27 experimental data sets, each of which has a unique combination of 4 parameters. Relevant parameters in Table 2.8 are referred to as: radius – notch root radius (mm), σ_f – failure tensile strength (MPa), θ_p – manufacturing angle (°) and infill density (%).

To show the reliability of the FIS methodology, it is necessary to have not only enough data for defining the fuzzy rules but also a group of data needed exclusively for validation. In the following sections, a new classification principle is adopted where all specimens with a radius equal to 1mm are treated as *unknown* data and classified as a validation group. This is to evaluate the performance of FIS in dealing with the *unseen* value - i.e. how well FIS will deal with the unseen data with a notch root radius equal to 1mm if the system has only seen data with radius of 0.5mm and 3mm.

2.7.3 Sugeno fuzzy inference system

As mentioned in previous sections, a more suitable Sugeno FIS is adopted in this section. Being in itself a recap and the introduction of the new Sugeno FIS, the general stages of setting up a Sugeno FIS are illustrated as follows. Initially, a group of historical data is fed to formulate the fuzzy rule base, which builds mappings between existing input and output. In order to make predictions of a new unknown output, the new known input data has to be first fuzzified into a membership value using MF. For consistency with the direct estimation, the triangular MF is still used here.

For various fuzzy rules, the parameters of MF could be different, so the fuzzification of a FIS, which contains several rules, has a parallel data processing pattern. Note here that these fuzzy rules have only helped to generate parameters of MF while they have not interfered with input data yet.

The derived membership values are then brought to the fuzzy inference engine, which contains a group of fuzzy calculus that can process the membership value with respect to fuzzy rules. The detailed calculus will be introduced in the later section, together with an illustrative example. The output of a Sugeno fuzzy inference engine is a combination of 2 values – m_i and n_i, where m_i

refers to the processed membership value of the new input for the ith fuzzy rule and n_i refers to the known output value (from training data) for the same rule.

As mentioned previously, the Sugeno FIS does not include any membership function calculation in the output stage apart from a weighted average calculation, as shown below:

$$W_a = \frac{\sum_1^k m_i * n_i}{\sum_1^k m_i}\ , \tag{9}$$

where k refers to the total amount of fuzzy rules and W_a refers to the calculated weighted average value. Eventually, the value of W_a is the estimated output value for the new input.

2.7.4 Sugeno fuzzy inference system with an illustrative example

Since the general stages of constructing a Sugeno FIS have been introduced, it is possible now to illustrate the detailed calculation with a synthetic example. Figure 2.9 shows the decomposition of a Sugeno FIS calculation for some fabricated data. Note that in Figure 2.9, the calculation and setup of MF for input parameters have been partly simplified, aimed at helping the readers to understand better.

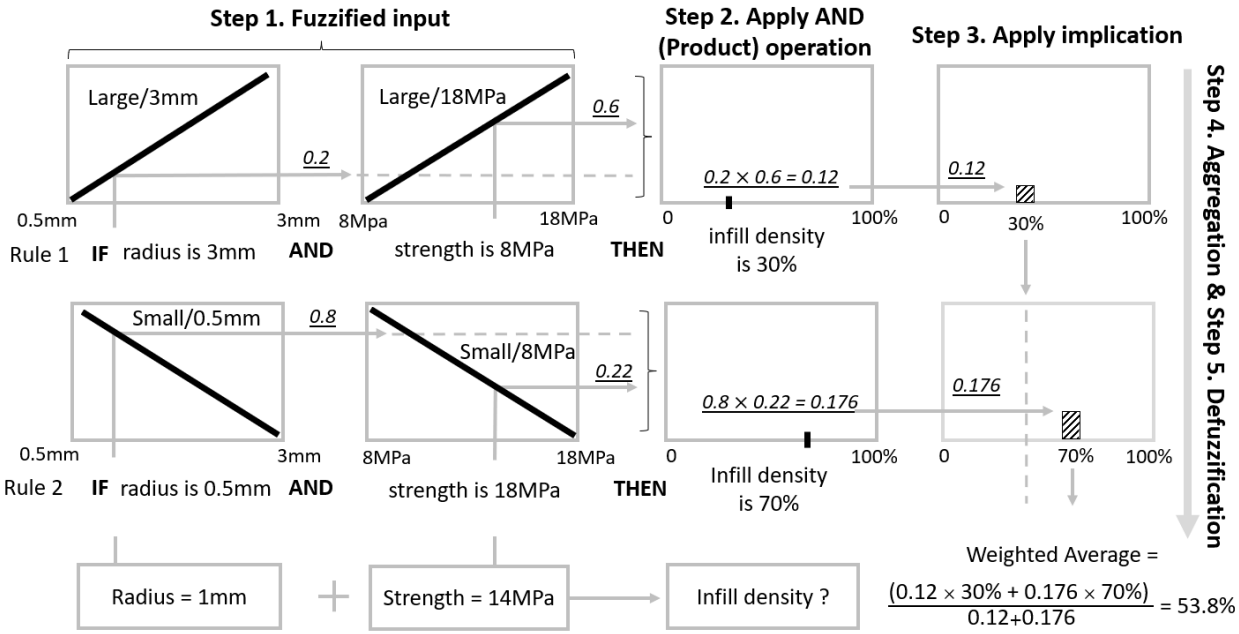

Figure 2.9 Decomposition of a Sugeno fuzzy inference system.

The process starts from the definition of 2 fuzzy rules, formulated based on the existing experimental data shown in Table 2.8, which in the linguistic form are:

Rule 1: "IF the radius is 3mm and strength is 8MPa, THEN infill density is 30%";

Rule 2: "IF the radius is 0.5mm and strength is 18MPa, THEN infill density is 70%".

As the next step, input parameters are fuzzified using triangular membership functions, resulting in membership values. For the first parameter of synthetic data, the radius ranges from 0.5mm to 3mm, and the membership value ranges from 0 to 1. Therefore, membership functions for the radius (the most left column in Figure 2.9) can be calculated as:

$$\mu(x) = \begin{cases} \dfrac{x-0.5}{3-0.5}, & \text{if the radius is large (rule 1)} \\ \dfrac{3-x}{3-0.5}, & \text{if the radius is small (rule 2)} \end{cases}, \tag{10}$$

With a new radius value equal to 1mm ($x = 1$mm) as input, the corresponding membership value of both rules can be found as $\frac{1-0.5}{3-0.5} = 0.2$ and $\frac{3-1}{3-0.5} = 0.8$. Similarly, membership values, $\frac{14-8}{18-8} = 0.6$ and $\frac{18-14}{18-8} = 0.4$, can be obtained for the second parameter - strength (the second column in Figure 2.9).

Then the next step - the *AND* operation, mentioned in both rules above, refers to implication: e.g. for 30% infill density (consequent of rule 1), the outcome of this implication stage is a membership value (the product of radius and strength membership values) $0.2 \times 0.6 = 0.12$. Therefore, combined with the 30% infill density, the calculation result for the first row is 0.12/30% (0.12 for the calculated membership value and 30% for the consequent value). Similarly, the calculation result for the second row is 0.176/70%, where 0.176 is obtained from $0.8 \times 0.22 = 0.176$.

Exercising all existing rules (two rules in our case), the weighted average of all outcomes is calculated as shown in Figure 2.9, resulting in the estimated infill density. Hence, in our illustrative example, with knowing data from rules 1 and 2, the estimated infill density for a new specimen (with "notch root radius - 1mm and tensile strength - 14Mpa") is $\frac{0.12\times30\%+0.176\times70\%}{0.12+0.176} = 53.8\%$. Note that membership functions of output parameters are now in the form of constants rather than functions, thanks to Sugeno FIS.

2.8 Inverse estimation results and adjustments

Returning to the original experimental data reported in Table 2.8, a new FIS can be constructed from all *known* (unshaded) specimens, following the procedure introduced in section 2.7. Then the new *unknown* data (shaded in Table 2.8) from the validation group is fed into the system, and the estimation results based on the validation group are noted in Table 2.9. The "experiment output" in Table 2.9 includes actual values of manufacturing angles and infill densities repeated from Table 2.8; they are eventually compared with the "estimation output".

2.8.1 Estimation error calculation

In order to evaluate the accuracy of the proposed inverse FIS methodology, estimated outputs (P_{est}) are compared with the actual experimental outputs (P_{exp}) see Table 2.9, where the *absolute* error is calculated according to:

$$Error = \left|P_{est} - P_{exp}\right|, \tag{11}$$

as the presence of "0" in the actual experimental manufacturing angle (and hence in a denominator for the case of relative error calculations) could cause numerical issues.

It can be seen from Table 2.9 ("Abs error – Exp. & Est." column) that the absolute estimation error between the experimental and the estimation results is 8.5° for $\boldsymbol{\theta_p}$ and 4.6% for infill density. Such estimation error shows that the two manufacturing parameters ($\boldsymbol{\theta_p}$ and infill density) can be estimated accurately using the inverse estimation scheme. Section 2.8.2 will introduce some necessary adjustments of these estimated results considering some particular specifications.

Table 2.9 Experimental output together with the estimation output, the corresponding adjustments and the estimation error

	Experiment Output		Estimation Output		Abs error – Exp. & Est.		Adjusted Estimation		Abs error – Exp. & adjusted Est.	
Spec	θ_p (°)	Infill (%)	θ_p (°)	Infill (%)	Error θ_p (°)	Error infill (%)	θ_p (°)	Infill (%)	Error θ_p (°)	Error infill (%)
2	0	30	5.3	30	5.3	0	0	30	0	0
5	0	50	33.7	60	33.7	10	30	60	30	10
8	0	70	9	70	9	0	15	70	15	0
11	30	30	24.1	30	5.9	0	30	30	0	0
14	30	50	30	64.3	0	14.3	30	60	0	10
17	30	70	30	61.4	0	8.6	30	60	0	10
20	45	30	37.5	30	7.5	0	45	30	0	0
23	45	50	30	61.4	15	8.6	30	60	15	10
26	45	70	45	70	0	0	45	70	0	0
			Average Error		**8.5**	**4.6**	**Average Error**		**6.7**	**4.4**

2.8.2 Necessary adjustments regarding particular specifications

Since the outcome of this inverse FIS is values of manufacturing parameters which are to be fed into 3D printers, it is very likely that the estimation results will be correct mathematically, but the values are somewhat meaningless to the printer due to possible printer specifications. Hence, the adjustments of results based on real applications (taking particular specifications of a 3D-printer into account) are necessary in order to avoid meaningless values. To take an example of the adjustment of manufacturing angle, which follows the principle of "proximity", if two estimated manufacturing angles are 4.3° and 12.9° for two different specimens, the adjusted estimation result will be 0° and 15°, respectively. Note here if the estimated value is equal to 7.5°, which is in the middle of the increment, the adjusted result will be rounded to 15° (see specimen 20 in Table 2.9) and adjustments in following chapters have the same rule.

Similarly, for infill density, if two estimated infill densities are 67.6% and 61.4% for two different specimens, the adjusted estimation result will be 70% and 60%, respectively. Both adjusted estimation results have been included in Table 2.9.

The average absolute error with adjustments is reported to be 6.7° and 4.4% for θ_p and infill

density, respectively. Compared with the estimation result without adjustments, the adjusted estimation has shown a decrease in absolute errors for both manufacturing parameters. Thus, it can be concluded that the adopted adjustments with respect to printer specifications are effective and can help reduce the estimation error.

Furthermore, it is interesting to note a high estimation error for the manufacturing angle of specimen 5 (see 30° absolute error). The author attempted to analyse this relatively high value and came up with the following explanations:

- the two adjacent rules influencing the estimation of specimen 5 are specimen 18 and 24 (see Table 2.8) since the strength of specimen 5, which is 13.8MPa, lies between 13.5MPa (specimen 24) and 13.9MPa (specimen 18);
- infill densities are also relatively close to each other (identical in specimens 5 and 24) ;
- therefore, intuitively, the estimated manufacturing angle of specimen 5 should lie somewhere between 30° (specimen 18) and 45° (specimen 24).

Moreover, it is seen that although specimen 18 and 24 have the same radius (3mm) and very close values of strength, the experimental manufacturing parameters are quite different (30°/70% vs 45°/50%). Such ambiguity causes the estimation inaccuracy for specimen 5. Summarising the above: the estimation result of FIS depends on the provided experimental data or fuzzy rules where ambiguous conformity could cause extra estimation error. Such ambiguity will be discussed in section 2.10.

2.9 Numerical validation

It can be seen from Table 2.9 that the average estimation error for manufacturing angle and infill density is seen to be 6.7° and 4.4%, respectively. At this stage, a validation test is designed in order to demonstrate the full capability and accuracy of FIS methodology. The author appreciates the unconventional usage of the word “validation” in a numerical rather than traditionally experimental sense but offers readers to follow them. It needs pointing out here that the author’s original attempt was to accomplish such validation experimentally. However, specimens used in previous sections were manufactured during a specific time, after which the 3D-printer has not yet been used for at least half a year. In such case, the consistency of manufactured specimens and potential validation specimens cannot be guaranteed. Hence, the numerical validation is chosen here as an alternative solution.

In this numerical validation test, illustrated in Figure 2.10, the author starts from the inverse FIS (denoted F_1) in order to estimate manufacturing parameters (manufacturing angle and infill

density) required to obtain the desired strength values and notch root radius. The author follows the process described above in section 2.7. These obtained manufacturing parameters, after adjustments, are then used together with the notch root radius in the next step – the direct FIS (denoted F_2) to *(re-)estimate* values of the strength. Eventually, these new (re-)estimated values of the strength are compared to the original experimental failure strength values. The accuracy of the comparison will indicate whether FIS methodologies worked well from a comprehensive perspective.

As shown in Table 2.10, the "manufacturing parameters" column presents the outcome of F_1. These data are then used in the new direct estimation FIS F_2, together with the radius, in order to (re-)estimate failure strength (presented in the "strength estimation" column). The new direct estimation still uses the aforementioned specimens to set up fuzzy rules, and the validation group is identical to that of inverse estimation. Estimated failure strength is then compared with experimental failure strength, and an absolute error is calculated. It can be seen (from Table 2.10) that the average absolute error is 0.55MPa, which is relatively small compared to actual strength values. To reiterate: this error refers to the difference in failure strength obtained from experiments and estimated using our inverse-adjusted-direct approach. It is noted that at the end of the direct estimation process, the estimation error already includes errors generated in both inverse and direct FIS. Therefore, it can be concluded that FIS has proven to show a good performance.

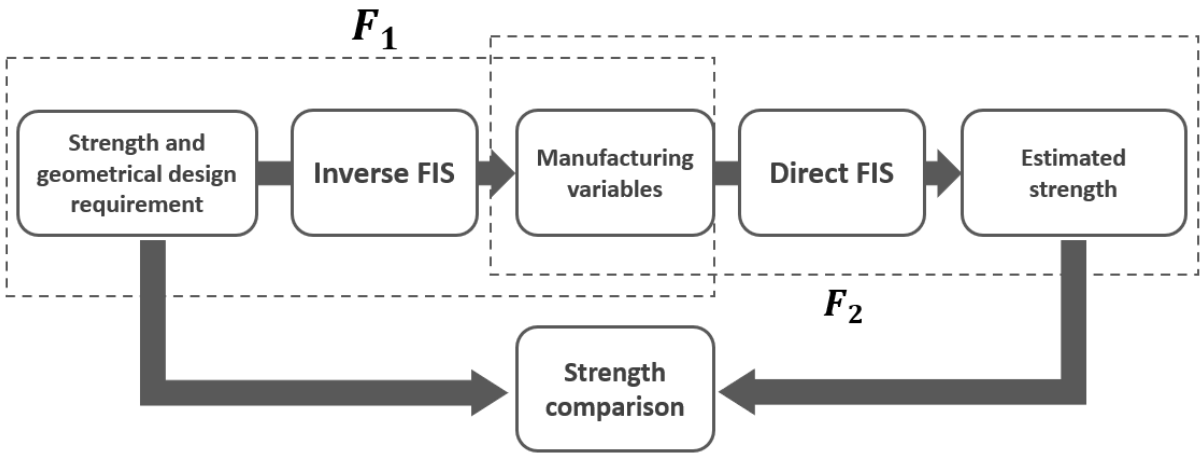

Figure 2.10 Explanation of the inverse and direct estimation using FIS where F1 refers to the inverse estimation and F2 is the direct validation estimation.

Table 2.10 Estimated manufacturing angle and infill density are brought back into the FIS direct estimation to estimate the failure strength, which is to be compared with the experimental failure strength for R=1 specimens.

	Manufacturing parameters (adjusted)		Strength		Absolute error
Specimens (R=1mm)	θ_p (°)	Infill(%)	Estimation σ_f(MPa)	Experimental σ_f(MPa)	σ_f
2	0	30	9.94	9.5	0.44
5	30	60	12.2	13.8	1.6
8	15	70	15.2	16.9	1.7
11	30	30	8.57	8.5	0.07
14	30	60	12.2	12	0.2
17	30	60	12.2	11.9	0.3
20	45	30	8.37	8.1	0.27
23	30	60	12.2	11.9	0.3
26	45	70	15.3	15.2	0.1
				Average Error	**0.55**

2.10 Study of cost-control relevant parameters with fuzzy system

As promised, in this section, the author would like to return to the ambiguity issue discussed in section 2.8. It is noted that specimen 23, for example, has a 45°/50% experimental setup, but the estimation result offers a preferred 30°/60% (see Table 2.9). The difference between both pairs cannot be disregarded; however, the 30°/60% provides a failure strength similar to 45°/50% (see Table 2.10). It can be referred to as the non-uniqueness of the 3D printing, i.e., different combinations of multiple parameters can lead to similar results.

Assuming there are no restrictions on manufacturing angles with respect to cost, this ambiguity of results can also be controlled by, for example, the material cost of the printing, where the solution with less infill density could be preferred. Hence, it has raised the extensive interest of the author that from the above inference process, parameters such as printing period and material consumption are worth extra attention, especially for manufacturers.

Table 2.11 presents the study, which includes not only strength and notch root radius but also

printing period and material consumption for the estimation of optimal manufacturing parameters. Both printing period and material consumption have been acquired from the software CURA with different design models loaded, where the assumption has been made that the estimated time and material usage shown in CURA is identical to reality.[73] The printing period refers to the time (minutes) needed to complete the 3D printing, while material consumption can quantify the weight of the material being consumed (grams). Both of them can be categorised as cost-relevant parameters which represent special industrial needs rather than manufacturing settings or geometrical design. Thus, they are used together with radius and strength as inputs of a new inverse FIS.

The setup of the new inverse FIS with two extra input parameters is similar to the one discussed in section 2.7. Table 2.11 reports that the new estimation error of recommended manufacturing angle is 8.3° (estimation *with* time and weight), which is larger than the error (6.7°) reported in Table 2.9 (estimation *without* time and weight). However, it is satisfying to see the new estimation error for infill density drops from 4.4% (without time and weight) to 0% (with time and weight). Such comparison leads to the following conclusions:

- Including additional parameters (such as printing time and material consumption) can lead to better FIS estimation accuracy for infill density while it has negative impacts on the estimation of manufacturing angle.
- Generalising further, it can be concluded that the manufacturing angle does not significantly influence the printing time and material consumption, contrary to infill density.

Once again, the above result proves that the fuzzy inference system is a useful tool that can be used to estimate manufacturing angles and infill densities with not only requirements of failure strength and notch root radius but also cost-control parameters such as printing time and material consumption. Additional relevant parameters can contribute to better estimation accuracy using FIS.

Table 2.11 Inverse FIS estimation of manufacturing parameters with printing time and material weight included.

	Input				Experiment output		Estimated adjusted output		Error without time and weight (from Table 2.9)		Error including time and weight	
No.	**Radius (mm)**	**σ_f (Mpa)**	**Time (mins)**	**Weight (g)**	**θ_p (°)**	**Infill (%)**	**θ_p (°)**	**Infill (%)**	**ABS error θ_p**	**ABS error infill**	**ABS error θ_p**	**ABS error infill**
1	0.5	9.7	93	8	0	30						
2	1	9.5	94	8	0	30	0	30	0	0	0	0
3	3	10.9	97	8	0	30						
4	0.5	13.1	101	9	0	50						
5	1	13.8	102	9	0	50	45	50	30	10	45	0
6	3	14.4	105	9	0	50						
7	0.5	17.4	109	10	0	70						
8	1	16.9	110	10	0	70	0	70	15	0	0	0
9	3	18.6	113	10	0	70						
10	0.5	8.2	93	8	30	30						
11	1	8.5	94	8	30	30	30	30	0	0	0	0
12	3	10	96	8	30	30						
13	0.5	11.5	101	9	30	50						
14	1	12	102	9	30	50	30	50	0	10	0	0
15	3	12.5	105	9	30	50						
16	0.5	12.2	109	10	30	70						
17	1	11.9	110	10	30	70	30	70	0	10	0	0
18	3	13.9	113	10	30	70						
19	0.5	8	92	8	45	30						
20	1	8.1	93	8	45	30	30	30	0	0	15	0
21	3	9.8	96	8	45	30						
22	0.5	11	100	9	45	50						
23	1	11.9	101	9	45	50	30	50	15	10	15	0
24	3	13.5	104	9	45	50						
25	0.5	15.1	108	10	45	70						
26	1	15.2	109	10	45	70	45	70	0	0	0	0
27	3	16.4	112	10	45	70						
							Average error		**6.7**	**4.4**	**8.3**	**0**

2.11 Conclusion

In this chapter, the key steps of setting up a Mamdani fuzzy inference system and a Sugeno fuzzy inference system has been presented and discussed. The FIS-based methodology is then used to estimate the failure strength of polylactide 3D-printed parts as a direct framework. Then, it also reports that FIS has the capability of inverse estimation.

For the direct estimation, by making use of a large number of experimental data, the performed validation exercise allows us to demonstrate that the use of this methodology leads to reliable and accurate estimations of the failure tensile strength. It is concluded that more experimental data improve the estimation accuracy markedly. Further studies can be conducted to find out the minimum number of experimental data that are required to reach the wanted estimation accuracy while the costs associated with the calibration process are minimised.

It is important to highlight that, thanks to its intrinsic versatility, the FIS methodology is expected to be equally successful in predicting other mechanical properties such as, for instance, strength under fatigue as well as under dynamic loading. Given the FIS methodology's *modus operandi*, the accuracy in estimating other mechanical responses is obviously expected to increase as the size of the data population used to train the method itself increases.

For the inverse estimation, FIS has shown its capability of estimating manufacturing angle and infill density with provided requirements of tensile strength and geometrical characteristic (notch root radius) in the 3D printing application. The necessity of having adjustments for estimation results has been discussed due to the specification of 3D printers, and it has been shown that adjustments are effective and not resulting in an evident reduction of the estimation accuracy. It was concluded that FIS has a highly accurate inverse estimation potential.

FIS has also shown its capability of dealing with not only manufacturing parameters but also cost-relevant parameters such as printing period and material consumption. Hence, it is a comprehensive solution which allows manufacturers to find the optimal manufacturing parameters and have a cost-control tool at the same time.

The FIS methodology is tested on different types of input parameters (i.e., manufacturing and geometrical variables) and is seen to be a simple, robust tool that can produce highly accurate estimations. Accordingly, the FIS approach has great potential as a decision-making tool for design problems. In particular, the FIS approach is expected to be very successful when used together with big data for its calibration. Potentially, in the near future, this approach could be effectively coupled with 5G, real-time data acquisition technologies, big data streams, artificial

intelligence and automated machine learning to model and predict the mechanical behaviour/strength of engineering components and structures. As a strong competitor of the FIS methodology in the above areas, the artificial neural network, which is famous for its self-learning capability, will be introduced in Chapter 3.

Chapter 3

Artificial Neural Network

The main focus of the present investigation is to introduce and analyse alternative data-driven methodologies in order to achieve the best data-driven methodology by comparing their estimation performance. Hence, as a strong competitor of the discussed in Chapter 2 FIS methodology, the artificial neural network has become one of the most commonly used algorithms in artificial intelligence, which has gained prevalent attention in all fields.[91] In this chapter, the main aspects of artificial neural network (NN) will be discussed in detail, including all necessary steps for building NN models.

Artificial intelligence (AI) is a popular idea in both academia and industry as it refers to the idea of allowing machines to make decisions based on predetermined rules. As a subset of AI, machine learning (ML) aims to build models based on existing data and patterns for the prediction of new data. NN is one of the machine learning models, and it is essentially a network of mathematical equations. The network processes the input variables with mathematical equations and then returns the prediction of the output variables, which are normally compared with the targeted output values for further network adjustment.

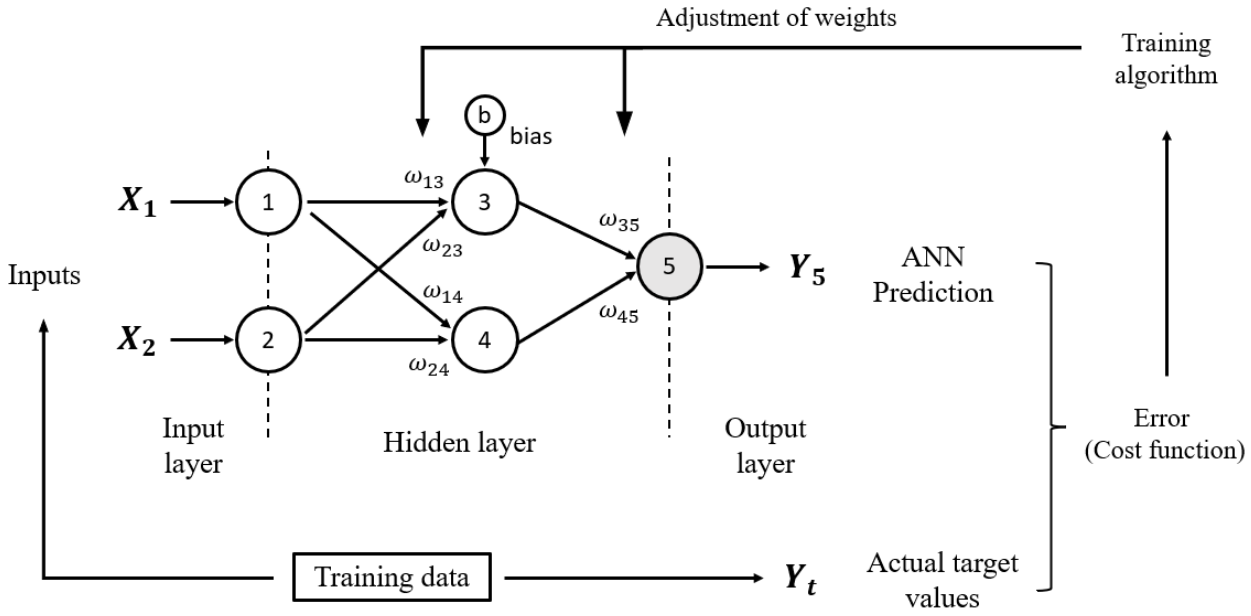

Figure 3.1 Decomposition of an artificial neural network.

3.1 Introduction of the artificial neural network

3.1.1 The main parameter of a neural network

The term *neural* refers to the artificial neurons in the structure of an NN as a neural network (NN) consists of an interconnected group of neurons and processes information similar to biological neurons in human brains. The typical structure of an NN is shown in Figure 3.1 in the form of a simplified network. The network includes two input variables - x_1, x_2 and one output variable - Y_5. The structure of the network consists of three different layers – (i) an input layer, (ii) a hidden layer, and (iii) an output layer.[92] There are two neurons in the input layer, two in the hidden layer, and one in the output layer, and these neurons connect to other neurons in adjacent layers. The required number of neurons in both input and output layers depends on the number of variables in the particular problem. However, various studies have suggested that the optimum number of neurons in hidden layers is preferably between 5 and 10.[93,94]

Being itself the main parameter of a NN, the weight connecting two neurons refers to the connection magnitude. To take an example of Figure 3.1, neuron 1 and 2 both contribute to neuron 3, while ω_{13} and ω_{23} represent individual importance that they have on neuron 3. Therefore, the value of neuron 3 can be calculated as follows:

$$Z_3 = (\omega_{13}x_1 + \omega_{23}x_2) + bias\,, \tag{12}$$

where Z_3 is the value of neuron 3 and bias is an extra input to neuron 3 in the form of a trainable/changeable constant, which allows the better fit of prediction results with respect to training data. To help the readers' understanding, bias is somehow similar to the constant in a linear equation. As such, the universal calculation of the neuron value can be expressed as:

$$Z = \sum(\omega x) + bias\,. \tag{13}$$

For the simplicity of calculation and illustration, bias will be omitted in the following section as the main focus here is to introduce the determination process of weights.

At the beginning, there is no deterministic knowledge of these connection weights, so they are initialised randomly. Then the inputs of training data are fed into the NN, together with initialised weights, which returns a predicted output value. The outputs in the training data (actual target values) are then compared with the predicted ones, where the error between both values indicates the estimation accuracy of the current NN. After being brought to a particular training algorithm, the error results in a group of updated weights, i.e., an updated network. Note here that the training algorithm (to be introduced in detail) constrains the initial random weights and upgrades them based on the error values. Once again, the training data is then fed into the updated network to start another upgrading iteration, and such an iterative upgrading process continues until a tolerable error is achieved. In general, the basic idea of NN is to minimise the error between the predicted and targeted values by upgrading weights in the network iteratively. This process is also recognised as the training process of a network, and once the error is within the tolerance, the network will be accurate enough to accept new inputs in order to make new predictions.

3.1.2 Activation function

After introducing the iterative calculations of NN, the topic in this section will return to the signal processing within the single neuron. Similar to biological neurons, after all signals are received and processed by the current neuron, it is necessary to determine whether and how much the current neuron is activated. This is where activation functions step in, as it is capable of helping the network learn various complicated patterns and avoid potential computational difficulties.

As introduced in Equation (*13*), the signal of a universal neuron includes a group of weighted sums of inputs, which are in the form of linear transformations. Despite there being multiple layers

of neurons attached, the superimposed transformations are still linear in nature. Such a network only behaves as a linear regression model, which cannot handle complicated non-linear problems.[95] Thus, the capability of adding non-linearity to a NN is a necessary characteristic of activation functions.

The necessity of activation functions is also reflected in computational expense. As inputs of the neuron consist of multiple functions of $\omega x + b$, it could result in computational difficulties, particularly for a complicated network with a large number of layers. Therefore, the activation function is desired to restrict the value of a neuron and should be computationally inexpensive as it needs calculating with every neuron.

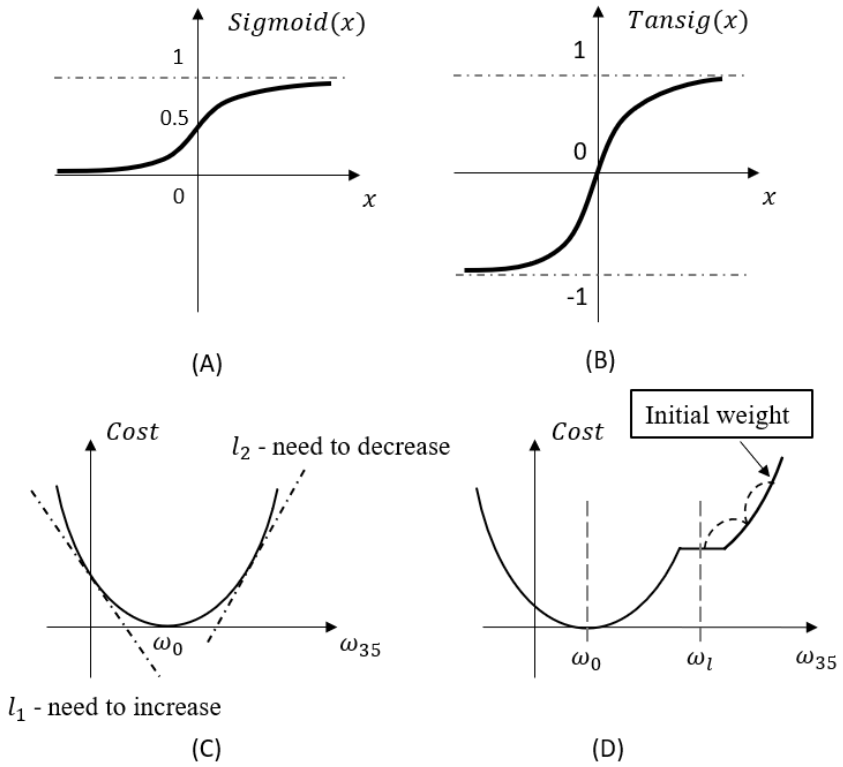

Figure 3.2 A) Sigmoid transfer function with x refers to the input signal; B) Tansig transfer function with x refers to the input signal; C) Cost function based on the Mean Squared Error; D) A example of more complex cost functions where the local minima is not optima.

There are various activation functions, such as the conventional Sigmoid function (Figure 3.2A), Sigmoid/Tanh-based functions (Tansig), exponential-based functions, rectified linear functions (ReLU), etc.[96] However, in the present research, in order to meet all requirements mentioned previously, the activation function adopted for the hidden layer is the Tansig transfer function which can be expressed in Equation (*14*) and Figure 3.2B. The selection of the Tansig function over the Sigmoid function will be explained in the section 3.1.5.

$$Tansig(x) = \frac{2}{1 + e^{-2x}} - 1 . \quad (14)$$

As such, combined with Equation (*12*), the output of neuron 3, for example, becomes as follows (with bias omitted for simplicity):

$$Y_3 = f(Z_3) = Tansig(\omega_{13}x_1 + \omega_{23}x_2) . \quad (15)$$

Note here that Z_3 is the signal received by the neuron in the form of a weighted sum, whereas Y_3 is the activation signal of the neuron, which is to be weighted and transmitted to the next neuron.

As for the output layer, since there are few calculations here and the main purpose is to output the derived results from the hidden layer, the pure linear function is sufficient for regression problems, although other activation functions could also be appropriate depending on the particular problem. Therefore, the signal transformation at the fifth neuron is as follows:

$$Y_5 = f(Z_5) = Z_5 = \omega_{35}Y_3 + \omega_{45}Y_4 . \quad (16)$$

3.1.3 Loss function

As mentioned in section 3.1.1, every predicted value from a network will be compared with the target value in order to update weights based on generated errors. Updated weights are then used for further predictions, and such iteration continues until an acceptable error is achieved. In this iterative process, the information is forwarded along the network, whereas the training feedback is then sent back to the system for adjusting the weights. Such a process could be referred to as feed-forward backpropagation.

The error between the prediction and the target can simply be calculated using the loss function, also known as the cost function:

$$Cost = (Y_5 - Y_t)^2 , \quad (17)$$

where Y_5 is the predicted output of each iteration and Y_t is the actual target value. The performance judgement of the network is based on the above equation as the network will be more accurate if Y_5 and Y_t are closer to each other, i.e., the less cost, the better. Cost/error derived from

such a function normally refers to the mean squared error (MSE), and the *square* here is for preventing positive and negative errors from cancelling out.

Based on Equation (*13*), Equation (*15*) and the linear activation function in the output layer, the cost function can be further extended as:

$$\begin{aligned} Cost &= (\omega_{35}Y_3 + \omega_{45}Y_4 - Y_t)^{\,2} \\ &= [\omega_{35}Tansig(\omega_{13}x_1 + \omega_{23}x_2) + \omega_{45}Tansig(\omega_{14}x_1 + \omega_{24}x_2) - Y_t]^2 \,. \end{aligned} \tag{18}$$

Essentially, the cost function is relevant to all weights. In order to study how each weight should be adjusted, suppose the cost function in Equation (*18*) is a function only relevant to ω_{35}. Thus, a quadratic function can be formed, as shown in Figure 3.2C, where the minimum value of the function is equal to zero when ω_{35} is equal to ω_0. At this point, the derivative of the cost function (slope of the curve) is also equal to zero, so the general question to answer has become how to locate ω_0. To take an example of Figure 3.2C, slope l_1 is negative and has to grow up to 0, whereas slope l_2 is positive, which has to drop to 0.

3.1.4 Gradient descent

Since the derivative of the cost function has become the main focus at this stage, with the assistance of the chain rule, the derivative can be expressed as:

$$\begin{aligned} Cost' = \frac{\partial Cost}{\partial \omega_{35}} &= \frac{\partial Cost}{\partial Y_5} \times \frac{\partial Y_5}{\partial Z_5} \times \frac{\partial Z_5}{\partial \omega_{35}} \\ &= 2(Y_5 - Y_t) \times 1 \times Y_3 \\ &= 2[\omega_{35}Tansig(\omega_{13}x_1 + \omega_{23}x_2) + \omega_{45}Tansig(\omega_{14}x_1 + \omega_{24}x_2) - Y_t] \times \\ &\quad Tansig(\omega_{13}x_1 + \omega_{23}x_2) \,, \end{aligned} \tag{19}$$

where $Cost'$ is the first derivative of the cost function, and Y_5, Y_3 & Y_t are all known with initialised weights given previous equations. Now that the gradient of the cost function with respect to ω_{35} is known, it is good timing to apply the gradient descent algorithm to optimise ω_{35} for the sake of minimum cost.

Gradient descent (GD) iteratively calculates the gradient at the current point and subtracts it from the current point after the gradient is scaled with a learning rate. The calculation result is the next point of interest, based on which GD keeps being executed. Based on Equation (*19*), the process can be written as follows:

$$\omega_{35}{}^{new} = \omega_{35} - L\frac{\partial Cost}{\partial \omega_{35}}\ , \tag{20}$$

where ω_{35} is the current weight value and $\omega_{35}{}^{new}$ is the new ω_{35} and is the feedback from the training algorithm. Together with other new weights, $\omega_{35}{}^{new}$ updates the old network.

The L refers to as learning rate in Equation (*20*), and it is a predetermined parameter that scales the gradient. It influences the learning step size in each iteration and determines the overall training period. For example, small learning rates lead to more precision at the cost of lower overall training efficiency, whereas large learning rates result in larger steps at the cost of risking overshooting the local minima. Therefore in the present investigation, the learning rate is set to be equal to 0.01, which is the common value in most past studies.[97,98]

3.1.5 Vanishing gradient problem

Now that the idea of gradient descent has been introduced, one of the typical problems with gradients in neural network is vanishing gradients. For particular activation functions, for example, the sigmoid function (see Figure 3.2A) could squish a large input into a small one which is between 0 and 1. Particularly for negative inputs with large absolute values, $|x|$, the change of output $Sigmoid(x)$ could be close to 0 even with a large input change. Correspondingly, the cost function becomes irresponsive, and the gradient descent iteration is extremely slow. This is often referred to as "Vanishing" gradient.

Vanishing gradient particularly influences deep networks where multiple layers of the structure are included. According to the chain rule, the derivatives of the initial layers are dependent on the multiplication of derivatives of the latter layers, so the gradient could exponentially decrease from the latter layers to the initial layers. Thus, such irresponsiveness in the training stage has a negative impact on both the efficiency and accuracy of the network.

One of the effective solutions to the vanishing gradient problem is to choose alternative activation functions, such as the Tansig activation function (see Figure 3.2B). With a large negative input, the output of a Tansig function is -1, which avoids the vanishment of the gradients.

Meanwhile, considering the NN used in the present investigation is a shallow network (only one hidden layer), the Tansig function is sufficient without causing a significant gradient vanishment problem. Therefore, it is another reason for choosing the Tansig activation function over the Sigmoid previously mentioned in section 3.1.2.

3.1.6 Gradient descent with momentum

Although the problem of vanishing gradients can be solved with an alternative activation function, the potential drawback of the conventional gradient descent method still needs a better solution, which will be illustrated in this section.

As introduced in section 3.1.4, GD is an optimisation algorithm for weights and biases based on their first derivatives with respect to the cost function. Figure 3.2C shows a simplified example of the cost function in which the local minima are normally the global minima, i.e., optima. However, for a more complicated function in real life, the local minima might not be the optima.

A good example is shown in Figure 3.2D, where a fabricated complex function has a plateau where the derivative of the cost function is equal to 0 here. If the initial weight starts from the right side of the plateau, the GD (short-dotted arcs) might cause no weight updates or changes at this point because $\frac{\partial Cost}{\partial \omega_{35}}$ is equal to 0. Consequently, the network could be "fooled" by the GD algorithm to believe the local minima is optima and, therefore, the iterations stop, returning ω_l rather than ω_0. In this case, the prediction accuracy is negatively influenced by this drawback of GD.

One of the solutions to this problem is to update GD with momentum. The idea of GD with momentum is to accumulate gradients in previous iterations before the local minima. So that even if there is no gradient change at the local minima, the accumulated gradients still "push" the algorithm to pass this plateau and eventually locate the global minima. Another benefit of momentum is its capability of speeding up and smoothing the convergency of Equation (*20*), particularly at the "low curvature" area because of the accumulated gradients.

At this stage, it is noted that all past gradients are equally weighted based on the above definition; however, the most recent gradient is almost always distinguished from the accumulated gradients due to various weights. This can be solved by giving the accumulated gradients a specific weightage/coefficient, as shown below.

The application of momentum starts from replacing the partial derivative in Equation (*20*) with a new term, V_t and, therefore, leading to a new Equation (*22*), which is also known as the Exponentially Moving Average (EMA) in statistics:

$$\omega_t = \omega_{t-1} - LV_t \,, \tag{21}$$

$$V_t = \beta V_{t-1} + (1-\beta)\frac{\partial Cost}{\partial \omega_{t-1}} \,, \tag{22}$$

where ω_t and ω_{t-1} are the updated weight linking the same neurons but in $(t-1)^{th}$ and $(t-2)^{th}$ iterations, respectively. Note here that the first iteration occurs when t is equal to 2, and when t is equal to 1, ω_1 is the initialised weight which is not applicable for Equation (21). L is still the learning rate defined previously. The momentum constant β controls the weight distribution between the accumulated gradients and the most recent gradient, and it is between 0 and 1.[99] It can be easily found that smaller β can lead to reduced importance of older gradients and eventually, Equation (21) is identical to the calculation of GD in Equation (*20*) when β is equal to 0. As such, β is set to 0.9 in the present investigation, the same as in many other cases.[100,101] The new term V_t includes both the scaled most recent gradient and all the previous accumulated gradients. An example of some basic calculations of V_t is shown in the following equations for readers' better comprehension:

$$V_1 = 0 \,, \tag{23}$$

$$V_2 = \beta V_1 + (1-\beta)\frac{\partial Cost}{\partial \omega_1} = (1-\beta)\frac{\partial Cost}{\partial \omega_1} \,, \tag{24}$$

$$V_3 = \beta V_2 + (1-\beta)\frac{\partial Cost}{\partial \omega_2} \,. \tag{25}$$

Summarising, the problem of plateau points can be effectively solved by adding momentum to the existing GD, including the past and accumulated gradients. With respect to the prediction accuracy and efficiency, the comparison of both GD and GD with momentum will be analysed in section 3.2.

3.1.7 Adjusting network with multiple training data

The above optimisation of weights is desired to be applied to each weight and bias (if applicable) so that a group of upgraded weights and biases are returned to the network. So far, such iteration is completed and is normally referred to as one epoch or one iteration in NN. As a result of finishing one epoch, the updated network can now make predictions closer to the target value compared with the previous network. However, the new predictions might still not meet expectations, so the training process continues until the error between the prediction and the target is within the predetermined tolerance.

Now that the process of adjusting a NN based on a single training dataset (x_1, x_2, Y_t) has been introduced, it is time to step into the network training with multiple training data. Suppose the group number of training data is n, each group of the training data shares the same initialised random weights with other groups at the beginning of the first feed-forward backpropagation iteration. In that case, the cost function is adjusted to:

$$Cost = \frac{1}{n}\sum_{i=1}^{n}\left(Y_{5_i} - Y_{t_i}\right)^2 , \tag{26}$$

where n is the total group number of training data, Y_{5_i} refers to the network-predicted value based on the ith group of training data input, and Y_{t_i} is the actual target value of the ith group of training data. Note here that the *Mean* in MSE is particularly interpreted in Equation (*26*), compared with that in Equation (*17*).

Correspondingly, the derivative of the cost function will be the mean result, where all groups of training data are brought into the network to formulate the mean $\frac{\partial Cost}{\partial \omega_t}$. The GD with momentum for multiple training data is identical to the one demonstrated in Equation (21). It is important to point out that after the weights are initialised or updated after an epoch, they remain the same until the end of the new epoch, no matter how much training data there are.

3.2 Artificial neural network for 3D-printed notched specimens

With the basis of NN introduced in section 3.1, in the following sections, the discussion will return to the analysis of experimental data obtained from testing the specimens previously presented in Chapter 1. The classification of the mentioned data will be introduced, and then the artificial neural network will be evaluated using the same data with respect to both direct and

inverse estimations.

3.2.1 Direct and inverse problems setup

To remind the reader, in the present study, the direct problem refers to estimating failure tensile strength based on the given infill density, manufacturing angle and notch root radius, as introduced in previous chapters. However, one of the industrial problems it to identify the optimal combination of manufacturing parameters provided the requirement of strength performance and geometrical design. Typically there is more than one solution to industrial problems, whereas the selection of the optimal one requires extra considerations on other criteria such as material-saving, timesaving, environment-friendly, etc. Thus, NN will be applied first to the direct estimation for the evaluation of NN performance in dealing with both types of parameters and then to the inverse problem for solving the aforementioned industrial problem. The outcome for both types of applications will be compared with other methodologies later in order to analyse accuracy and efficiency.

3.2.2 Experimental data and classification for the direct estimation

As a recap for the reader here, the experimental data demonstrated in Table 3.1 (similar to Table 2.6 in section 2.6) was originally adopted from Ahmed and Susmel[73] from which each three repeating tested results have been averaged for simplicity in the present investigation. Eventually, there are 27 groups of testing results here, the failure tensile strength σ_f, together with the corresponding manufacturing angle θ_p, the infill density and the geometrical notch root radius. Each data group is designed to have a unique combination of manufacturing and geometrical parameters.

For a typical neural network, past studies have concluded that the proportion between the amount of training data and testing data is empirically determined to be 70% vs 30% or 80% vs 20%.[102] Another particular consideration here is the attempt to evaluate the performance of NN to deal with the *unseen* values of data. For example, the notch root radius in Table 3.1 has three different levels of value, which are 0.5mm, 1mm and 3mm. All specimens with a radius equal to 1mm are assumed to be *unknown*, composing the validation group, so that the system does not have any chances to be trained based on those data with 1mm radius. As such, the validation group consists of results from the second, fifth, eighth, eleventh, fourteenth, seventeenth, twentieth,

twenty-third and twenty-sixth specimens (shaded in Table 3.1), and the rest data from 18 specimens compose the training group.

Table 3.1 Summary of experimental data for testing U-notched specimens (direct estimation)

	Input			Output
Specimen	θ_p (°)	Infill (%)	Radius (mm)	σ_f (MPa)
1	0	30	0.5	9.7
2	0	30	1	9.5
3	0	30	3	10.9
4	0	50	0.5	13.1
5	0	50	1	13.8
6	0	50	3	14.4
7	0	70	0.5	17.4
8	0	70	1	16.9
9	0	70	3	18.6
10	30	30	0.5	8.2
11	30	30	1	8.5
12	30	30	3	10
13	30	50	0.5	11.5
14	30	50	1	12
15	30	50	3	12.5
16	30	70	0.5	12.2
17	30	70	1	11.9
18	30	70	3	13.9
19	45	30	0.5	8
20	45	30	1	8.1
21	45	30	3	9.8
22	45	50	0.5	11
23	45	50	1	11.9
24	45	50	3	13.5
25	45	70	0.5	15.1
26	45	70	1	15.2
27	45	70	3	16.4

3.3 Neural network setup for direct estimation

After the introduction of estimation problem setup and the classification of the data, this section will explain the detailed settings of the NN used for the direct estimation for readers' comprehensive understanding, although a part of the NN setup has previously been introduced in section 3.1. The network type for the direct estimation is feed-forward backpropagation, and the training function is determined to be GD and GD with momentum for further comparison with respect to their estimation accuracy and efficiency. Note here that the selection of the training functions has no impact on other setups of the network. As detailed in the previous section, the function used for performance judgement of the network is selected to be Mean Squared Error (MSE).

Apart from the input and output layer, there is one hidden layer in the network. Such choice is based on the conclusion from past studies: although increasing number of hidden layers can lead to great accuracy, but both the complexity and the training time of the network are also multiplied. Besides, a "too accurate" network can be messed up with redundant details (noises) during the training process and the overall performance, therefore, becomes worse (also known as "overfitting").[103] Considering the database in the presented study is relatively simple, one hidden layer is sufficient here.

In the hidden layer, there are five neurons, each of which has a Tansig activation function. Such choice is based on empirical decisions from past studies. Paola and Schowengerdt[104] reported that with six hidden-layer neurons, their network had the fastest classification. Xing and Li[105] also reported that the optimal number of hidden-layer neurons was five in order to achieve the best accuracy of their network. Hence, the number of neurons in hidden layer here is determined to be five.

Different from the Tansig activation function of hidden-layer neurons, the activation function of the output layer neuron is determined to be PURELIN which refers to the pure linear function. This is because the NN here is applied to solve a regression problem (not binary classification where the sigmoid function is more suitable) and the output values are unbounded. Therefore, the linear activation function is sufficient here.

As for the learning rate, it is determined to be 0.01 in the present investigation as it has been reported by Wilson and Martinez[106] that 0.01 is the learning rate which leads to the maximum of estimation accuracy and the minimum of training time. Moreover, since the default epoch number has been set to 1000 in the "nntool" of MATLAB, author keeps this hyperparameter as default

after trying other epoch numbers. Hence the network with both GD and GD with momentum are designed to be executed for 1000 epochs.

After the configuration of the neural network has been confirmed, weights and biases are then initialised to new values in preparation for training. The initialisation is based on generating a random number from the standard normal distribution (with unit standard deviation and zero mean).[107] One of benefits of using the standard normal distribution here is that all weights and biases closer to zero (but not too close) could avoid numerical instabilities, particularly for initial layers after a few layers of multiplications.

3.4 Direct estimation results

The input of the training data specified in the previous classification is first fed into the network for fitting the weights and biases. The estimated output, in this case, failure tensile strength, is then compared with the targeted output values in the training group. The comparison indicates the estimation accuracy of the generated network, which is in the form of estimation relative percentage error (similar to Equation (*8*) in section 2.4), calculated as:

$$Error = \left| \frac{\sigma_e - \sigma_f}{\sigma_f} \right| \times 100\% , \tag{27}$$

where σ_e is the estimated failure strength, and σ_f is the targeted failure strength from training data. Errors for all validation data are then averaged as a general estimation error which represents the estimation accuracy of the network.

Table 3.2 Estimation and experimental results with the comparison of the estimation errors for both GD and GDM.

	Strength			Relative error	
Specimens (R=1mm)	**Estimation σ_f (GD) (MPa)**	**Estimation σ_f (GDM) (MPa)**	**Experimental σ_f (MPa)**	**σ_f (%) for GD**	**σ_f (%) for GDM**
2	9.63	9.76	9.5	1.37	2.74
5	13.34	13	13.8	3.33	5.8
8	17.68	17.35	16.9	4.62	2.66
11	9.2	8.26	8.5	8.24	2.82
14	11.16	11.67	12	7	2.75
17	15.2	11.7	11.9	27.73	1.68
20	8.52	8.49	8.1	5.19	4.81
23	10.85	11.12	11.9	8.82	6.55
26	15.16	14.77	15.2	0.26	2.83
			Average Error	**7.4**	**3.6**

Table 3.2 presents the estimation results for the network using gradient descent (GD) and gradient descent with momentum (GDM) training functions, respectively. It is reported that the neural network with either training function has shown a satisfying performance with respect to estimation accuracy. It has proven that the artificial neural network can effectively be applied to estimate the failure tensile strength with not only manufacturing parameters but also geometrical design parameters.

With respect to individual accuracy, the general estimation error for GDM is 3.6% which is less than half of that for GD (7.4%). So it is seen that the gradient descent with momentum training function leads to a better estimation accuracy. It is noted that there is an error spike (27.73%) for the GD algorithm, σ_f of specimen 17. It could be because both specimen 17 and 23 share the same experimental failure strength (11.9MPa) while they have completely different manufacturing angles and infill densities. Compared with GD, GDM appears to be more robust when the training group contains these types of “ambiguous” data.

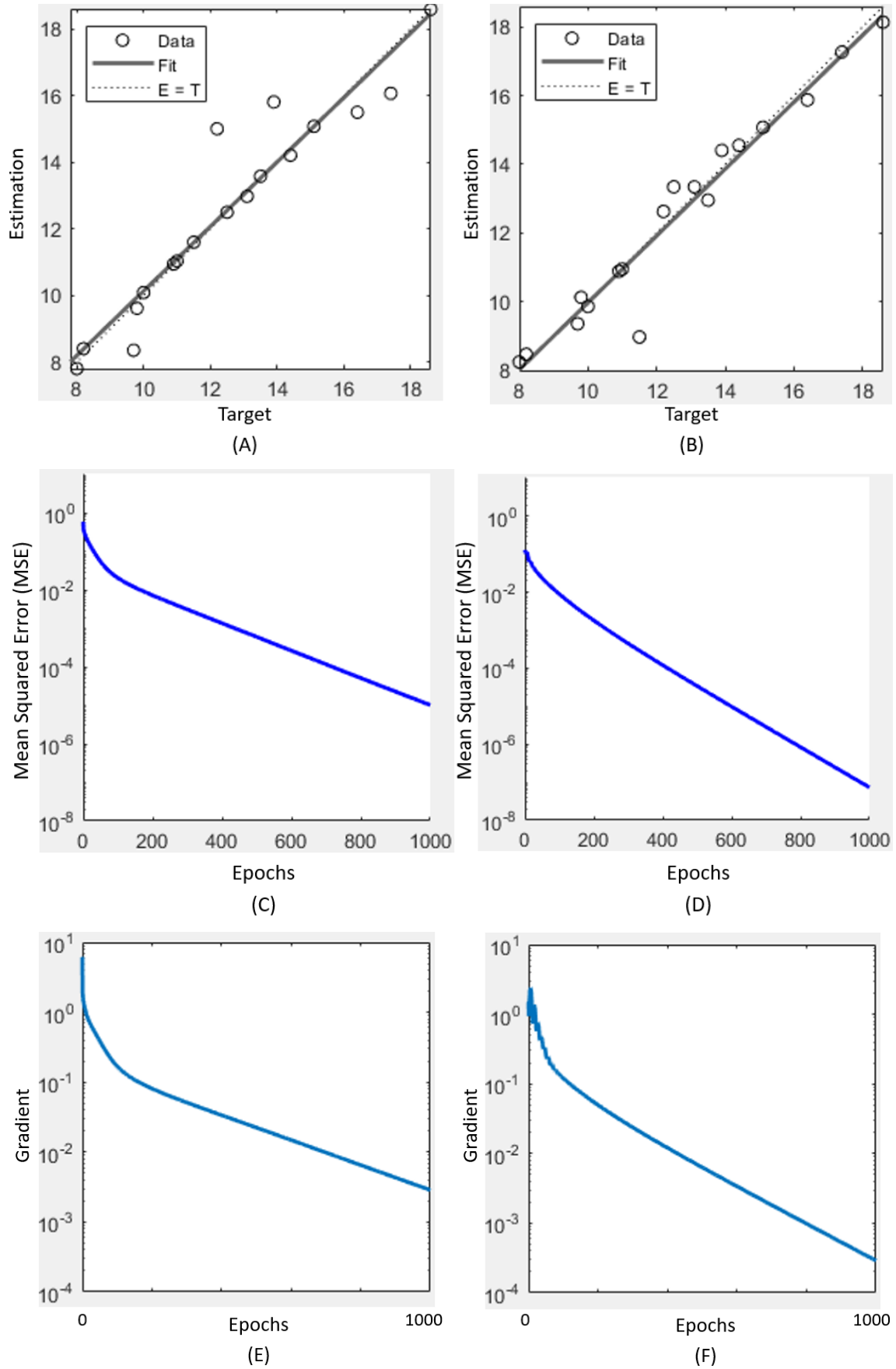

Figure 3.3 NN for the direct estimation (A) Regression result of GD; (B) Regression result of GDM; (C) Training performance of GD; (D) Training performance of GDM; (E) Gradient training state of GD; (F) Gradient training state of GDM.

Figure 3.3A and Figure 3.3B are the regression results of the network with respect to 18 training data with GD and GDM training functions, respectively. The x axis here refers to the target value (experimental data) and the y axis represents the estimated value using NN. Ideally, if the network can produce perfectly accurate estimations, estimated values are supposed to be equal to target values. The correlation of these both values indicates the strength of linear relationship between them, which is quantified using an R-value here, also known as coefficient of correlation.[108] So in other words, the R-value shows how well the training data fit the regression network model. One of the typical formulas to calculate the R-value can be expressed as:

$$R = \frac{n(\sum xy) - (\sum x)(\sum y)}{\sqrt{\left[n\sum(x^2) - (\sum x)^2\right]\left[n\sum(y^2) - (\sum y)^2\right]}}, \tag{28}$$

where n refers to the number of elements. As such, both GD and GDM have shown a good regression performance in Figure 3.3A and Figure 3.3B. The R-value for GDM is reported to be 0.97, which is slightly larger than that of GD (0.95). The result indicates that the network with GDM algorithm can produce estimations with higher accuracy. This conclusion is in accordance with the error comparison result shown in Table 3.2, i.e., GDM is more accurate.

As for the efficiency of both training functions, Figure 3.3C and Figure 3.3D show the change in MSE with respect to epoch numbers. With increasing epoch numbers, the MSE decreases for both GD and GDM, whereas when it comes to the 1000th epoch, the final MSE is approximately at 10^{-5} for GD and 10^{-7} for GDM. Therefore, with the same amount of iteration, the difference between the estimated value and the actual targeted value is smaller for GDM than for GD. In other words, the GDM training function leads to the faster convergence of the cost function.

Different from the criterion of MSE, the efficiency for using both training functions is compared in Figure 3.3E and Figure 3.3F. Both gradients decrease as the epoch number increases; however, the final gradient at the 1000th epoch is at 10^{-3} for GD, and the gradient for GDM is at 10^{-4}. Note here that the smaller gradient means the network is closer to convergence. Hence, the comparison once again indicates that the application of the GDM function leads to a better estimation efficiency than the GD function.

Summarising, the artificial neural network has shown a great performance with respect to the direct estimation of failure tensile strength of a 3D-printed part based on the given manufacturing angle, infill density and notch root radius. The application of the gradient descent with momentum

training function effectively improves the estimation accuracy and efficiency of the neural network.

3.5 Inverse estimation with the artificial neural network

As mentioned in section 3.2.1, the current industrial problem is to identify the optimal manufacturing parameters (the manufacturing angle and the infill density) with the given requirement of strength and design (the failure tensile strength and the notch root radius). Dwelling on the success of NN in direct estimation, this section will introduce the application of NN in inverse estimation. As the mathematical basis of a NN has been illustrated in previous sections, it will not be explained here.

The experimental data is then classified as shown in Table 3.3, similar to Table 2.8 in section 2.7.1, which includes experimental data repeated from Table 3.1 but rearranged, and both training and validation group classifications are identical to the ones used in the previous direct estimation.

The neural network used for the inverse estimation is also a feed-forward backpropagation network which uses both GD and GDM algorithms as training functions. Although in the direct estimation, GDM has proven to be better than GD, it is still worth the comparison in the inverse estimation in order to check the consistency with the previous conclusion (GDM has shown to have better accuracy and efficiency). Identical to the configuration of NN in the direct estimation, there is one input layer, one hidden layer and one output layer. The hidden layer has five neurons with the Tansig activation function, and the output layer has one output neuron whose activation function is the pure linear function.

Table 3.3 Summary of experimental data for the inverse estimation.

	Input		Output	
Specimen	Radius (mm)	σ_f (MPa)	θ_p (°)	Infill density(%)
1	0.5	9.7	0	30
2	1	9.5	0	30
3	3	10.9	0	30
4	0.5	13.1	0	50
5	1	13.8	0	50
6	3	14.4	0	50
7	0.5	17.4	0	70
8	1	16.9	0	70
9	3	18.6	0	70
10	0.5	8.2	30	30
11	1	8.5	30	30
12	3	10	30	30
13	0.5	11.5	30	50
14	1	12	30	50
15	3	12.5	30	50
16	0.5	12.2	30	70
17	1	11.9	30	70
18	3	13.9	30	70
19	0.5	8	45	30
20	1	8.1	45	30
21	3	9.8	45	30
22	0.5	11	45	50
23	1	11.9	45	50
24	3	13.5	45	50
25	0.5	15.1	45	70
26	1	15.2	45	70
27	3	16.4	45	70

3.6 Inverse estimation results and adjustments

With the data classification and the configuration of the adopted NN introduced in the last section, the topic of this section will focus on the inverse estimation results and their adjustments. The rearranged inputs shown in Table 3.3 are fed into the network for the inverse estimation. Initially, with the same configuration used in the direct estimation, the network is reported not to lead to a convergency. This could be due to the more non-linearity in the inverse estimation (from failure tensile strength and notch root radius to manufacturing parameters). After the learning rate

has been changed from 0.01 (used in direct estimation) to 0.0001 for more precision, the network succeeds in producing convergent results with both GD and GDM algorithms. Correspondingly, with a lower learning rate, the total epoch number is now redesigned up to 30000 for a complete convergency process.

The estimation results in the inverse estimation are values of the manufacturing parameters to be applied to machines and devices. Therefore, it is possible that the estimation results are mathematically correct, but the values are meaningless to 3D printers. Similar effects have been noted in section 2.8. As such, similar to the adjustment steps in the FIS chapter, it is of great necessity to adjust the inverse estimated results with respect to the specifications of the software and printing. Thus, the adjustment of the manufacturing angle is based on the "proximity" principle. Mathematically, to take an example of adjustments between 0° and 15°, the proximity principle can be expressed as follows:

$$If\ 0° \leq \theta_p < 7.5°, \theta_p = 0°\ ;$$

$$If\ 7.5° \leq \theta_p < 15°, \theta_p = 15°\ .$$

Similarly, according to the particular specification, the infill density has an increment of 10%, and it follows the same principle of proximity.

Table 3.4 and Table 3.5 present the inverse estimation results from the generated neural network using both GD and GDM algorithms, respectively. The estimated results have been adjusted with respect to the specifications of the aforementioned 3D printer and software. The experiment output in both tables refers to the actual targeted values of the manufacturing angles and infill densities and is eventually compared with adjusted estimation results.

Table 3.4 Summary of estimation results from the network using the gradient descent algorithm.

	Estimation Output		Adjusted Estimation		Experiment Output		Absolute Error	
Spec	**θ_p (°)**	**Infill(%)**	**θ_p (°)**	**infill(%)**	**θ_p (°)**	**infill(%)**	**Error θ_p (°)**	**Error infill(%)**
2	38.21	30.25	45	30	0	30	45	0
5	11.71	61.88	15	60	0	50	15	10
8	1.71	67.59	0	70	0	70	0	0
11	39.57	28.43	45	30	30	30	15	0
14	24.48	46.72	30	50	30	50	0	0
17	25.12	45.96	30	50	30	70	0	20
20	39.78	28.14	45	30	45	30	0	0
23	25.17	45.91	30	50	45	50	15	0
26	7.66	66.41	15	70	45	70	30	0
					Average Error		**13.3**	**3.3**

Table 3.5 Summary of estimation results from the network using the gradient descent with momentum algorithm.

	Estimation Output		Adjusted Estimation		Experiment Output		Absolute Error	
Spec	**θ_p (°)**	**Infill(%)**	**θ_p (°)**	**infill(%)**	**θ_p (°)**	**infill(%)**	**Error θ_p (°)**	**Error infill(%)**
2	18.53	31.88	15	30	0	30	15	0
5	14.03	60.14	15	60	0	50	15	10
8	-0.06	69.49	0	70	0	70	0	0
11	38.79	28.4	45	30	30	30	15	0
14	32.87	50.92	30	50	30	50	0	0
17	32.62	50.41	30	50	30	70	0	20
20	60	30.46	60	30	45	30	15	0
23	32.60	50.37	30	50	45	50	15	0
26	-1.1	65.25	0	70	45	70	45	0
					Average Error		**13.3**	**3.3**

It is interesting to point out in Table 3.5, both specimens 8 and 26 have negative manufacturing angles. Note that in fuzzy inference system (FIS), the estimation result is constrained by the existing knowledge or expert experience; therefore, it is unlikely to have negative values for θ_p. However, as a universal approximator, neural network does not have such boundary restrictions; hence, it is possible to have negative values in this investigation. Particularly for θ_p, negative values are still "achievable" in the manufacturing of 3D-printed components. Same negative values will appear in later chapters as well.

Different from the relative percentage error calculated in Equation (*27*), the inverse estimation accuracy is evaluated in the form of absolute error, as shown in Equation (*29*). Due to the presence of "0" at θ_p of the experiment output, the relative error calculation could cause a meaningless value. As such, the absolute error calculation is adopted here based on the estimated outputs (P_{est}) and targeted experiment outputs (P_{exp}).

$$Error = \left|P_{est} - P_{exp}\right|. \tag{29}$$

As to the comparison between GD and GDM algorithms, it is noted that the inverse estimation network with GD and GDM share the same absolute error after the results adjustments. However, the absolute error of using GDM has a smaller standard deviation of the estimation errors for θ_p (calculated as 13.12°) than that of using GD (calculated as 14.91°). Since the smaller standard deviation means data are more clustered around the mean, the estimation results of using GDM are considered to be more concentrated. Hence, the GDM training algorithm is considered to have better estimation accuracy than GD in inverse estimation.

It is noted here that the error spike talked in the direct estimation shows up again here, this time not for specimen 17 but for specimen 26 for both GD and GDM and specimen 2 for GD. The error spike mainly happens to the estimation of manufacturing angle as the infill density is more dominant in determining failure strength. Hence, the estimation of the less dominant parameter, manufacturing angle, in this case, could sometimes be inaccurate. Particularly, such inaccuracy tends to happen to the boundary data as there are no more "outer" data helping constrain both boundary data. In this case, both boundary data are similar to the extrapolation points with respect to the rest data points. Therefore, the estimation accuracy could decrease, particularly at both boundaries.

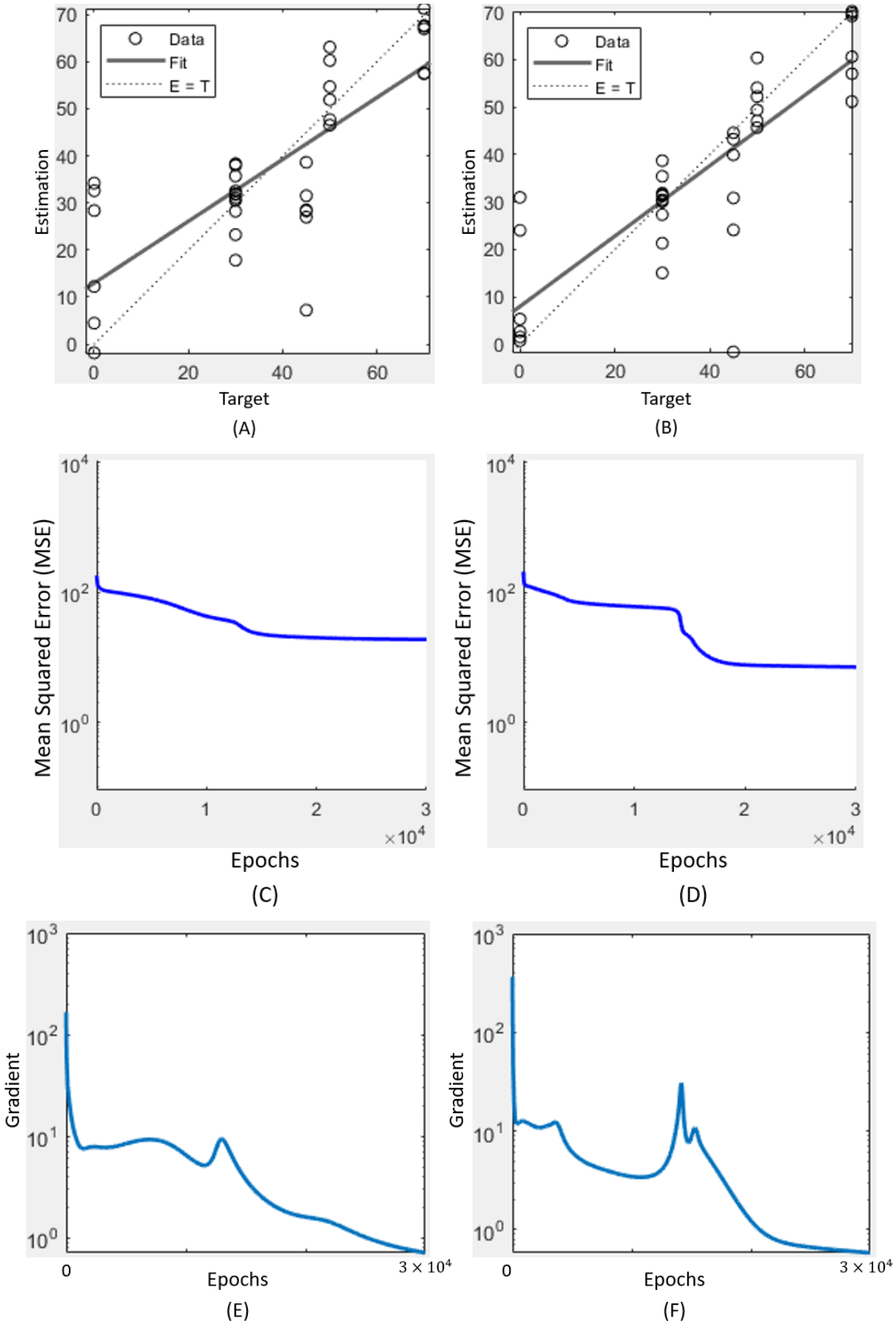

Figure 3.4 NN for inverse estimation (A) Regression with GD; (B) Regression with GDM; (C) Training performance with GD; (D) Training performance with GDM; (E) Gradient training state with GD; (F) Gradient training state with GDM.

As for the estimation efficiency, Figure 3.4A and Figure 3.4B are the regression results of the network with GD and GDM algorithms, respectively. The R-value for inverse estimation is reported to be 0.78 for GD and 0.82 for GDM, respectively, from which once again, GDM has shown better regression fitting than GD. Figure 3.4C and Figure 3.4D show the change of MSE with all epochs, and both GD and GDM have a final MSE at approximately 10^1. However, in detail, it can be seen that the MSE in Figure 3.4D is still smaller than that in Figure 3.4C, which means the convergence of using GDM is faster than GD, and the final estimation accuracy of using GDM could be slightly better. According to Figure 3.4E and Figure 3.4F, the GDM has a smaller final gradient value (reported to be 0.58) than that of GD (reported to be 0.71) at 30000 epochs, which once again shows a consistent conclusion to the previous ones.

Generally, the generated network has shown good estimation performance with respect to both the efficiency and accuracy of the inverse estimations. However, the current estimated and adjusted results are to be validated once more for whether these manufacturing parameters could lead to the desired mechanical property of the printed parts.

3.7 Numerical validation

As the NN methodology has successfully given accurate adjusted estimation results for the inverse estimation, it is now suggested to have a validation test to evaluate the adjustments in inverse estimations and the full capability of the NN methodology. Similar "numerical" validation test has been conducted in previous sections of FIS, and for the sake of completeness, it is here conducted again for NN. Considering the high accuracy of the estimation results for the direct problem, the "validation" here refers to the unconventional usage in a numerical rather than traditionally experimental sense.

For a recap for readers, the idea of such a validation test is explained here again. The numerical validation process is illustrated in Figure 3.5 seen in Chapter 2, which starts from using the inverse estimation of NN (denoted F_1) to inversely estimate manufacturing parameters based on required failure strength and geometrical design. The inverse estimation follows the aforementioned process in this chapter. From the inverse estimation, the estimated manufacturing angle and infill density are then brought into the direct estimation of NN (denoted F_2), together with the notch root radius, to *(re-)estimate* the corresponding failure strength. Note that at the start of this chapter, for the introduction of NN, the actual manufacturing parameters from the validation group were used instead of the inversely estimated ones in the direct NN.

The newly estimated strength values from F_2 are then compared with those of the original experimental values (target value), i.e. product design requirements. The comparison indicates the estimation performance of the NN framework and the effect of the adopted adjustments.

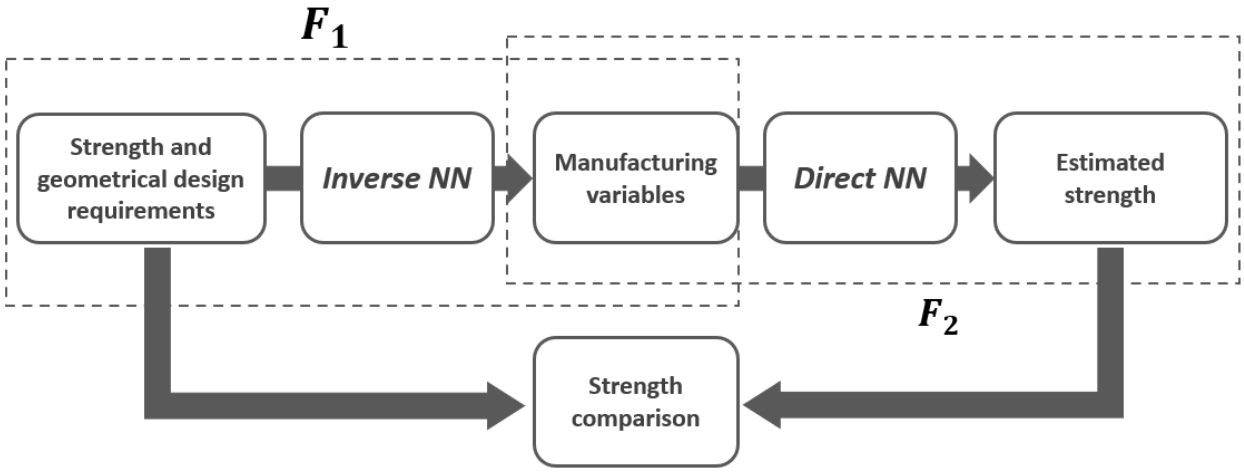

Figure 3.5 Explanation of inverse and direct estimation using NN where F1 refers to the inverse estimation and F2 is the direct validation estimation.

The re-estimated results are shown in Table 3.6, which contains the comparison between the numerical validated and experimental failure tensile strength. It is calculated that the average absolute error between the estimated and experimental strength is 0.58MPa, which is relatively small compared with experimental results. It is noted here that this 0.58MPa have already included the intrinsic estimation error from both inverse and adjusted-direct estimations. Therefore, it can be concluded here that the inverse estimation and adjustments using the NN are effective, and the estimated manufacturing parameters with NN can be applied to 3D printers with high accuracy. Note that the comparison of these numerically validated results of using NN with other methodologies will be illustrated in later chapters.

Table 3.6 Estimated manufacturing angle and infill density are brought back into the NN direct estimation to estimate the failure strength, which is to be compared with the experimental failure strength for R=1 specimens.

	Manufacturing parameters (adjusted)		Strength		Absolute error
Specimens (R=1mm)	θ_p (°)	Infill(%)	Estimation σ_f	Experimental σ_f	σ_f (abs)
2	15	30	9.94	9.5	0.44
5	15	60	12.2	13.8	1.6
8	0	70	15.2	16.9	1.7
11	45	30	8.57	8.5	0.07
14	30	50	12.2	12	0.2
17	30	50	12.2	11.9	0.3
20	60	30	8.57	8.1	0.47
23	30	50	12.2	11.9	0.3
26	0	70	15.3	15.2	0.1
				Average Error	**0.58**

3.8 Study of cost-control relevant parameters with neural network

In the previous chapter, studies have been conducted, including printing period and material weight/consumption as additional cost-relevant inputs for the inverse estimations. It has previously been proven that the addition of both cost-relevant parameters can lead to better estimation accuracy of using FIS. As such, for the sake of completeness and contrast, experimental data with additional parameters are here fed to the existing NN model. Considering the better accuracy and efficiency of using the GDM algorithm, an study is conducted based on the NN model with the GDM algorithm. Note here that the configuration of the network is identical to the previous network used for inverse estimation except for including two extra input parameters.

Table 3.7 Inverse NN estimation of manufacturing parameters with printing period and material weight included.

	Input				Experiment output		Estimated adjusted output		Error without time and weight (from Table 3.5)		Error including time and weight	
No.	Radius (mm)	σ_f (Mpa)	Time (mins)	Weight (g)	θ_p (°)	Infill (%)	θ_p (°)	Infill (%)	ABS error θ_p	ABS error infill	ABS error θ_p	ABS error infill
1	0.5	9.7	93	8	0	30						
2	1	9.5	94	8	0	30	0	30	15	0	0	0
3	3	10.9	97	8	0	30						
4	0.5	13.1	101	9	0	50						
5	1	13.8	102	9	0	50	15	50	15	10	15	0
6	3	14.4	105	9	0	50						
7	0.5	17.4	109	10	0	70						
8	1	16.9	110	10	0	70	15	70	0	0	15	0
9	3	18.6	113	10	0	70						
10	0.5	8.2	93	8	30	30						
11	1	8.5	94	8	30	30	30	30	15	0	0	0
12	3	10	96	8	30	30						
13	0.5	11.5	101	9	30	50						
14	1	12	102	9	30	50	30	50	0	0	0	0
15	3	12.5	105	9	30	50						
16	0.5	12.2	109	10	30	70						
17	1	11.9	110	10	30	70	45	70	0	20	15	0
18	3	13.9	113	10	30	70						
19	0.5	8	92	8	45	30						
20	1	8.1	93	8	45	30	45	30	15	0	0	0
21	3	9.8	96	8	45	30						
22	0.5	11.0	100	9	45	50						
23	1	11.9	101	9	45	50	45	50	15	0	0	0
24	3	13.5	104	9	45	50						
25	0.5	15.1	108	10	45	70						
26	1	15.2	109	10	45	70	30	70	45	0	15	0
27	3	16.4	112	10	45	70						
								Average error	**13.3**	**3.3**	**6.7**	**0**

Table 3.7 presents the inverse estimation results of the manufacturing angle and infill density based on the “new” inputs, which are notch root radius, failure tensile strength, printing period and material weight. The acquisition of the printing period and material weight data has been

introduced in the FIS chapter. The printing period refers to the overall time in minutes it takes for the printing process, and the material weight is the weight of filaments consumed for the printing process. Both parameters are directly linked with manufacturing cost, so they are also considered cost-relevant. Once again, the hypothesis here is that the printing period and the material weighted acquired from the software CURA are identical to the actual experimental values.

It can be seen from Table 3.7 that the addition of both cost-relevant parameters leads to an obvious decrease in absolute estimation error: from 13.3° to 6.7° for manufacturing and from 3.3% to 0% for infill density, respectively. Once again, it proves that for both FIS and NN methodologies, including both cost-relevant parameters could generally lead to better estimation accuracy. Generalising further, as the error of the manufacturing angle had no change in the study in the FIS chapter, it can be concluded that there is more estimation accuracy improvement for the manufacturing angle, particularly for the NN model.

3.9 Conclusion

In the present investigation, key steps of artificial neural network setup have been discussed and demonstrated. Gradient descent with moment algorithm has shown improvements in both estimation accuracy and efficiency of the artificial neural network methodology, compared with the conventional gradient descent algorithm.

Generally, NN has provided a great estimation accuracy both in the direct problem and the inverse problem. It is also a comprehensive solution which can be applied with various types of parameters. Including the cost-relevant parameters when using NN has shown a positive influence on the estimation accuracy for both manufacturing angle and infill density. Hence, manufacturers could find the optimal manufacturing parameters and have a cost-control tool at the same time by adopting NN models.

Summarising, The NN methodology has appeared to be a robust and precise prediction tool. NN methodology not only has the potential to become a decision-making tool in design problems but also could be particularly effective in control systems due to its self-governing factor. Considering the computation pattern the NN has, it is expected to be very successful when used together with big data for parameter calibration. This, at the same time, is also a requirement of computing power. Accordingly, the results calculated from the NN approach could be highly accurate when large groups of data are included. Apart from the capability of modelling and predicting the mechanical behaviour/strength of engineering components and structures, the NN

approach will also play a significant role in the real-time control system, big data streams, artificial intelligence, automated driving, etc.

Although NN has shown great potential as a precise and robust data-driven technique, the time-consuming training process can sometimes compromise its advantages of precision when the efficiency of the technique is a priority. Hence, in Chapter 4, a combination of the previous two methodologies will be introduced, known as the adaptive fuzzy inference system, which takes advantage of both previous approaches.

Chapter 4

Adaptive Neural Fuzzy Inference System

After introducing both FIS and NN methodologies in the previous chapters, it is seen that both methodologies have their advantages and disadvantages. FIS is able to handle inaccurate or indeterministic inputs by including engineering uncertainties in the form of membership values. Prior knowledge, expert opinions and intuitions could provide a flexible and tuneable simple-structured system for interpretations. However, some aspects of the FIS approach still need a better understanding, such as there are no effective standard solutions to transform human knowledge or expert intuition into fuzzy rules and data. As such, aimed at using the recursive learning capability of NN to determine the MF parameters, Jang first proposed an integrated approach named adaptive neural fuzzy inference system (ANFIS).[109]

This chapter first introduces the architecture and the training process of ANFIS. The main aspects of the adaptive neural fuzzy inference system (ANFIS) will be discussed in detail, including all necessary steps for building up ANFIS models. Furthermore, as one of the main focuses of the present investigation, ANFIS will be adopted for both previously introduced direct and inverse estimations, and the performance of the methodology will be evaluated with respect to the estimation accuracy and efficiency.

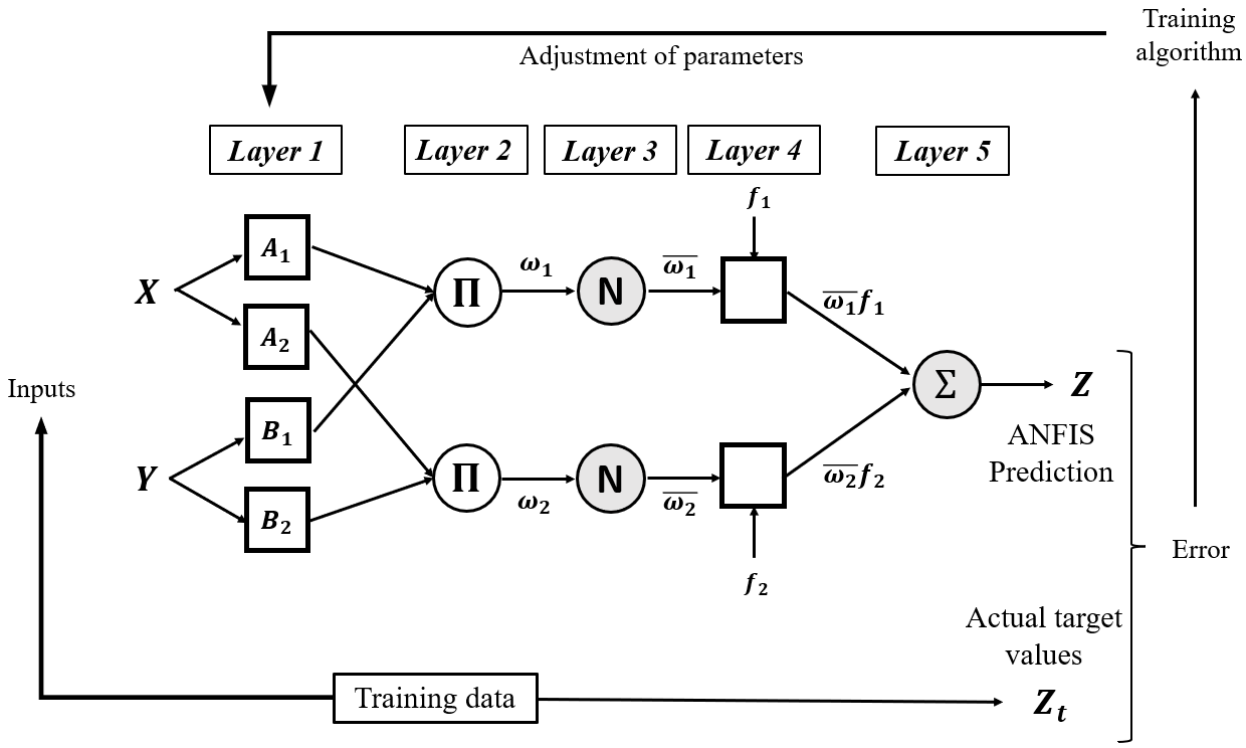

Figure 4.1 Decomposition of an adaptive neural fuzzy inference system.

4.1 Architecture

ANFIS is an integration of Sugeno FIS and NN methodologies, as it includes the uncertainty reasoning process of FIS and the iterative learning and connection pattern of NN. As shown in Figure 4.1, the structure of a typical ANFIS is similar to that of a feed-forward and backpropagation NN.

Note here that although it is the main purpose to introduce the architecture of ANFIS, it is also necessary to introduce the basic FIS in the adaptive network. The FIS involved in the ANFIS shown in Figure 4.1 has two inputs, X and Y, and one output, Z. Suppose there are two fuzzy rules in the adopted FIS:

Rule 1: If X is A_1 and Y is B_1, then $f_1 = p_1x + q_1y + r_1$;

Rule 2: If X is A_2 and Y is B_2, then $f_2 = p_2x + q_2y + r_2$;

where A_1, A_2, B_1 & B_2 are linguistic labels or specific values of the input variable X and Y, respectively; f_1 and f_2 are output MFs, and are selected as linear equation here. x and y are values from input 1 and input 2, respectively; p_i , q_i & r_i are constant coefficients ensuring the establishment of both rules. Note that linear equations are used here as the iterative calculation

process (thanks to the neural-like structure) can help identify these unknown parameters. However, there is no such calculation scheme back in the fuzzy inference system (FIS) chapter, which used constant as MF outputs.

As far as the structure is concerned, it is seen in Figure 4.1 that there are five layers of nodes which are similar to the neurons used in conventional NN. Each of these layers is interpreted as follows:

Layer 1 – The first layer is a fuzzification layer where each node holds the fuzzified membership value of the crisp input. The output of the nodes at this layer can be represented as:

$$O_i^1 = \begin{cases} \mu_{A_i}(x), & \forall i = 1, 2, \\ \mu_{B_i}(y), & \forall i = 1, 2, \end{cases} \tag{30}$$

where $\mu(x)$ is the membership function which fuzzifies the crisp inputs into membership values. In order for completeness and comparison with the previously introduced FIS approach, here, the membership function is still selected as triangular MF due to its simplicity. As a recap here for readers, the triangular MF can be expressed as Equation (*31*) or in a simplified form as Equation (*32*):

$$\mu(x) = \begin{cases} 0, & x \le a \\ \dfrac{x-a}{b-a}, & a < x \le b \\ \dfrac{c-x}{c-b}, & b < x < c \\ 0, & x \ge c \end{cases}, \tag{31}$$

$$\mu(x) = \max\left(\min\left(\frac{x-a}{b-a}, \frac{c-x}{c-b}\right), 0\right), \tag{32}$$

where a, b & c are the MF parameters for the ANFIS. Parameters in this layer are referred to as *premise* parameters, as the fuzzification of inputs is dependent on these premise parameters before the fuzzified data is transmitted to other nodes. Note here that these MF parameters are adaptive (square nodes in Figure 4.1) and equivalent to the weights in NN, which will be updated recursively during the system training process. The update of these parameters will be introduced in the next section, together with the training strategy.

Layer 2 – This layer contains the implication of the acquired membership values from the first layer. The product of input signals (membership values) is the output of the nodes at this layer, and the implication process is similar to the introduction of implication in the FIS chapter. The node output can be calculated as follows:

$$O_i^2 = \omega_i = \mu_{A_i}(x) \times \mu_{B_i}(y)\,, \qquad \forall i = 1, 2, \tag{33}$$

where ω_i refers to the firing strength of the node, i.e., the product of both relevant membership values acquired from the previous layer.

Layer 3 – Layer 3 is known as the normalisation layer, where the previously acquired firing strength is normalised with respect to each fuzzy rule. The normalisation result, which is also the output of the nodes at this layer, is calculated by the ratio of the specific firing strength for the ith rule to the sum of all firing strengths, as shown in Equation (*34*).

$$O_i^3 = \overline{\omega_i} = \frac{\omega_i}{\sum \omega_i}\,, \qquad \forall i = 1, 2, \tag{34}$$

where $\overline{\omega_i}$ is the normalised firing strength of the node. The normalisation process aims to avoid the negative impact that a possible extremely large or small firing strength could have on further calculations. The ratio in Equation (*34*) represents the importance of each fuzzy rule, i.e., which rule is activated more significantly.

Layer 4 – This is the layer where the previously acquired normalised firing strength is added to the existing rules, more specifically, the output MF (f_1 & f_2) of the existing rules. The product of the normalised firing strength and the output MF is the output of the nodes at this layer as follows:

$$O_i^4 = \overline{\omega_i} f_i = \overline{\omega_i}(p_i x + q_i y + r_i), \qquad \forall i = 1,2. \tag{35}$$

As a reminder, $f_i = p_i x + q_i y + r_i$ is the previously mentioned fuzzy rule in the present investigation, and p_i, q_i & r_i here are noted as *consequent* parameters as they are the last parameters within the system that could determine the final estimation results. The consequent parameters are also adaptive (square nodes) and will be updated during the training of the system.

Layer 5 – This layer is known as the output layer or the defuzzification layer, where the signals from the previous nodes are aggregated and defuzzified. The output of the node is the estimation result of the adaptive system and can be represented as Equation (*36*). It is noted that the expansion of the equation is identical to the weighted average calculations previously introduced as a defuzzification technique in the FIS chapter.

$$O_i^5 = \sum_i \overline{\omega_i} f_i = \frac{\sum_i \omega_i f_i}{\sum_i \omega_i}, \qquad \forall i = 1,2. \tag{36}$$

4.2 Learning strategy of ANFIS

As previously mentioned, ANFIS has a similar architecture to NN due to the benefit of recursive calculations. Therefore, the basic learning strategy of the adaptive system is similar to that of NN. The term "adaptive" here refers to the relevant parameters that are tuneable and supposed to be updated based on the specific training strategy in order to minimise the estimation error between the estimated results and the actual target results. Suppose there are P entries in the existing training data set, the estimation error for the pth entry can be represented as:

$$E_p = \left(Z_p - Z_{t_p}\right)^2, \qquad 1 \le p \le P, \tag{37}$$

where E_p refers to the squared error for the pth training data; Z_p and Z_{t_p} are the estimation results and actual target value of results for the pth training data, respectively. Note here that for an ANFIS model, the update of parameters occur after all training data have been fed into the system, i.e., after each epoch or iteration. Hence, the general estimation error E can be expressed as:

$$E = \sum_{p=1}^{P} E_p . \tag{38}$$

As mentioned previously, the training process of ANFIS is similar to that of NN, so the gradient descent training algorithm is adopted here for the update of relevant parameters. The estimated output Z_p is a function relevant to both premise and consequent parameters (see Equation (*39*)). As such, according to the calculation of the cost function in Equation (*19*), the

partial derivative of the error function with respect to each of the relevant parameters can be calculated using the chain rule, as shown in Equation (*40*):

$$Z_p = \frac{\omega_1 r_1 + \omega_2 r_2}{\omega_1 + \omega_2} = \frac{\mu_{A_1}\mu_{B_1} r_1 + \mu_{A_2}\mu_{B_2} r_2}{\mu_{A_1}\mu_{B_1} + \mu_{A_2}\mu_{B_2}} , \tag{39}$$

$$\frac{\partial E_p}{\partial a} = \sum_{Z^* \in S} \frac{\partial E_p}{\partial Z^*} \times \frac{\partial Z^*}{\partial a} , \tag{40}$$

where S refers to the set of nodes whose outputs are dependent on a. Here a is one of the parameters of the network. As the update of the corresponding parameter occur after all training data entries, the derivative of the general estimation error can be written as:

$$\frac{\partial E}{\partial a} = \sum_{p=1}^{P} \frac{\partial E_p}{\partial a} . \tag{41}$$

Thus, according to the previous application of the gradient descent algorithm in NN, the update function of the parameter a can be summarised as:

$$a^{new} = a - L\frac{\partial E}{\partial a} , \tag{42}$$

where L is the learning rate of the gradient descent algorithm and a^{new} is the updated parameter.

Note here that in the present investigation, the update of the relevant parameter happens after every epoch or iteration, normally known as batch learning or offline learning.[110] However, there is another learning paradigm for parameter update, named pattern learning or online learning. In the former case, since the update happens after all training data entries for batch learning, the derivative calculation is particularly dependent on Equation (*41*). In the latter case, parameters are updated immediately after a training data entry to the system with the online learning, so the update formula is particularly dependent on the derivative calculated in Equation (*40*). Considering the nature of pattern learning, if the calculation happens for every training data entry, the pattern learning will have relatively more computations, leading to worse computation efficiency. Thus, for the computational efficiency and completeness of the paradigm adopted in

the NN chapter, batch learning is selected in the investigation of ANFIS.

4.3 Hybrid learning strategy in ANFIS

As the basic learning strategy of ANFIS is still a gradient descent algorithm, it is desired to accomplish the parameter update in the adaptive system effectively. However, the high computational cost (even with momentum) of the GD algorithm has become one of its main drawbacks, especially when there are numerous parameters in the current system. Hence, a hybrid learning rule, first proposed by Jang,[111] could be an alternative and more efficient solution here. The hybrid learning rule is a combination of the gradient descent algorithm and the least squares estimate (LSE) approach for identifying relevant parameters, which will be introduced in the following section. Generally, in the hybrid learning strategy, the GD algorithm is applied to identify the premise parameters and the LSE is used to calculated consequent parameters.

4.3.1 Least squares estimation

For the complete introduction of the hybrid learning algorithm, the least squares estimate will be introduced in detail with a simplified example in this section. LSE is a methodology for estimating parameters by minimising the overall difference between the observed data points. Suppose there is a collection of observed data points (d_i, y_i) where $i = 1,2, \dots, l$. In order to fit a straight line to these data points, a synthetic function is defined as:

$$y_i = \beta_0 + \beta_1 d_i + n_i \,, \tag{43}$$

where β_0 and β_1 refer to the intercept and the slope of the straight line, respectively, and they are both the parameters of interest in this problem. n_i here is referred to as a disturbance term, which represents the distance from the observed data point to the point on the straight line which shares the same d_i.

The difference between y_i of the aforementioned data points and y of the point on the straight line with the same d_i is taken as residual. Such a definition leads to an expression similar to an error term, noted as:

$$R_i = y_i - f\left(d_i, \tilde{\beta}\right), \qquad \forall i = 1,2, \dots, l, \tag{44}$$

where R_i is the residual and $\tilde{\beta}$ refers to a column vector whose elements are β_0 and β_1. Here the term "least squares" indicates that the goal of the LSE approach is to identify the optimal $\tilde{\beta}$ that leads to the least squares of the residual. Hence, a more general equation can be written as follows:

$$\tilde{y} = \overline{\overline{H}}\tilde{x} + \tilde{n}\,, \tag{45}$$

where $\tilde{y}$, $\tilde{x}$ and $\tilde{n}$ are all column vectors, and $\overline{\overline{H}}$ is a matrix. Here since the $\tilde{\beta}$ is the vector of interest, it is equivalent to the $\tilde{x}$ in Equation (*45*); and the matrix of $\overline{\overline{D}}$, which contains all known d_i, is equivalent to $\overline{\overline{H}}$ here. To rewrite Equation (*43*) in a consistent form of Equation (*45*):

$$\tilde{y} = \begin{pmatrix} 1 & d_1 \\ 1 & d_2 \\ \vdots & \vdots \\ 1 & d_l \end{pmatrix}\tilde{\beta} + \tilde{n} = \overline{\overline{D}}\tilde{\beta} + \tilde{n}\,. \tag{46}$$

Returning to the term "least squares", based on Equation (*45*), the $\tilde{x}$, which minimises the residual squares, can be defined as follows:

$$\hat{x} = argmin\left\|\tilde{y} - \overline{\overline{H}}\tilde{x}\right\|^2, \tag{47}$$

where $\hat{x}$ refers to the least square estimate given by the argument that minimises the residual function. In order to solve Equation (*47*), a partial derivative of the function with respect to $\tilde{x}$ can be rewritten, as shown in Equation (*48*), and the partial derivative has to be equal to 0 in order to locate the minimum.

$$\frac{\partial}{\partial\tilde{x}}\left(\tilde{y} - \overline{\overline{H}}\tilde{x}\right)^T\left(\tilde{y} - \overline{\overline{H}}\tilde{x}\right) = \tilde{0}^T\,, \tag{48}$$

where T refers to the transpose of the vector and matrix. As mentioned earlier, $\tilde{x}$ and $\tilde{y}$ are column vectors, so $\left(\tilde{y} - \overline{\overline{H}}\tilde{x}\right)$ is still a column vector, with its transpose being a row vector. Thus, $\left(\tilde{y} - \overline{\overline{H}}\tilde{x}\right)^T\left(\tilde{y} - \overline{\overline{H}}\tilde{x}\right)$ is now a scalar, and the derivative of a scalar with respect to a column vector should be a row vector, which is represented as $\tilde{0}^T$. Now the partial derivative can be expanded and solved as follows:

$$\frac{\partial}{\partial \tilde{x}}\left(\tilde{y}^T\tilde{y} - \tilde{x}^T\bar{\bar{H}}^T\tilde{y} - \tilde{y}^T\bar{\bar{H}}\tilde{x} + \tilde{x}^T\bar{\bar{H}}^T\bar{\bar{H}}\tilde{x}\right)$$

$$= \frac{\partial}{\partial \tilde{x}}\left(-2\tilde{y}^T\bar{\bar{H}}^T\tilde{x} + \tilde{x}^T\bar{\bar{H}}^T\bar{\bar{H}}\tilde{x}\right) \tag{49}$$

$$= -2\tilde{y}^T\bar{\bar{H}} + 2\,\tilde{x}^T\bar{\bar{H}}^T\bar{\bar{H}}\,,$$

where $\tilde{y}^T\tilde{y}$ is not dependent on $\tilde{x}$, so the partial derivative of this term is 0 and omitted. The term $\tilde{x}^T\bar{\bar{H}}^T\tilde{y}$ is scalar, which is equal to its transpose, $\tilde{y}^T\bar{\bar{H}}\tilde{x}$. The calculation of the partial derivative $\frac{\partial}{\partial \tilde{x}}(\,\tilde{x}^T\bar{\bar{H}}^T\bar{\bar{H}}\tilde{x}) = 2\tilde{x}^T\bar{\bar{H}}^T\bar{\bar{H}}$ is further explained below.

Suppose the row vector $\tilde{x}^T$ and the column vector $\tilde{x}$ are $(x_1\ x_2)$ and $\begin{pmatrix}x_1\\x_2\end{pmatrix}$, respectively, and a new matrix is adopted here, which satisfies: $\bar{\bar{A}} = \bar{\bar{H}}^T\bar{\bar{H}} = \begin{pmatrix}a_{11} & a_{12}\\ a_{21} & a_{22}\end{pmatrix}$. Hence, $\tilde{x}^T\bar{\bar{H}}^T\bar{\bar{H}}\tilde{x}$ can be further expanded as:

$$\alpha = \tilde{x}^T\bar{\bar{H}}^T\bar{\bar{H}}\tilde{x} = \tilde{x}^T\bar{\bar{A}}\tilde{x} = (x_1\ x_2)\begin{pmatrix}a_{11} & a_{12}\\ a_{21} & a_{22}\end{pmatrix}\begin{pmatrix}x_1\\x_2\end{pmatrix}$$

$$= (x_1a_{11} + x_2a_{21} \quad x_1a_{12} + x_2a_{22})\begin{pmatrix}x_1\\x_2\end{pmatrix} \tag{50}$$

$$= {x_1}^2a_{11} + x_1x_2a_{21} + x_1x_2a_{12} + {x_2}^2a_{22}\,,$$

$$\frac{\partial\alpha}{\partial x_1} = 2x_1a_{11} + x_2a_{21} + x_2a_{12}\,, \tag{51}$$

$$\frac{\partial\alpha}{\partial x_2} = x_1a_{21} + x_1a_{12} + 2x_2a_{22}\,. \tag{52}$$

Both derivatives of α with respect to x_1 and x_2 are calculated in Equation (*51*) and (*52*), and it is noticed that due to its definition and nature, $\bar{\bar{A}}$ is a symmetric matrix in this case. As such, a_{21} is identical to a_{12}, and both derivatives can now be rewritten as:

$$\frac{\partial\alpha}{\partial x_1} = 2x_1a_{11} + 2x_2a_{21}\,, \tag{53}$$

$$\frac{\partial \alpha}{\partial x_2} = 2x_1 a_{21} + 2x_2 a_{22}\,. \tag{54}$$

At this stage, it is easy to find that both Equation (*53*) and (*54*) together formulate the two times of the expansion of $(x_1\ x_2)\begin{pmatrix} a_{11} & a_{12} \\ a_{21} & a_{22} \end{pmatrix}$ in Equation (*50*). Summarising, the partial derivative of α with respect to $\tilde{x}$ can be represented as:

$$\frac{\partial \alpha}{\partial \tilde{x}} = 2\,\tilde{x}^T \bar{\bar{A}} = 2\,\tilde{x}^T \bar{\bar{H}}^T \bar{\bar{H}}\,, \tag{55}$$

Thus, the calculation of the partial derivative $\frac{\partial}{\partial \tilde{x}}(\,\tilde{x}^T \bar{\bar{H}}^T \bar{\bar{H}} \tilde{x}) = 2\tilde{x}^T \bar{\bar{H}}^T \bar{\bar{H}}$ ends here. Returning to the end of Equation (*49*), the partial derivative is equal to zero row vector so that the $\hat{x}$ leading to the least squares can be further calculated as:

$$\frac{\partial}{\partial \tilde{x}} = -\,2\tilde{y}^T \bar{\bar{H}} + 2\,\tilde{x}^T \bar{\bar{H}}^T \bar{\bar{H}}\,, \tag{56}$$

$$-\,2\tilde{y}^T \bar{\bar{H}} + 2\hat{x}^T \bar{\bar{H}}^T \bar{\bar{H}} = \tilde{0}^T\,, \tag{57}$$

$$\hat{x} = \left(\bar{\bar{H}}^T \bar{\bar{H}}\right)^{-1} \bar{\bar{H}}^T \tilde{y}\,. \tag{58}$$

Therefore, the least square estimate of the proposed synthetic function in Equation (*43*) can be acquired, and it is necessary to point out that the final matrix shown in Equation (*58*) is also known as *pseudo inverse*. Note here that it needs pointing out that a particular hypothesis for Equation (*58*) is that $\bar{\bar{H}}^T \bar{\bar{H}}$ is non-singular, i.e., $\bar{\bar{H}}^T \bar{\bar{H}}$ is an invertible matrix. After the introduction of the LSE approach, the topic of the next section will return to applying the LSE approach to identify the parameters in ANFIS.

4.3.2 Calculation of consequent parameters in ANFIS

Now that the computation process of the LSE approach has been illustrated in section 4.3.1, consequent parameters can be calculated using the above equations. Note that with Equation (*58*) applied to the ANFIS, a more general calculation of consequent parameters can be given as:

$$VX = Y\,, \tag{59}$$

where V is a matrix, each row vector of which represents a pattern of the training data set. X is the vector of all consequent parameters, and Y is the vector of targeted output values from the training data.[112] For an easier understanding, $\hat{x}$ from Equation (*58*) is equivalent to X in Equation (*59*), $\overline{\overline{H}}$ is V, and $\tilde{y}$ is Y. Thus, Equation (*59*) can be further written as:

$$X = (V^T V)^{-1} V^T Y\,. \tag{60}$$

At this stage, Equation (*60*) is sufficient for the calculation of consequent parameters. However, considering the expensiveness in computation with the matrix inverse, a sequential formula of LSE is suggested here for the better efficiency of the system. Suppose the ith row vector of matrix V is noted as v_i and the ith element of vector Y is y_i; then X can be calculated iteratively using the following formulas:[113]

$$\left.\begin{aligned} X_{i+1} &= X_i + S_{i+1} v_{i+1} (y_{i+1}^T - v_{i+1}^T X_i) \\ S_{i+1} &= S_i - \frac{S_i v_{i+1} v_{i+1}^T S_i}{1 + v_{i+1}^T S_i v_{i+1}}, \qquad i = 0,1,\dots,n-1 \end{aligned}\right\}, \tag{61}$$

where S_i normally refers to the *covariance matrix*, and the final LSE result of consequent parameters is X_n. The initial condition of Equation (*61*), as introduced previously, is as follows:

$$X_0 = 0 \; and \; S_0 = \gamma I\,, \tag{62}$$

where γ is a positive big number, and I is the identity matrix of $M \times M$ (M is the number of linear parameters in f, see Figure 4.1).

4.3.3 General parameters identification process

For a more transparent illustration, the process of a hybrid learning will be explained in this section: at the beginning, with inputs of training data (18 combinations of θ_p, infill density and notch root radius) being fed into the ANFIS, the value range of each input parameter is identified

(for example in our case, [0,45] for θ_p, [30,70] for infill density and [0.5,3] for notch root radius). Users then need to specify the number and type of MFs (number of triangles in case of triangular MF) for each input parameter. Next, the initial premise parameters, i.e., both feet and peak of the triangle MF – a, b & c in Equation (*31*), are determined based on the user-defined information. In this process, for the consistency, the initial premise MF parameters used here are identical to the ones used in Chapter 2 with fuzzy inference system (FIS) (see details in section 2.3.4).

With initial premise parameters being determined, the inputs of the training data are fed into the system, fuzzified and transmitted from one node to the other until the consequent parameters in the defuzzification layer. As stated in Equation (*62*), the initial consequent parameters are all equal to 0 ($p_i = q_i = r_i = 0$), although it is inaccurate due to both initialised premise and consequent parameters.

At this stage, a simple example will be presented to show how the consequent parameters are calculated. Suppose there is only one training data entry, also the single fuzzy rule: $IF\ \theta_p = 0^\circ$ & infill density = 30% $THEN\ \sigma_f = 9.7$MPa (notch root radius will not be included in the simplified example). Vectors X and V in Equation (*59*) can now be represented as:[114]

$$V = (\ \overline{\omega_1}x\ \ \overline{\omega_1}y\ \ \overline{\omega_1}\ \ \ldots\ \ \overline{\omega_4}\ \ \overline{\omega_4}x\ \ \overline{\omega_4}y\ )$$

$$X = (\ p_1\ \ q_1\ \ r_1\ \ \ldots\ \ p_4\ \ q_4\ \ r_4\ )$$

To just look at $\overline{\omega_1}$ and ($p_1\ \ q_1\ \ r_1$) first, $V = (\ \overline{\omega_1}x\ \ \overline{\omega_1}y\ \ \overline{\omega_1}\ )$ and $X = (\ p_1\ \ q_1\ \ r_1\ )$ are brought back to Equation (*61*) (in this case, $x = 0$ and $y = 30$). Note that now with the input of 0° and 30%, the existing rule is the only fuzzy rule activated; thus, $\overline{\omega_1}$ is equal to one (both antecedents are 100% activated – 0° and 30%). Therefore, Equation (*61*) can now be further represented as:

$$
\begin{aligned}
S_1 &= S_0 - \frac{S_0 v_1 v_1^T S_0}{1 + v_1^T S_0 v_1} \\
&= S_0 - \frac{S_0 [0 \quad 30 \quad 1] \begin{bmatrix} 0 \\ 30 \\ 1 \end{bmatrix} S_0}{1 + \begin{bmatrix} 0 \\ 30 \\ 1 \end{bmatrix} S_0 [0 \quad 30 \quad 1]} \\
&= S_0 - \frac{901}{1 + 901} \approx 1 - 0.99889 \\
&= 0.00111
\end{aligned}
\tag{63}
$$

$$
\begin{aligned}
X_1 &= X_0 + S_1 v_1 (y_1^T - v_1^T X_0) \\
&= 0 + 0.00111 \times [0 \quad 30 \quad 1] \times (9.7 - 0) \\
&= 0.00111 \times [0 \quad 30 \quad 1] \times 9.7 \\
&= [0 \quad 0.32301 \quad 0.010767]
\end{aligned}
\tag{64}
$$

Thus, the first group of consequent parameters can be calculated as $p_1 = 0$, $q_1 = 0.32301$ & $r_1 = 0.010767$. The same calculation will be conducted for the rest of rules if applicable. Following the consequent parameters, there is no more unknown parameters in the forward pass of the adaptive network and the estimated result can be calculated with all input data being fed into the network.

At this stage, the first half of the hybrid learning has been finished; then, the error between the estimated results and the outputs of training data is calculated, noted as E_p (introduced in section 4.2). Similarly, the rest of the training data are fed into the system, with the same initial premise and consequent parameters, to calculate each estimation error. Eventually, the general estimation error E can be calculated using Equation (*40*) and (*41*). Accordingly, with the help of the gradient descent algorithm, a new pair of premise parameters can be calculated with Equation (*42*). The calculation of gradient descent has been introduced in Chapter 3 and the only difference is that in Chapter 3, it was the weight value to be updated whereas it is MF parameters (a, b & c) here to be updated in ANFIS. So far, the first epoch of the hybrid learning has finished.

Based on the updated premise parameters from the first epoch, the inputs are again fed into the system, fuzzified with the updated MFs. With all parameters updated and calculations repeated, a new pair of consequent parameters are calculated using Equation (*61*), leading to a new estimation result. Correspondingly, a new error is then calculated for the next gradient descent operation.

Summarising, as shown in Table 4.1, in the forward pass, input data are fed forward to calculate each node output until consequent parameters are identified, and eventually, an error function is calculated. In the backward pass, the error function propagates from the output of the system to the input, and the updated premise parameters are acquired using the gradient descent approach.

Table 4.1 Various passes in the hybrid learning strategy for ANFIS

	Forward Pass	**Backward Pass**
Premise parameters	Fixed	Gradient descent (GD)
Consequent parameters	Least Squares Estimate (LSE)	Fixed
Signals	Node outputs	Error function

4.4 Adaptive neural fuzzy inference system for 3D-printed notched specimens (Direct estimation)

Starting from this section, the discussion will return to the application of the ANFIS model to formulate the relationship between various parameters of fused deposition modelling (FDM). The estimation performance of the adopted ANFIS approach will be evaluated with respect to the experimental results. The data used in this chapter with ANFIS is identical to the ones used in the NN and FIS chapters. For readers' convenience, the complete data sets will be presented again in later sections.

With the provided manufacturing angle (θ_p), infill density and notch root radius, ANFIS is applied directly to estimate the failure tensile strength (σ_f) of FDM parts. As shown in Table 4.2, shaded data sets are classified as validation data since testing the ANFIS model with unseen data (all specimens with a radius equal to 1mm) is still one of the research objectives for this chapter. Correspondingly, the rest of the data in the table are taken as training data.

It can be seen from Table 4.2 that there are three levels of inputs for θ_p ($0°, 30° \,\&\, 45°$) and infill (30%, 50% & 70%), whereas there are two levels of radius (0.5mm & 3mm). Hence, at the beginning of setting up the MFs for ANFIS, the number of MFs for all three input parameters is

3 for θ_p, 3 for infill and 2 for radius. The type of MF for all input parameters, similar to previous chapters, is determined to be triangle MF. The output MF is selected as constant since all data are deterministic in the present investigation.

The training method is determined to be hybrid learning instead of pure backpropagation, as it is more computation-efficient (illustrated in section 4.3). The training epochs are initially set to 100, and it is reported that the training error converges at approximately *40* epochs.

Table 4.2 Summary of experimental data for testing U-notched specimens (direct estimation).

	Input			Output
Specimen	θ_p (°)	Infill (%)	Radius (mm)	σ_f (MPa)
1	0	30	0.5	9.7
2	0	30	1	9.5
3	0	30	3	10.9
4	0	50	0.5	13.1
5	0	50	1	13.8
6	0	50	3	14.4
7	0	70	0.5	17.4
8	0	70	1	16.9
9	0	70	3	18.6
10	30	30	0.5	8.2
11	30	30	1	8.5
12	30	30	3	10
13	30	50	0.5	11.5
14	30	50	1	12
15	30	50	3	12.5
16	30	70	0.5	12.2
17	30	70	1	11.9
18	30	70	3	13.9
19	45	30	0.5	8
20	45	30	1	8.1
21	45	30	3	9.8
22	45	50	0.5	11
23	45	50	1	11.9
24	45	50	3	13.5
25	45	70	0.5	15.1
26	45	70	1	15.2
27	45	70	3	16.4

Table 4.3 Estimation and experimental results, together with the estimation error in the form of relative percentage error for using ANFIS to estimate the failure tensile strength of 3D-printed parts.

Specimens (R=1mm)	Estimated σ_f (MPa)	Experimental σ_f (MPa)	Relative Percentage Error (%)
2	9.93	9.5	4.53
5	13.4	13.8	2.9
8	17.6	16.9	4.14
11	8.55	8.5	0.59
14	11.7	12	2.5
17	12.5	11.9	5.04
20	8.36	8.1	3.21
23	11.5	11.9	3.36
26	15.4	15.2	1.32
		Average Error	**3.06**

With the premise MF parameters and consequence parameters being identified, the inputs of the validation data are then fed into the system for the estimation results. The results are shown in Table 4.3, which compares the estimated and the actual targeted results. The estimation accuracy is evaluated in the form of the relative percentage error. The average error for direct estimation using ANFIS is calculated as 3.06%, and the maximum estimation error is less than 5%, which both prove that the ANFIS has great estimation accuracy and stability for direct estimation.

As for the efficiency of the ANFIS model, with the hybrid learning approach, the convergency happens approximately at *40* epochs with an error value of 1.324×10^{-5}. However, a simple comparative test is conducted with a pure backpropagation training approach and the result reports that the least error term is approximately equal to 2.58×10^{-3} at *100* epochs where the error function is not convergent yet. Therefore, it has been proven that the hybrid learning approach improves computational efficiency, as promised.

4.5 Inverse estimation with ANFIS

As previously introduced, both FIS and NN can be used to solve the problem of identifying the optimal manufacturing parameters with specific requirements of mechanical property and geometrical design. Owing to the success of ANFIS in direct estimation, it is another objective to evaluate the performance of applying ANFIS on inverse estimation. Similar to the previous inverse problem setup, both notch root radius and failure tensile strength are taken as new inputs, and the manufacturing angle and infill density are marked as outputs. Experimental data are rearranged as shown in Table 4.4 (similar approach as in previous chapters), particularly for the inverse estimation. The shaded data sets belong to the validation group, with the rest of the data sets being the training group.

During the setup of the ANFIS model for the inverse estimation, both radius and σ_f become new inputs, so the number of MFs for initial MFs is 2 for radius (0.5mm & 3mm) and 18 for σ_f (18 different values/levels of σ_f). Note here that there are 18 deterministic training data sets, so 18 fuzzy rules have been established for the adaptive system. The training approach remains the same, which is the aforementioned hybrid learning process for consistency with direct estimation. The training epoch is initially set equal to 100 epochs.

It needs to be pointed out that the ANFIS-estimated manufacturing angles are adjusted based on a "proximity" principle to the nearest 15° increment, similar to adjustments in previous chapters. The adjustment of the infill density follows the same principle, whereas the increment is 10%. The estimation accuracy of the ANFIS model is evaluated in the form of absolute estimation errors to avoid numerical issues related to 0° manufacturing angle.

Table 4.4 Summary of experimental data for testing U-notched specimens (inverse estimation)

	Input		Output	
Specimen	Radius (mm)	σ_f (MPa)	θ_p (°)	Infill density(%)
1	0.5	9.7	0	30
2	1	9.5	0	30
3	3	10.9	0	30
4	0.5	13.1	0	50
5	1	13.8	0	50
6	3	14.4	0	50
7	0.5	17.4	0	70
8	1	16.9	0	70
9	3	18.6	0	70
10	0.5	8.2	30	30
11	1	8.5	30	30
12	3	10	30	30
13	0.5	11.5	30	50
14	1	12	30	50
15	3	12.5	30	50
16	0.5	12.2	30	70
17	1	11.9	30	70
18	3	13.9	30	70
19	0.5	8	45	30
20	1	8.1	45	30
21	3	9.8	45	30
22	0.5	11	45	50
23	1	11.9	45	50
24	3	13.5	45	50
25	0.5	15.1	45	70
26	1	15.2	45	70
27	3	16.4	45	70

Table 4.5 Summary of the adjusted inverse estimation results from ANFIS.

	Estimation Output		Adjusted Estimation		Experiment Output		Absolute Error	
Spec (R=1mm)	θ_p (°)	Infill (%)	θ_p (°)	Infill (%)	θ_p (°)	Infill (%)	Error θ_p (°)	Error infill (%)
2	4.03	29.6	0	30	0	30	0	0
5	7.59	54.4	15	50	0	50	15	0
8	6	63.2	0	60	0	70	0	10
11	14.4	25.9	15	30	30	30	15	0
14	23.3	58	30	60	30	50	0	10
17	22.6	55.1	30	60	30	70	0	10
20	31.7	24.5	30	20	45	30	15	10
23	22.6	55.1	30	60	45	50	15	10
26	33.7	66	30	70	45	70	15	0
					Average Error		**8.3**	**5.6**

Table 4.5 presents the estimated and adjusted results for the inverse estimation using the ANFIS model. It can be seen from the table that the absolute estimation error for θ_p and infill density are 8.3° and 5.6%, respectively. It is noted that both absolute error values are approximately equal to half of the value of increments (7.5° for θ_p and 5% for infill). Hence, both inverse estimation errors have shown that the ANFIS model has a good estimation performance for the inverse estimation. It is also seen that there is no sudden error spike for ANFIS, which once again proves the stability and robustness of the approach.

As for the efficiency of using the ANFIS model in the inverse estimation, it is reported that the error function of the manufacturing angle converges at approximately *55* epochs and *65* epochs for the error function of infill density. The convergency in the inverse estimation needs more epochs compared with that in the direct estimation, which was approximately *40* epochs. Hence, the efficiency of using the ANFIS model for the inverse estimation is seen to be good but not as good as that for the direct estimation.

At this stage, ANFIS has shown good performance in both direct and inverse estimations, and both the estimation accuracy and efficiency are satisfying. For the consistency and comparison with the previous FIS and NN study, a numerical validation test is still needed to identify whether

the inversely estimated results could eventually lead to an appropriate outcome, which is desired mechanical property in this case.

4.6 Numerical validation

As seen in Table 4.5, the absolute estimation error for both manufacturing angle and infill density is 8.3° and 5.6%, respectively. For the numerical validation test process shown in Figure 4.2 (similar to previous chapters), ANFIS is used first to estimate the optimal manufacturing parameters with the given requirement of mechanical property and geometrical design (denoted as F_1). With the adjusted results, ANFIS is then used for the direct estimation from inversely estimated manufacturing angle, infill density, and notch root radius to the failure tensile strength (denoted as F_2).

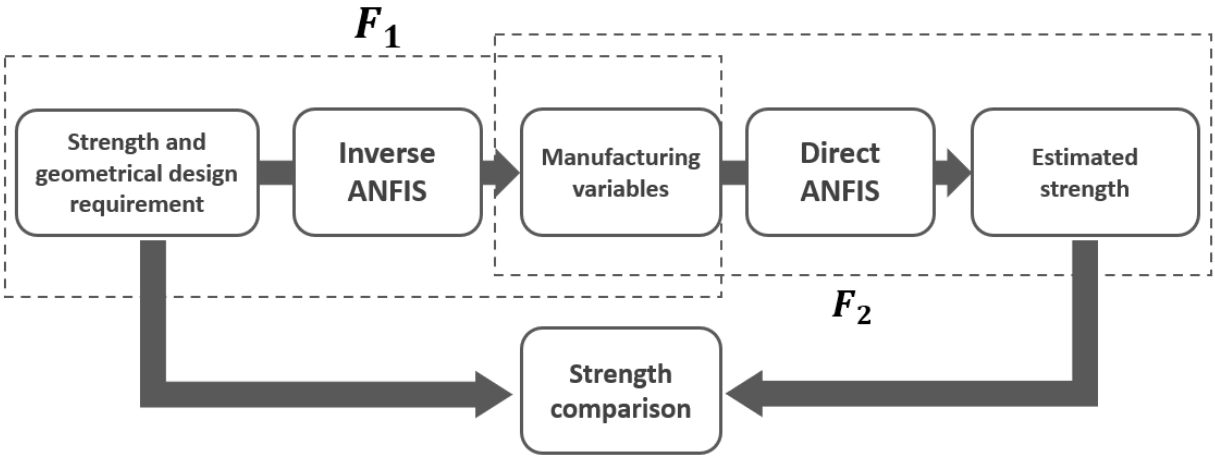

Figure 4.2 Explanation of inverse and direct estimation using ANFIS where F1 refers to the inverse estimation and F2 is the direct validation estimation.

As listed in Table 4.6, the "manufacturing parameters" column contains the estimated and adjusted results from the inverse estimation F_1. These inversely estimated parameters are then taken as new inputs in the direct estimation F_2. With the training data remaining the same, the difference between the direct estimation in the numerical validation and the previously introduced vanilla direct problem is that the inputs of the testing data are inversely estimated manufacturing parameters for the former.

The final average absolute estimation error for the numerical validation is calculated as 0.85MPa, which is relatively small compared with the actual failure tensile strength. Since this error value already includes the calculation error generated previously in both inverse and direct

estimations, such validation result has proven that the inverse estimation with the ANFIS model can provide effective manufacturing parameters to be used by the software and the 3D printer.

Table 4.6 Estimated manufacturing angle and infill density are brought back into the ANFIS direct estimation to estimate the failure tensile strength, which is to be compared with the experimental failure strength for R=1 specimens.

	Manufacturing parameters (adjusted)		Strength		Absolute error
Specimens (R=1mm)	θp(°)	Infill(%)	Estimation σ_f(MPa)	Experimental σ_f(MPa)	σ_f (MPa)
2	0	30	9.92	9.5	0.42
5	15	50	12.2	13.8	1.6
8	0	60	15.5	16.9	1.4
11	15	30	9.06	8.5	0.56
14	30	60	12.1	12	0.1
17	30	60	12.1	11.9	0.2
20	30	20	8.53	8.1	0.43
23	30	60	12.1	11.9	0.2
26	30	70	12.5	15.2	2.7
				Average Error	**0.85**

4.7 Study of cost-control relevant parameters with adaptive neural fuzzy inference system

After analysing the full capability of ANFIS, this section will evaluate the performance of ANFIS dealing with cost-control parameters, i.e., printing period and material consumption as additional industrial requirements. Since both parameters are industrial-concerned, they are considered industrial requirements, together with the mechanical property. The data of the printing period and the material consumption are once again extracted from the CURA software[115] with different design models loaded. For the completeness and consistency of the investigation of the cost-control parameters, the training and testing specimens remain in the same classification in both direct and inverse estimation.

Table 4.7 Inverse ANFIS estimation of manufacturing parameters with printing period and material weight included.

	Input				Experiment output		Estimated adjusted output		Absolute error without time and weight (from Table 4.5)		Absolute error including time and weight	
No.	**Radius (mm)**	**σ_f (Mpa)**	**Time (mins)**	**Weight (g)**	**θ_p (°)**	**Infill (%)**	**θ_p (°)**	**Infill (%)**	**ABS error θ_p**	**ABS error infill**	**ABS error θ_p**	**ABS error infill**
1	0.5	9.7	93	8	0	30						
2	1	9.5	94	8	0	30	0	30	0	0	0	0
3	3	10.9	97	8	0	30						
4	0.5	13.1	101	9	0	50						
5	1	13.8	102	9	0	50	15	50	15	0	15	0
6	3	14.4	105	9	0	50						
7	0.5	17.4	109	10	0	70						
8	1	16.9	110	10	0	70	15	70	0	10	15	0
9	3	18.6	113	10	0	70						
10	0.5	8.2	93	8	30	30						
11	1	8.5	94	8	30	30	30	30	15	0	0	0
12	3	10	96	8	30	30						
13	0.5	11.5	101	9	30	50						
14	1	12	102	9	30	50	30	50	0	10	0	0
15	3	12.5	105	9	30	50						
16	0.5	12.2	109	10	30	70						
17	1	11.9	110	10	30	70	15	70	0	10	15	0
18	3	13.9	113	10	30	70						
19	0.5	8	92	8	45	30						
20	1	8.1	93	8	45	30	30	30	15	10	15	0
21	3	9.8	96	8	45	30						
22	0.5	11	100	9	45	50						
23	1	11.9	101	9	45	50	30	50	15	10	15	0
24	3	13.5	104	9	45	50						
25	0.5	15.1	108	10	45	70						
26	1	15.2	109	10	45	70	45	70	15	0	0	0
27	3	16.4	112	10	45	70						
							Average error		**8.3**	**5.6**	**8.3**	**0**

Table 4.7 reports that with printing period and material consumption as new inputs to the inverse ANFIS, the new estimation error for the manufacturing angle and infill density are 8.3° and 0%, respectively. It is seen that including both cost-relevant parameters does not influence the estimation accuracy of the manufacturing angle but has a significantly positive influence on the infill density (from 5.6% average error to 0%).

As for the efficiency of using ANFIS with two extra cost-relevant parameters, it is reported that the final error of the manufacturing angle (10^{-2}) is much higher than that of infill density (10^{-4}). Moreover, even if it takes only approximately *65* epochs for the error function to converge with infill density, it takes more time for the computation in each epoch due to the additional input parameters (more parameter calculations). Hence, the calculation for the extra-parameter study is even more time-consuming than using the NN in the previous chapter. More specifically, the overall time it takes for the error function to converge for infill density in the extra-parameter study is approximately twice the time it takes for the original inverse estimation with only two input parameters. This is due to the additional input parameters, together with their MFs, could lead to a dramatic increase in computations, which makes the whole computation process much slower than the previous inverse estimation with only two inputs (θ_p and infill density).

Summarising, including the cost-relevant parameters improves the infill density estimation accuracy of ANFIS, but the manufacturing angle has little impact from including the printing period and the material consumption. Moreover, with the increasing number of inputs for the ANFIS, it could lead to expensive computations since, correspondingly, the number of premise parameters will increase dramatically.

4.8 Conclusion

In the present investigation, the main aspects of ANFIS and the steps of setting up an adaptive system have been discussed and analysed, with particular attention paid to the iterative calculation in the system. Here ANFIS has shown its capability of both direct and inverse estimations, where the direct estimation using ANFIS has a better estimation accuracy than the inverse. The adjustment of the ANFIS inverse estimation results, i.e., manufacturing parameters, has proven effective for achieving the desired mechanical property.

Due to the fact that ANFIS is a combination approach of both FIS and NN, ANFIS is seen to deal with not only mechanical parameters but also geometrical and cost-control relevant ones, with a recursive computation process assuring the general estimation accuracy. Hence, it can be concluded that ANFIS is a comprehensive data-driven methodology that can be widely applied in

engineering fields, particularly for problems such as manufacturing parameters optimisation, mechanical property prediction, etc.

Summarising, The ANFIS methodology has appeared to be a precise and robust prediction tool. Potentially, the ANFIS methodology could become an effective decision-making tool in design problems and a self-governing control system. Considering the computation process of the ANFIS, it is expected to be very successful when used together with big data but also requires computing power at the same time, considering the potential expensive computation of MF parameters. Accordingly, ANFIS could give a highly accurate estimation and appears to be the most accurate methodology compared with FIS and NN, which will be illustrated in detail in the next chapter. In addition to the modelling and prediction of the mechanical behaviour/strength of engineering components and structures, ANFIS methodology could also play an essential role in various applications such as real-time control systems, artificial intelligence, automated driving, etc.

Chapter 5

Comparative Study of All Adopted Methodologies

After introducing the main aspects of FIS, NN and ANFIS methodologies, a comparative study is introduced in this chapter for all previous approaches with respect to their estimation efficiency, accuracy and other criteria. It is desired to achieve the conclusion of which methodology is optimal, but it is also expected that each of these methodologies might have its advantages and disadvantages in different cases.

5.1 Design of Experiments

Before comparing both the estimation accuracy and efficiency of FIS, NN and ANFIS, as discussed in Chapter 1, it is the author's attempt to present a comparative study of another statistical approach as a contrast method here, which is known as the design of experiments (DOE).

5.1.1 Direct estimation with design of experiments

The basis of DOE has been introduced in section 1.2.4 and the DOE approach will be used in this section for direct estimation. For consistency, the training and validation data classification here is identical to the previous pattern for the other methodologies. According to the MS Excel built-in data analysis tool, the coefficients for the direct estimation are calculated as shown in Table 5.1.

Table 5.1 The MS Excel analysed ANOVA results which include both the coefficients and the corresponding P-values for the direct estimation.

	Coefficients	P-value
Intercept, b	4.915952	0.000268
θ_p	-0.04524	0.007479
Infill	0.154167	2.31×10^{-7}
Radius	0.613333	0.013386

Therefore, the statistical model of the direct estimation can be expressed as follows:

$$\sigma_f = 4.915952 - 0.04524\theta_p + 0.154167Infill + 0.613333Radius\,, \tag{65}$$

Note here that together with the coefficients, P-value is also included in Table 5.1, and it normally indicates how incompatible the data are with a null hypothesis.[116] Here, the null hypothesis suggests that no statistical relationship exists between the observed variables (inputs) and the observed phenomena (outputs). The null hypothesis presumes to be valid until existing evidence indicates otherwise.[117] Hence, in other words, the smaller P-value means there is a greater statistical incompatibility of the data with the null hypothesis.[118]

It can be found in Table 5.1 that all P-values are smaller than 0.05, which is typically considered a threshold of the P-value with respect to statistical incompatibility. So all input variables are significant to some extent, whereas the infill density appears to have the largest incompatibility among all variables, including the intercept, b. Therefore, it is consistent with the previous conclusion that the infill density is the most dominant variable with respect to the failure tensile strength in the present investigation. According to the DOE model, the intercept is the second significant variable, while the manufacturing angle and the notch root radius are dividedly third and least important variables.

Table 5.2 Estimation results vs experimental results, together with the relative percentage error of the estimation.

Spec	Estimated outputs	Experimental outputs	Error (%)
2	10.2	9.5	6.51
5	13.2	13.8	3.75
8	16.3	16.9	3.48
11	8.8	8.5	4.07
14	11.9	12	0.85
17	15	11.9	25.64
20	8.1	8.1	0.15
23	11.2	11.9	5.9
26	14.3	15.2	5.83
		Average	6.2

Returning to Equation (*66*), after the determination of relevant coefficients, the inputs of the validation data are fed into the equation, and the corresponding σ_f are calculated. These estimated results, together with estimation errors (relative percentage error), are shown in Table 5.2. It is reported that the average estimation error for using DOE is 6.2% in the direct estimation. It is interesting to point out that the estimation error of specimen 17 is significantly larger than others, which could be because of the identical experimental results (11.9MPa) in specimen 23.

5.1.2 Inverse estimation with design of experiments

Following the direct estimation results of using DOE, the inverse estimation results will be presented in this section. With the same classification of the training and validation data group, the inverse estimation using DOE has a similar parameter setup to the previous inverse estimations: both manufacturing angle and infill density are to be estimated as unknown manufacturing parameters while notch root radius and failure tensile strength are taken as input parameters. Since the statistical model introduced in the last section is for a single output variable, there will be two models to be identified for both manufacturing parameters in this section.

As shown in Table 5.3, the coefficients of manufacturing angle and infill density are calculated, and the corresponding statistical models can be expressed as follows:

$$\theta_p = 47.51581 + 1.20154Radius - 1.95903\sigma_f\,, \tag{66}$$

$$Infill = -8.4621 - 3.11979Radius + 5.08661\sigma_f\,, \tag{67}$$

where Equation (*67*) and (*66*) are for modelling the manufacturing angle and the infill density, respectively.

It is seen from Table 5.3 that, on the one hand, for the manufacturing angle, P-values for the radius and the strength are much larger than 0.05, which means the manufacturing angle could be less significant to the notch root radius and the failure tensile strength. On the other hand, for the infill density, P-values for the radius and the strength are both less than those of the manufacturing angle. Meanwhile, the P-value for the failure strength is much smaller than that of the radius. Therefore, such contrast indicates that the infill density is more dominant in determining the geometrical and strength parameters. Furthermore, the infill density appears to be more directly relevant to the failure tensile strength compared with the notch root radius.

Table 5.3 The MS Excel analysed ANOVA results which include both the coefficients and the corresponding P-values for the inverse estimation.

	θ_p		*Infill*	
	Coefficients	***P-value***	***Coefficients***	***P-value***
Intercept, b	47.51581	0.033188	-8.4621	0.341068
radius	1.20154	0.757503	-3.11979	0.073775
σ_f	-1.95903	0.24585	5.08661	2.28E-06

Table 5.4 reports the estimation results of using DOE, together with the adjusted results according to the CURA software specifications. Due to the presence of "0" manufacturing angle, the absolute error is used here to evaluate the inverse estimation accuracy of using DOE. It is reported that the average absolute error for the manufacturing angle and the infill density is 13.3° and 4.4%, respectively.

Table 5.4 Summary of the adjusted inverse estimation results of using DOE.

	Estimation Output		Adjusted Estimation		Experiment Output		Absolute Error	
Specimen (R=1mm)	θ_p (°)	Infill (%)	θ_p (°)	Infill (%)	θ_p (°)	Infill (%)	Error θ_p (°)	Error infill (%)
2	30	36.9	30	40	0	30	30	10
5	21.8	58.4	15	60	0	50	15	10
8	15.6	74.4	15	70	0	70	15	0
11	32.2	31.4	30	30	30	30	0	0
14	25.2	49.4	30	50	30	50	0	0
17	25.4	49	30	50	30	70	0	20
20	32.8	29.7	30	30	45	30	15	0
23	25.4	49	30	50	45	50	15	0
26	19	65.6	15	70	45	70	30	0
						Average Error	13.3	4.4

Table 5.5 Estimated manufacturing angle and infill density are brought back into the DOE direct estimation to estimate the failure strength, which is compared with the experimental failure strength for R=1 specimens.

	Manufacturing parameters (adjusted)		Strength		Absolute error
Specimens (R=1mm)	θp(°)	Infill(%)	Estimation σ_f(MPa)	Experimental σ_f(MPa)	σ_f (MPa)
2	30	40	10.3	9.5	1.4
5	15	60	14.2	13.8	1.0
8	15	70	15.9	16.9	0.4
11	30	30	8.8	8.5	0.7
14	30	50	11.9	12	0.7
17	30	50	11.9	11.9	0.8
20	30	30	8.8	8.1	1.1
23	30	50	11.9	11.9	0.8
26	15	70	15.9	15.2	1.3
				Average Error	**0.9**

As explained in previous chapters, a numerical validation is applied here to demonstrate the accuracy of the inverse estimation and also for further comparison with the results from other methods. The estimated manufacturing angle and infill density from the inverse estimation are brought back to the direct estimation framework for the newly estimated failure strength. The final average absolute estimation error between the estimated and experimental results is 0.9MPa (see Table 5.5) and it will be further compared with the results of other methods regarding the estimation accuracy.

5.1.3 Conclusion of using the design of experiments

It is reported from the previous sections that with the DOE methodology, the average direct estimation accuracy is equal to 6.2% (failure tensile strength), and the average inverse estimation accuracies are 13.3° for the manufacturing angle and 4.4% for the infill density, respectively. The results indicate that the DOE has a good estimation accuracy in both direct and inverse estimations. They will also be compared with the results of using other three methodologies in following sections regarding the estimation performance.

5.2 Comparison of all methodologies with respect to the estimation accuracy

5.2.1 Accuracy of direct estimations

As one of the main statistical characteristics, the estimation accuracy of the adopted methodologies is of great importance for the investigation. Table 5.6 reports the previously calculated relative percentage estimation error for direct problems. Each of the five columns represents the calculated error for the corresponding methodology, including FIS (Sugeno), NN (GD algorithm), NN (GDM algorithm) and ANFIS.

Note that in the initial study of the direct estimation using FIS (section 2.6), the validation group includes 12 specimens (specimen 2, 4, 6, 8, 11, 13, 15, 17, 20, 22, 24 & 26). However, for investigating the performance of all methodologies to deal with the unseen value (radius equal to 1mm), the validation group has then been updated to have nine specimens (specimen 2, 5, 8, 11, 14, 17, 20, 23 & 26) in the inverse estimation. Hence, for the consistency of the validation specimens in various methodologies, the validation group in the direct estimation of using FIS has been amended to the latest nine specimens.

Table 5.6 Comparison of the direct estimation relative percentage error using all adopted methodologies.

Spec	FIS Sugeno Error (%)	NN GD Error (%)	NN GDM Error (%)	ANFIS Error (%)	DOE Error (%)	FIS ABS Error (MPa)	NN GD ABS Error (MPa)	NN GDM ABS Error (MPa)	ANFIS ABS Error (MPa)	DOE ABS Error (MPa)
2	4.63	1.02	2.37	4.53	6.51	0.44	0.1	0.23	0.43	0.62
5	2.9	3.36	5.77	2.9	3.75	0.4	0.46	0.8	0.4	0.52
8	4.14	4.63	2.66	4.14	3.48	0.7	0.78	0.45	0.7	0.59
11	0.82	8.23	3.23	0.59	4.07	0.07	0.7	0.27	0.05	0.34
14	4.17	6.96	2.77	2.5	0.85	0.5	0.84	0.33	0.3	0.1
17	5.04	27.73	1.69	5.04	25.64	0.6	3.30	0.2	0.6	3.05
20	3.33	5.22	4.85	3.21	0.15	0.27	0.42	0.39	0.26	0.01
23	3.36	8.86	6.59	3.36	5.9	0.4	1.05	0.78	0.4	0.7
26	0.66	0.29	2.82	1.32	5.83	0.1	0.04	0.43	0.2	0.88
AVE	**3.2**	**7.4**	**3.6**	**3.06**	6.2	**0.39**	**0.86**	**0.43**	**0.37**	**0.76**

Apart from the update in the validation group, the type of FIS is also updated in the comparative study. Considering the Sugeno fuzzy system adopted for the inverse estimation is more suitable with deterministic output values, the Sugeno FIS is applied in this chapter for both direct and inverse FIS estimation for consistency. As such, new estimation results (with new Sugeno FIS and updated validation group) are calculated, and their estimation errors are also presented in the "FIS Sugeno" column, Table 5.6.

It is seen that the NN with GD method has the worst estimation error, equal to 7.4% but replacing the GD with GDM for the NN leads to a significant drop in error from 7.4% to 3.6%. Meanwhile, the estimation error is 6.1% for the DOE method, 3.2% for the Sugeno FIS method separately, following the least estimation error of the ANFIS, which is equal to 3.06%. It is also reported that apart from specimen 17 for NN with the GD algorithm and specimen 17 for DOE, the rest of the three methodologies have been shown to provide accurate results with stable error fluctuations.

Hence, with the same training and testing setup, it can be concluded that the FIS, NN and ANFIS are all effective methodologies for the prediction of mechanical property with given manufacturing and geometrical parameters. The ANFIS has the best estimation accuracy for direct estimation, although the FIS and the NN with the GDM algorithm both lead to a similar level of

estimation error to that of ANFIS with little deduction in estimation accuracy.

Note that Table 5.6 also includes the absolute error for the direct estimation, which is because the direct estimations are evaluated in the form of relative percentage error, whereas the inverse estimations are evaluated by absolute errors. In order to compare both direct and inverse estimation results with respect to the estimation accuracy, the absolute errors for the direct estimations are also calculated in Table 5.6.

5.2.2 Accuracy for inverse estimations

Table 5.7 reports the absolute error for the inverse estimations of using all three methodologies, together with each corresponding numerical validation result. Note that in the direct estimation, the GDM has shown a significantly better performance than the GD algorithm. Hence, the NN with the GD algorithm is not included in Table 5.7 for the simplicity of comparison. Note here that the term "Num valid ABS error" in the table refers to the absolute error of comparing the numerical validated failure strength and the actual experimental one.

It is seen that ANFIS lead to an 8.3° of absolute error for the manufacturing angle, whereas both NN with GDM and DOE lead to an absolute error of 13.3°. The FIS methodology gives the least absolute error or manufacturing angle, which is 6.7°. Therefore, compared with other two methodologies, the FIS methodology gives the better estimation result of the manufacturing angle.

As for the infill density, Table 5.7 reports that the ANFIS approach gives an estimation error of 5.6MPa, while the general estimation error for DOE, FIS and NN are calculated as 4.4MPa, 4.4MPa and 3.3MPa, respectively. Thus, although the FIS and ANFIS both have good estimations, NN has the best estimation accuracy with respect to the infill density of the 3D printing.

Since the conclusion of the analysis of the manufacturing angle and the infill density are different, it is necessary to have a comprehensive conclusion which takes both variables into account. Hence, as previously introduced, the estimated values of both variables are fed into corresponding direct systems (numerical validation) to generate a new estimation of the failure tensile strength. The absolute estimation error between the actual experimental tensile strength and this newly estimated failure strength is calculated, which is the outcome of the numerical validation process shown in Table 5.7. The outcome error of the numerical validation can be interpreted as the comprehensive inverse estimation error. In order to evaluate the inverse estimation process, the error from the numerical validation is then compared with the error of the single direct estimation in Table 5.6. Note that the comprehensive estimation error here already includes the intrinsic error generated during the adjustments with respect to the specifications of CURA software. Hence, it is expected that the comprehensive errors are slightly larger than those

from the direct estimations.

Table 5.7 Comparison of the inverse estimation absolute error using all adopted methodologies.

Spec	FIS angle ABS error	FIS Infill ABS error	FIS Num valid ABS error	NN angle ABS error	NN infill ABS error	NN Num valid ABS error	ANFIS angle ABS error	ANFIS infill ABS error	ANFIS Num valid ABS error	DOE angle ABS error	DOE infill ABS error	DOE Num valid ABS error
2	0	0	0.44	15	0	0.44	0	0	0.42	30	10	1.4
5	30	10	1.6	15	10	1.6	15	0	1.6	15	10	1.0
8	15	0	1.7	0	0	1.7	0	10	1.4	15	0	0.4
11	0	0	0.07	15	0	0.07	15	0	0.56	0	0	0.7
14	0	10	0.2	0	0	0.2	0	10	0.1	0	0	0.7
17	0	10	0.3	0	20	0.3	0	10	0.2	0	20	0.8
20	15	0	0.27	15	0	0.47	15	10	0.43	15	0	1.1
23	0	10	0.3	15	0	0.3	15	10	0.2	15	0	0.8
26	0	0	0.1	45	0	0.1	15	0	2.7	30	0	1.3
AVE	**6.7**	**4.4**	**0.55**	**13.3**	**3.3**	**0.58**	**8.3**	**5.6**	**0.85**	13.3	4.4	**0.9**

It is seen that from Table 5.6, the absolute direct estimation error for FIS, NN-GDM, ANFIS and DOE are equal to 0.39MPa, 0.43MPa, 0.37MPa and 0.76MPa, respectively, in the direct estimation. In the inverse estimation, the error acquired from the numerical validation for FIS, NN-GDM, ANFIS and DOE is equal to 0.55MPa, 0.58MPa, 0.85MPa and 0.9MPa, respectively. Hence, it can be concluded from the above comparison that:

- The estimation errors of the inverse-validation operation are higher than those of the direct estimations for all three methodologies, i.e., the direct estimation framework is always more accurate compared with the inverse estimation framework;
- The ANFIS methodology has the best estimation accuracy in direct estimation, whereas the FIS methodology has the best accuracy in inverse-validation estimation;
- Although all methodologies can give accurate estimation results, DOE appears to have the least estimation accuracy for both direct and inverse estimations. It is consistent with the existing studies comparing DOE with other approaches in other applications.[70,119]

To summarise, in the single direct estimation problems, ANFIS is able to give the best estimation results, whereas in the inverse problems, FIS appears to give better estimation results. Both differences are non-neglectable but within the acceptable fluctuation range.

5.3 Estimation efficiency

In the present investigation of using the FIS methodology, the determination of the membership functions is based on i) the type of the adopted MF (triangle MF in this case); ii) historical data which has been used for generating fuzzy rules (training group). After the determination of the MFs, each membership value is calculated with respect to inputs from the validation group and then processed with product operation and implication process. Finally, the desired estimation result is calculated with the weighted average of the previously calculated membership values.

Generally, FIS is a computationally cheap methodology without a recursive calculation process. Based on the code developed by the author, the return of both direct and inverse estimations results are instant and the estimation time is within seconds even with additional cost-relevant parameters. Conventionally, tuning the membership parameters could have been time-consuming as they depend on the user's intuition and knowledge. However, due to the parameters of MF in the present investigation depending on the existing historical data, the tuning process has been integrated with the historical data. Hence, the FIS methodology is efficient without a redundant calculation process.

As for the neural network, the recursive updates of weight values and partial derivatives both add more computations to the system. As illustrated in Chapter 3, the total number of epochs for an NN could be up to 10^4 in order to reach the convergence of the cost function, which could take 1min for the author's computer to accomplish in the present investigation. With additional cost-relevant parameters included, it took 2mins for the author's computer to accomplish the estimation.

For the recursive calculations of the ANFIS approach, the weight updates in NN are replaced by the updates of the MFs parameters. Meanwhile, the parameters of output MF needs further calculations, which in this case are linear parameters to be determined, p_i, q_i & r_i. In this case, there are more parameters to be determined compared with NN. Hence, although it is reported in Chapter 5 that it takes approximately only *60* epochs for the cost function to converge, the calculation of each epoch for ANIFS actually takes much more time compared with that of NN. According to the author's tests, the general time it takes for the convergency of the cost function could be up to 1.5mins. With additional cost-relevant parameters included, it took 3.5mins for the

estimation on author's computer. Considering the influence of the increasing number of parameters in the recursive calculations on the overall efficiency, the time consumption of the ANFIS methodology will increase exponentially if more parameters are included in the system.

Last but not least, as a MS Excel built-in data analysis tool, DOE is a quick and accessible method. Without the recursive calculation process, DOE is relatively computational cheap and has little requirements of computational power. Hence, DOE estimation is an efficient estimation method, benefiting from its simple calculations and low study cost, compared to other methods.

5.4 Comparison of FIS, NN and ANFIS methodologies

After both estimation accuracy and the efficiency of all methodologies have been compared, the present section will include a general comparison and conclusion. The FIS approach appears to be the most efficient methodology with the parallel data processing pattern. In the present investigation, MF parameter tunning process has been changed to an integrated process thanks to the deterministic historical data. This saves the time which could have been spent on tuning the MF parameters for optimisation purposes.

NN and ANFIS have good estimation performance with respect to the accuracy, but they are computationally expensive due to the nature of the recursive calculations. In the present investigation, the calculation time for both methodologies appears to be acceptable, thanks to the simplicity of the test setup. However, note that both methodologies could become more time-consuming when applied with big-data tests or with the increasing number of parameters.

Although the DOE methodology is not accurate as FIS, NN and ANFIS methodologies, it is still a quick, easy and effective MS Excel built-in tool for some modelling problems, especially for those who had no experience in other data-driven methodologies. Besides, DOE has a unique capability (also an advantage) of identifying the main factors and quantifying the significance of each input variable through a few parameters, such as the P-value in the present investigation. Hence, instead of being used alone, it is suggested that the design of experiments could be used together with other more accurate data-driven methodologies to reach a better estimation accuracy and identify main factors simultaneously.

Therefore, when it comes to the actual cases, the factors of applications and methodologies, such as the number of available data, time limit, estimation accuracy and hardware capability, may require further considerations and compromises for the selection of the methodology. Generally, for the current stage, with estimation accuracy as the priority, the FIS methodology could be an efficient choice. However, when an extensive database is available, and the computing

power is not a compromising factor, the ANFIS methodology could help achieve the most accurate estimation results.

Chapter 6

Conclusion and Future Work

In the present study, addressing the lack of knowledge of the complex physical relationship between the manufacturing parameters and the mechanical property of FDM 3D-printed parts, multiple data-driven methodologies have been adopted and applied to formulate the mathematical relationship. The manufacturing parameters here refer to the manufacturing angle and the infill density of the FDM process, while the mechanical property in this study particularly refers to the failure tensile strength of the printed parts.

First of all, the 27 specimens in previous chapters have proven to be sufficient for evaluating the performance of the frameworks and methodologies as it covers all possible configurations of manufacturing and geometrical parameters. Based on that, two frameworks – direct and inverse have been developed. The direct estimation framework is designed to estimate the failure tensile strength of the FDM parts with the provided manufacturing angle and infill density. With the aim of extending the methodology applications, the inputs of the direct estimation include the notch root radius as a geometrical design characteristic. The results of all adopted methodologies have proven that the data-driven approaches can be applied with not only manufacturing parameters but also geometrical design parameters for the prediction of tensile strength with good accuracy.

The inverse estimation framework is designed to identify the optimal combinations of the various manufacturing parameters ensuring given requirements of strength and geometry. In this case, the inputs of the inverse estimation system are the failure tensile strength and the notch root radius, and the outputs of the system are the manufacturing angle and the infill density. The inverse estimation results for all analysed methodologies are adjusted according to the specifications of the CURA software for meaningful and usable values, and the inverse-estimated results have been validated with a numerical validation process. Generally, it has been proven that

all the adopted data-driven methodologies could support the inverse estimation framework.

Since the aim of the inverse estimation is to help industries identify the optimal manufacturing parameters, a study has been conducted to include cost-control relevant parameters as extra inputs for the inverse estimation framework. It has been reported that including additional cost-relevant parameters, such as printing time and material consumption, could lead to a more accurate estimation of process parameters with all the adopted methodologies. In the following sections, a summary of achieved goals and conclusions from previous chapters will be summarised.

6.1 Fuzzy inference system

The main aspects of a fuzzy inference system have been illustrated where the conventional linguistic labels are replaced by deterministic values. Hence, it has saved much time for the determination and the tunning process of the membership function parameters. FIS has shown good estimation accuracy for both direct and inverse estimations.

It has been reported that the additional data for the system could effectively lower the estimation error. Furthermore, by excluding each input parameter at a time, the key parameter that leads to the best estimation results is reported to be the infill density, followed by the manufacturing angle. Meanwhile, the additional input parameter – manufacturing void size d_v, interconnected with the infill density, is reported to cause worse estimation accuracy. Hence, the presence of repeating or interconnected parameters should be avoided for FIS methodology.

By including the notch root radius as an additional geometrical parameter, the supportive study has reported that FIS can be applied with not only manufacturing parameters but also geometrical design parameters for the prediction of tensile strength. As such, FIS is seen to have great potential as a decision-making tool in design and fracture-related problems.

The Sugeno FIS adopted in the inverse estimation has been illustrated with particular emphasis on the difference between the Sugeno FIS and the previously adopted Mamdani FIS. The performance of the FIS approach in dealing with unseen data has been evaluated with a good estimation result. The corresponding inverse estimation results are adjusted according to the specifications of the compatible 3D-printing software, and the estimated results have been validated with a numerical validation process. Although the inverse estimation accuracy of using FIS is less than that of direct estimation, the developed inverse framework is still trustworthy, considering its satisfying accuracy.

With the additional cost-relevant parameters, such as printing time and material consumption, a better FIS estimation accuracy has been achieved, particularly in estimating the infill density.

Hence, it can be concluded in general that the FIS methodology is a precise and efficient tool for problems such as property predictions.

6.2 Artificial neural network

The main aspects of the artificial neural network have been illustrated with particular emphasis on comparing both the gradient descent and the gradient descent with momentum algorithms with respect to their estimation accuracy and efficiency. It has been reported that the accuracy of using GDM is higher than that of using GD for direct estimation. Meanwhile, the convergence of the cost function with GDM is faster than that with GD, which means the GDM algorithm is relatively more efficient. Hence, the NN with GDM algorithm is reported to be a generally better solution concerning accuracy and efficiency than the NN with GD.

It has been reported that the inverse estimation of using NN with both GDM and GD has a good performance with respect to accuracy. Considering the final gradient value, the GDM is seen to be more efficient than the GD algorithm. With the extra cost-relevant parameters included as inputs, the estimation accuracy of both manufacturing parameters is seen to improve.

Summarising, comparing both the direct and inverse estimations of using NN, the estimation accuracy of the direct estimation is better than that of the inverse estimation, which is also consistent with that of the FIS methodology. As for the efficiency, considering the number of epochs and the overall time it takes for the cost function convergency, the NN is a precise methodology but has requirements of computation power. Due to the nature of the recursive calculations, NN could be time-consuming depending on the number of parameters and the configurations of the network.

6.3 Adaptive neural fuzzy inference system

The previous chapter has illustrated the main aspects of the adaptive neural fuzzy inference system with particular introductions of the hybrid learning strategy. It has been reported that the direct estimation results of using the ANFIS approach have the best accuracy among all three adopted methodologies. For the inverse estimation, the estimation accuracy of using ANFIS is still good and at the same level as that for the FIS approach.

Meanwhile, generally the number of epochs it takes for ANFIS computation is less than that of NN and the overall time it takes for ANFIS in the direct estimation is similar to that for NN. It is noted that although it takes fewer epochs for ANFIS to achieve the best estimation system,

ANFIS methodology could still be more time-consuming and computing-power-consuming than NN. This is because, for the ANFIS methodology, there are more parameters to calculate in each epoch, especially when a big data group or multiple input parameters are included.

Similar to FIS, with additional cost-relevant parameters as inputs, the ANFIS methodology is seen to have an estimation accuracy improvement in the infill density, with no change to the manufacturing angle. Hence, it is seen that the ANFIS approach is a highly accurate methodology with requirements of relatively more computing power, compared with FIS and NN methods.

6.4 Design of experiments

In the previous chapter, the main aspects of the design of experiments have been illustrated, and the DOE methodology has been used for both direct and inverse estimations. Although it has the least accuracy among all the adopted methodologies, DOE is seen to still provide accurate estimation results as a contrast approach.

Note that DOE might not be the most accurate methodology but considering its MS built-in and ease-to-use feature, it is still a quick and efficient beginner-friendly tool, particularly for simpler problems without the requirement of deep learning. However, due to the same MS built-in feature, the calculation process is less transparent than the FIS methodology. Hence, users might have less control over the general calculation process, which makes it like one of the “Black Box” solutions.

6.5 Comparison of all the adopted data-driven methodologies

Generally, all the adopted methodologies have shown a good estimation performance of being applied to formulate the relationships between the various manufacturing/geometrical parameters and the failure tensile strength of FDM 3D-printed parts. It is important to point out that the FIS methodology is seen to be simple and accurate without high requirements of computing power. However, for unseen data which lies outside of the input range, it becomes impossible to predict with these “outliers” due to the nature of the fuzzy system.

For big data or self-adaptive/self-learning applications, NN has been reported to be the best solution, although it requires a large amount of training data and a relatively high computing power. It is important to point out that due to the recursive computation pattern, NN is capable of dealing with the “outliers” mentioned above, which is one of its main advantages.

The ANFIS is a combination of the previous two methodologies and has been reported to have

the best estimation accuracy. ANFIS is the prior choice if the most significant criterion is estimation accuracy. However, it might be less efficient than the FIS approach due to its expensive computations.

Last but not least, the DOE methodology has the advantage of identifying and quantifying the significance of each input variable, and the MS built-in characteristic makes it easy to use in simpler predictions or shallow learning with less non-linearity. It is an efficient beginner-friendly tool for those who have yet to gain experience in other data-driven methodologies.

6.6 Future work

Specifically, considering the advantage of the DOE approach in identifying and quantifying the significance of each input parameter, in the future, it is expected to have an efficient hybrid method which is a combination of both FIS and DOE methodology. Such a hybrid methodology is expected to select the main factors in the problem with the benefit of the DOE approach in the first step. Then the FIS approach could be applied with main factors for a more accurate estimation result.

Generally, the existing data-driven methodologies have shown good estimations of the tensile strength of FDM 3D-printed parts based on the manufacturing angle and the infill density. Hence, future work could be conducted by including more process parameters of the FDM process, such as layer thickness, temperatures, etc., together with the identification of the significance of each parameter. The optimisation of the printing process could produce high-quality parts with minimal defects, improved accuracy and consistency. This could also be particularly useful in applications where the FDM process is sensitive to variations in temperature, humidity and other environmental factors.

As for the properties to be estimated, other important properties can be taken into account, but other properties, such as the surface finish and the fracture behaviour under dynamic loading, could also be analysed with the same framework. Due to the intrinsic versatility of the data-driven methodology, all the considered methodologies are expected to be the same success. This could potentially lead to the application of developing smart materials that can adapt their properties in response to changes in their environment. For example, a material with a controlled thermal expansion coefficient could compensate for warping or distortion during the printing process, leading to more accurate and reliable printed parts.

Another potential avenue of investigation is the application of the proposed methodologies to other 3D printing fields, such as Laser Sintering systems. In this case, the inputs of interest could

be laser power, laser speed, laser scan spacing, etc., and the outputs of interest could be tensile modulus, ultimate tensile strength, elongation at break (ductility), the size difference between the nominal and actual sizes, etc.

Summarising, it has been proven that data-driven methodologies are robust tools that can produce highly accurate estimations even with various variables. Hence, it can be foreseen that these methodologies could be effective decision-making tools in not only 3D printing but also other fields as long as there are data to be used to formulate the relationships. Accordingly, it can be expected that data-driven methodologies will be increasingly important to human society, particularly in the digital era.

Bibliography

1 Ribeiro F. 3D printing with metals. *Comput Control Eng J*. 1998;9: 31–38.

2 Chen Z, Li Z, Li J, et al. 3D printing of ceramics: A review. *J Eur Ceram Soc*. 2019;39: 661–687.

3 Wickramasinghe S, Do T, Tran P. FDM-Based 3D printing of polymer and associated composite: A review on mechanical properties, defects and treatments. *Polymers (Basel)*. 2020;12: 1–42.

4 Luo Y, Lin Z, Guo G. Biodegradation Assessment of Poly (Lactic Acid) Filled with Functionalized Titania Nanoparticles (PLA/TiO 2) under Compost Conditions. *Nanoscale Res Lett*. 2019;14.

5 Gunaydin, Kadir & S. Türkmen H. Common FDM 3D Printing Defects. *Int Congr 3D Print (Additive Manuf Technol Digit Ind*. 2018: 1–8.

6 Masood SH. Advances in Fused Deposition Modeling. *Compr Mater Process*. 2014;10: 69–91.

7 General Electric. What is Additive Manufacturing | GE Additive. Ge.com. Available at: https://www.ge.com/additive/additive-manufacturing. Published 2022 Accessed August 19, 2022.

8 Dwiyati ST, Kholil A, Riyadi R, Putra SE. Influence of layer thickness and 3D printing direction on tensile properties of ABS material. *J Phys Conf Ser*. 2019;1402: 066014.

9 Yousefi AA. Effects of 3D printer nozzle head temperature on the physical and mechanical properties of PLA based product. In: *Developement of Carbon Nanotube / Resorcinol-Formaldehyde Gels View Project Flexible Polymer Solar Cell View Project Morteza Behzadnasab Iran Poly*. ; 2016:3–5.

10 Chacón JM, Caminero MA, García-Plaza E, Núñez PJ. Additive manufacturing of PLA structures using fused deposition modelling: Effect of process parameters on mechanical properties and their optimal selection. *Mater Des*. 2017;124: 143–157.

11 Ning F, Cong W, Hu Y, Wang H. Additive manufacturing of carbon fiber-reinforced plastic composites using fused deposition modeling: Effects of process parameters on tensile properties. *J Compos Mater*. 2017;51: 451–462.

12 Chicos LA, Pop MA, Zaharia SM, et al. Infill Density Influence on Mechanical and

Thermal Properties of Short Carbon Fiber-Reinforced Polyamide Composites Manufactured by FFF Process. *Materials (Basel)*. 2022;15.

13 Maszybrocka J, Dworak M, Nowakowska G, Osak P, Łosiewicz B. The Influence of the Gradient Infill of PLA Samples Produced with the FDM Technique on Their Mechanical Properties. *Materials (Basel)*. 2022;15.

14 Tyson E. How to use 3D print infill settings-increase strength , save filament. Rigid.ink. Available at: https://www.3dsourced.com/rigid-ink/3d-print-optimal-infill-settings/. Published 2021 Accessed August 17, 2022.

15 Tanveer MQ, Haleem A, Suhaib M. Effect of variable infill density on mechanical behaviour of 3-D printed PLA specimen: an experimental investigation. *SN Appl Sci*. 2019;1: 1–12.

16 Ramesh M, Panneerselvam K. Mechanical investigation and optimization of parameter selection for Nylon material processed by FDM. In: *Materials Today: Proceedings*. Vol 46. Elsevier Ltd; 2019:9303–9307.

17 Porter JH, Cain TM, Fox SL, Harvey PS. Influence of infill properties on flexural rigidity of 3D-printed structural members. *Virtual Phys Prototyp*. 2019;14: 148–159.

18 Schmitt M, Mehta RM, Kim IY. Additive manufacturing infill optimization for automotive 3D-printed ABS components. *Rapid Prototyp J*. 2020;26: 89–99.

19 Somireddy M, Czekanski A. Anisotropic material behavior of 3D printed composite structures – Material extrusion additive manufacturing. *Mater Des*. 2020;195: 108953.

20 Ezeh OH, Susmel L. Reference strength values to design against static and fatigue loading polylactide additively manufactured with in-fill level equal to 100%. *Mater Des Process Commun*. 2019;1.

21 Ng CT, Susmel L. Notch static strength of additively manufactured acrylonitrile butadiene styrene (ABS). *Addit Manuf*. 2020;34: 101212.

22 Ziemian C, Sharma M, Ziemi S. Anisotropic Mechanical Properties of ABS Parts Fabricated by Fused Deposition Modelling. In: *Mechanical Engineering*. IntechOpen; 2012:159–180.

23 Koch C, Van Hulle L, Rudolph N. Investigation of mechanical anisotropy of the fused filament fabrication process via customized tool path generation. *Addit Manuf*. 2017;16: 138–145.

24 Zaldivar RJ, Witkin DB, McLouth T, Patel DN, Schmitt K, Nokes JP. Influence of processing and orientation print effects on the mechanical and thermal behavior of 3D-Printed ULTEM ® 9085 Material. *Addit Manuf*. 2017;13: 71–80.

25 Weake N, Pant M, Sheoran A, Haleem A, Kumar H. Optimising parameters of fused filament fabrication process to achieve optimum tensile strength using artificial neural network. *Evergreen*. 2020;7: 373–381.

26 Nurizada A, Kirane K. Induced anisotropy in the fracturing behavior of 3D printed parts analyzed by the size effect method. *Eng Fract Mech*. 2020;239.

27 Floor J, Van Deursen B, Tempelman E. Tensile strength of 3D printed materials: Review and reassessment of test parameters. *Mater Test*. 2018;60: 679–686.

28 Mirsayar MM. A generalized criterion for fatigue crack growth in additively manufactured materials – Build orientation and geometry effects. *Int J Fatigue*. 2021;145: 106099.

29 Ezeh OH, Susmel L. Fatigue strength of additively manufactured polylactide (PLA): effect of raster angle and non-zero mean stresses. *Int J Fatigue*. 2019;126: 319–326.

30 Wang Y, Wang W, Susmel L. Constant/variable amplitude multiaxial notch fatigue of additively manufactured AISI 316L. *Int J Fatigue*. 2021;152.

31 Popescu D, Zapciu A, Amza C, Baciu F, Marinescu R. FDM process parameters influence over the mechanical properties of polymer specimens: A review. *Polym Test*. 2018;69: 157–166.

32 Kannan S, Vezhavendhan R, Kishore S, Kanumuru KV. Investigating the effect of orientation, infill density with Triple raster pattern on the tensile properties for 3D Printed samples. *IOP SciNotes*. 2020;1: 024405.

33 Yerbolat G, Shynggys A, Ali MH. Mechanical property prediction method based on multi-material 3D printer. In: *2018 Joint 7th International Conference on Informatics, Electronics and Vision and 2nd International Conference on Imaging, Vision and Pattern Recognition, ICIEV-IVPR 2018*. Institute of Electrical and Electronics Engineers Inc.; 2019:498–502.

34 Munteanu A, Chitariu DF. The neural networks used in FDM printing study. In: *MATEC Web of Conferences*. Vol 178. EDP Sciences; 2018.

35 Esakki B, Rajamani D, Arunkumar P. An Intelligent Modeling System to Predict Mechanical Strength Characteristics of Selective Inhibition Sintered Parts using Fuzzy Logic Approach. *Mater Today Proc*. 2018;5: 11727–11737.

36 Tu R, Gitman I, Susmel L. Fuzzy inference system for failure strength estimation of plain and notched 3D-printed polylactide components. *Fatigue Fract Eng Mater Struct*. 2022;45: 1663–1677.

37 Kalogirou SA. Designing and Modeling Solar Energy Systems. In: *Solar Energy Engineering*. Academic Press; 2009:553–664.

38 Wang K. Computational Intelligence in Agile Manufacturing Engineering. In: *Agile Manufacturing: The 21st Century Competitive Strategy*. Elsevier Science Ltd; 2001:297–315.

39 Rajamani D, Esakki B, Arunkumar P, Velu R. Fuzzy Logic-Based Expert System for Prediction of Wear Rate in Selective Inhibition Sintered HDPE Parts. In: *Materials Today: Proceedings*. Vol 5. Elsevier; 2018:6072–6081.

40 Gitman MB, Klyuev A V., Stolbov VY, Gitman IM. Complex Estimation of Strength Properties of Functional Materials on the Basis of the Analysis of Grain-Phase Structure Parameters. *Strength Mater*. 2017;49: 710–717.

41 Gitman IM, Klyuev A V, Gitman MB, Stolbov VY. Multi-scale approach for strength properties estimation in functional materials. *ZAMM Zeitschrift fur Angew Math und Mech*. 2018;98: 945–953.

42 Walczak S, Cerpa N. Artificial Neural Networks. In: *Encyclopedia of Physical Science and Technology*. Academic Press; 2003:631–645.

43 Lecun Y, Bengio Y, Hinton G. Deep learning. *Nature*. 2015;521: 436–444.

44 Reddy DR. Speech Recognition by Machine: A Review. *Proc IEEE*. 1976;64: 501–531.

45 Kocić J, Jovičić N, Drndarević V. An end-to-end deep neural network for autonomous driving designed for embedded automotive platforms. *Sensors (Switzerland)*. 2019;19.

46 Krizhevsky A, Sutskever I, Hinton GE. ImageNet classification with deep convolutional neural networks. *Commun ACM*. 2017;60: 84–90.

47 Gu GX, Chen CT, Buehler MJ. De novo composite design based on machine learning algorithm. *Extrem Mech Lett*. 2018;18: 19–28.

48 Liang L, Liu M, Martin C, Sun W. A deep learning approach to estimate stress distribution: a fast and accurate surrogate of finite-element analysis. *J R Soc Interface*. 2018;15.

49 Everton SK, Hirsch M, Stavroulakis PI, Leach RK, Clare AT. Review of in-situ process monitoring and in-situ metrology for metal additive manufacturing. *Mater Des*. 2016;95: 431–445.

50 Shevchik SA, Kenel C, Leinenbach C, Wasmer K. Acoustic emission for in situ quality monitoring in additive manufacturing using spectral convolutional neural networks. *Addit Manuf*. 2018;21: 598–604.

51 Williams G, Meisel NA, Simpson TW, McComb C. Design repository effectiveness for 3D convolutional neural networks: Application to additive manufacturing. *J Mech Des Trans ASME*. 2019;141.

52 Khadilkar A, Wang J, Rai R. Deep learning–based stress prediction for bottom-up SLA 3D

printing process. *Int J Adv Manuf Technol*. 2019;102: 2555–2569.

53 Sood AK, Ohdar RK, Mahapatra SS. Experimental investigation and empirical modelling of FDM process for compressive strength improvement. *J Adv Res*. 2012;3: 81–90.

54 Sood AK, Equbal A, Toppo V, Ohdar RK, Mahapatra SS. An investigation on sliding wear of FDM built parts. *CIRP J Manuf Sci Technol*. 2012;5: 48–54.

55 Vahabli E, Rahmati S. Improvement of FDM parts' surface quality using optimized neural networks - Medical case studies. *Rapid Prototyp J*. 2017;23: 825–842.

56 Mohamed OA, Masood SH, Bhowmik JL. Investigation of dynamic elastic deformation of parts processed by fused deposition modeling additive manufacturing. *Adv Prod Eng Manag*. 2016;11: 227–238.

57 Uçar T, Karahoca A, Karahoca D. Tuberculosis disease diagnosis by using adaptive neuro fuzzy inference system and rough sets. *Neural Comput Appl*. 2013;23: 471–483.

58 Al-Hmouz A, Shen J, Al-Hmouz R, Yan J. Modeling and simulation of an Adaptive Neuro-Fuzzy Inference System (ANFIS) for mobile learning. *IEEE Trans Learn Technol*. 2012;5: 226–237.

59 Mensah RA, Xiao J, Das O, Jiang L, Xu Q, Alhassan MO. Application of adaptive neuro-fuzzy inference system in flammability parameter prediction. *Polymers (Basel)*. 2020;12.

60 Raju R, Manikandan N, … DP-A in A, 2021 U. Comparative Studies on FDM based AM Process Using Regression Analysis and ANFIS Model. In: *Advances in Additive Manufacturing Processes*. ; 2021:200–215.

61 Heshmat M, Maher I, Abdelrhman Y. Surface roughness prediction of polylactic acid (PLA) products manufactured by 3D printing and post processed using a slurry impact technique: ANFIS-based modeling. *Prog Addit Manuf*. June 2022: 1–12.

62 Sedigh A, Ghelich P, Quint J, Samandari M, Tamayol A, Tomlinson RE. Approximating Scaffold Printability Utilizing Computational Methods. *bioRxiv*. July 2022: 2022.07.11.499589.

63 Yadav D, Chhabra D, Gupta RK, Phogat A, Ahlawat A. Modeling and analysis of significant process parameters of FDM 3D printer using ANFIS. In: *Materials Today: Proceedings*. Vol 21. Elsevier; 2020:1592–1604.

64 Nawafleh N, AL-Oqla FM. An innovative fuzzy-inference system for predicting the mechanical behavior of 3D printing thermoset carbon fiber composite materials. *Int J Adv Manuf Technol*. 2022;121: 7273–7286.

65 Durakovic B. Design of experiments application, concepts, examples: State of the art. *Period Eng Nat Sci*. 2017;5: 421–439.

66 Paulo F, Santos L. Design of experiments for microencapsulation applications: A review. *Mater Sci Eng C*. 2017;77: 1327–1340.

67 Yu P, Low MY, Zhou W. Design of experiments and regression modelling in food flavour and sensory analysis: A review. *Trends Food Sci Technol*. 2018;71: 202–215.

68 Schlueter A, Geyer P. Linking BIM and Design of Experiments to balance architectural and technical design factors for energy performance. *Autom Constr*. 2018;86: 33–43.

69 Durakovic B, Torlak M. Simulation and experimental validation of phase change material and water used as heat storage medium in window applications. *J Mater Environ Sci*. 2017;8: 1837–1846.

70 Aengchuan P, Phruksaphanrat B. A comparative study of design of experiments and fuzzy inference system for plaster process control. *Lect Notes Eng Comput Sci*. 2017;2229: 184–188.

71 Cimbala MJ. Taguchi Orthogonal Arrays. *Instrumentation, Meas Stat*. 2014: 4–6.

72 Walfish S. Statistical essentials - Part 4: Regression and design of experiments. *BioPharm Int*. 2008;21: 34–38.

73 Ahmed AA, Susmel L. Static assessment of plain/notched polylactide (PLA) 3D-printed with different infill levels: Equivalent homogenised material concept and Theory of Critical Distances. *Fatigue Fract Eng Mater Struct*. 2019;42: 883–904.

74 Wu W, Ye W, Wu Z, Geng P, Wang Y, Zhao J. Influence of layer thickness, raster angle, deformation temperature and recovery temperature on the shape-memory effect of 3D-printed polylactic acid samples. *Materials (Basel)*. 2017;10.

75 Ultimaker 2 Extended+ | 3DGBIRE Ltd. Available at: https://3dgbire.com/pages/ultimaker-2-extended-plus-tech-specs. Accessed November 7, 2022.

76 Zadeh LA. Fuzzy Sets. *Inf Control*. 1965;8: 338–353.

77 Özcan F, Atiş CD, Karahan O, Uncuoğlu E, Tanyildizi H. Comparison of artificial neural network and fuzzy logic models for prediction of long-term compressive strength of silica fume concrete. *Adv Eng Softw*. 2009;40: 856–863.

78 Akkurt S, Tayfur G, Can S. Fuzzy logic model for the prediction of cement compressive strength. *Cem Concr Res*. 2004;34: 1429–1433.

79 Zhao J, Bose BK. Evaluation of membership functions for fuzzy logic controlled induction motor drive. *IECON Proc (Industrial Electron Conf*. 2002;1: 229–234.

80 Harliana P, Rahim R. Comparative Analysis of Membership Function on Mamdani Fuzzy Inference System for Decision Making. In: *Journal of Physics: Conference Series*. Vol

930. ; 2017:12029.

81 Ali OAM, Ali AY, Sumait BS. Comparison between the Effects of Different Types of Membership Functions on Fuzzy Logic Controller Performance. *Int J Emerg Eng Res Technol*. 2015;3: 76–83.

82 Princy S, Dhenakaran SS. Comparison of Triangular and Trapezoidal Fuzzy Membership Function. *J Comput Sci Eng*. 2016;2: 46–51.

83 Kaur A, Kaur A. Comparison of Mamdani-Type and Sugeno-Type Fuzzy Inference Systems for Air Conditioning System. *Int J Soft Comput Eng*. 2012;2: 323–325.

84 Saletic DZ, Velasevic DM, Mastorakis NE. Analysis of basic defuzzification techniques. *Recent Adv Comput Comput Commun*. 2002: 247–252.

85 Voskoglou MG. Comparison of the COG Defuzzification Technique and Its Variations to the GPA Index. *Am J Comput Appl Math*. 2016;6: 187–193.

86 Mamdani EH, Assilian S. An experiment in linguistic synthesis with a fuzzy logic controller. *Int J Man Mach Stud*. 1975;7: 1–13.

87 Samavat T, Nazari M, Ghalehnoie M, et al. A Comparative Analysis of the Mamdani and Sugeno Fuzzy Inference Systems for MPPT of an Islanded PV System. *Int J Energy Res*. 2023;2023: 1–14.

88 Sugeno M. *Industrial Applications of Fuzzy Control*. North-Holland; 1985.

89 Gitman IM, Gitman MB, Batin SE, Boyarshinov DA. Stochastic stability of performance properties for materials with non-deterministic microstructure. *ZAMM Zeitschrift fur Angew Math und Mech*. 2020: 1–18.

90 Gitman IM, Gitman MB, Stolbov VY, Batin SE, Boyarshinov DA. Methodology to estimate the minimum number of experiments and key microstructural parameters in macroscopic strength properties evaluation. *ZAMM Zeitschrift fur Angew Math und Mech*. 2019;99: 1–9.

91 Amin Rashidifar M, Amin Rashidifar A. Analysis of Vibration of a Pipeline Supported on Elastic Soil Using Differential Transform Method. *Am J Mech Eng*. 2013;1: 96–102.

92 Goldberg Y. Neural Network Methods for Natural Language Processing. *Synth Lect Hum Lang Technol*. 2017;10: 1–311.

93 Rong-Ji W, Xin-Hua L, Qing-Ding W, Lingling W. Optimizing process parameters for selective laser sintering based on neural network and genetic algorithm. *Int J Adv Manuf Technol*. 2009;42: 1035–1042.

94 Mahmood MA, Visan AI, Ristoscu C, Mihailescu IN. Artificial neural network algorithms for 3D printing. *Materials (Basel)*. 2021;14: 1–29.

95 Ioffe S, Szegedy C. Batch normalization: Accelerating deep network training by reducing internal covariate shift. In: *32nd International Conference on Machine Learning, ICML 2015*. Vol 1. International Machine Learning Society (IMLS); 2015:448–456.

96 Dubey SR, Singh SK, Chaudhuri BB. Activation functions in deep learning: A comprehensive survey and benchmark. *Neurocomputing*. 2022;503: 92–108.

97 Smith SL, Kindermans PJ, Ying C, Le Q V. Don't decay the learning rate, increase the batch size. In: *6th International Conference on Learning Representations, ICLR 2018 - Conference Track Proceedings*. ; 2018.

98 Takase T, Oyama S, Kurihara M. Effective neural network training with adaptive learning rate based on training loss. *Neural Networks*. 2018;101: 68–78.

99 Tham M. Dealing with measurement noise. University of Newcastle, Londres (1998 b). Available at: https://web.archive.org/web/20100329135531/http://lorien.ncl.ac.uk/ming/filter/filewma.htm. Published 1998 Accessed November 2, 2022.

100 Cutkosky A, Mehta H. Momentum improves normalized SGD. In: *37th International Conference on Machine Learning, ICML 2020*. Vol PartF16814. International Machine Learning Society (IMLS); 2020:2238–2246.

101 Wang K, Dou Y, Sun T, Qiao P, Wen D. An automatic learning rate decay strategy for stochastic gradient descent optimization methods in neural networks. *Int J Intell Syst*. 2022;37: 7334–7355.

102 Gholamy A, Kreinovich V, Kosheleva O. Why 70/30 or 80/20 Relation Between Training and Testing Sets : A Pedagogical Explanation. *Dep Tech Reports*. February 2018: 1–6.

103 Karsoliya S. Approximating Number of Hidden layer neurons in Multiple Hidden Layer BPNN Architecture. *Int J Eng Trends Technol*. 2012;3: 714–717.

104 Paola JD, Schowengerdt R a. The Effect of Neural-Network Structure on a Classification. *Neural Comput*. 1997;85721: 1–7.

105 Xing Y, Li F. Research on the influence of hidden layers on the prediction accuracy of GA-BP neural network. *J Phys Conf Ser*. 2020;1486.

106 Wilson DR, Martinez TR. The general inefficiency of batch training for gradient descent learning. *Neural Networks*. 2003;16: 1429–1451.

107 Kumar V, Tripathi MM. Weight and bias initialization of ANN for load forecasting using cuckoo search algorithm. *Proc - 2019 7th Int Conf Green Hum Inf Technol ICGHIT 2019*. 2019: 60–65.

108 Schober P, Schwarte LA. Correlation coefficients: Appropriate use and interpretation.

Anesth Analg. 2018;126: 1763–1768.

109 Jang JSR. ANFIS: Adaptive-Network-Based Fuzzy Inference System. *IEEE Trans Syst Man Cybern*. 1993;23: 665–685.

110 Burlutskiy N, Petridis M, Fish A, Chernov A, Ali N. An Investigation on Online Versus Batch Learning in Predicting User Behaviour. In: *Research and Development in Intelligent Systems XXXIII*. ; 2016:135–149.

111 Jang JSR. Fuzzy Modeling Using Generalized Neural Networks and Kalman Filter Algorithm. *AAAI'91 Proc ninth Natl Conf Artif Intell*. 1991;2: 762–767.

112 Loganathan C, Girija & K V. *Investigations on Hybrid Learning in ANFIS*. Vol 4.2014.

113 Jang J-SR, Sun C-T, Mizutani E. *Neuro Fuzzy and Soft Computing: A Computational Approach to Learning and Machine Intelligence*. Prentice-Hall Inc.; 1996.

114 Chen C, John R, Twycross J, Garibaldi JM. An extended ANFIS architecture and its learning properties for type-1 and interval type-2 models. *2016 IEEE Int Conf Fuzzy Syst FUZZ-IEEE 2016*. 2016: 602–609.

115 Ultimaker Cura: Powerful, easy-to-use 3D printing software. Available at: https://ultimaker.com/software/ultimaker-cura. Accessed November 7, 2022.

116 Wasserstein RL, Lazar NA. The ASA's Statement on p-Values: Context, Process, and Purpose. *Am Stat*. 2016;70: 129–133.

117 Haldar SK. Statistical and Geostatistical Applications in Geology. In: *Mineral Exploration*. Elsevier; 2018:167–194.

118 Nahm FS. What the P values really tell us. *Korean J Pain*. 2017;30: 241–242.

119 Aengchuan P, Aungkulanon P. Comparative Study of Fuzzy Inference System and Design of Experiment for Clean Room Equipment Factory. *Int J Mater Mech Manuf*. 2019;7: 33–37.